AD_____

Award Number: W81XWH-05-1-0279

TITLE: Development of a Novel Therapeutic Paradigm Utilizing a Mammary Gland-Targeted, Bin-1 Knockout Mouse Model

PRINCIPAL INVESTIGATOR: Alexander Muller, Ph.D.

CONTRACTING ORGANIZATION: Lankenau Institute for Medical Research
                           Wynnewood, PA 19096

REPORT DATE: March 2008

TYPE OF REPORT: Annual

PREPARED FOR: U.S. Army Medical Research and Materiel Command
               Fort Detrick, Maryland 21702-5012

DISTRIBUTION STATEMENT: Approved for Public Release;
                        Distribution Unlimited

The views, opinions and/or findings contained in this report are those of the author(s) and should not be construed as an official Department of the Army position, policy or decision unless so designated by other documentation.

REPORT DOCUMENTATION PAGE

1. REPORT DATE 01-03-2008	2. REPORT TYPE Annual	3. DATES COVERED 14 Mar 2007 – 13 Mar 2008
4. TITLE AND SUBTITLE Development of a Novel Therapeutic Paradigm Utilizing a Mammary Gland-Targeted, Bin-1 Knockout Mouse Model		5a. CONTRACT NUMBER
		5b. GRANT NUMBER W81XWH-05-1-0279
		5c. PROGRAM ELEMENT NUMBER
6. AUTHOR(S) Alexander Muller, Ph.D. Email: mullera@mlhs.org		5d. PROJECT NUMBER
		5e. TASK NUMBER
		5f. WORK UNIT NUMBER
7. PERFORMING ORGANIZATION NAME(S) AND ADDRESS(ES) Lankenau Institute for Medical Research Wynnewood, PA 19096		8. PERFORMING ORGANIZATION REPORT NUMBER
9. SPONSORING / MONITORING AGENCY NAME(S) AND ADDRESS(ES) U.S. Army Medical Research and Materiel Command Fort Detrick, Maryland 21702-5012		10. SPONSOR/MONITOR'S ACRONYM(S)
		11. SPONSOR/MONITOR'S REPORT NUMBER(S)

12. DISTRIBUTION / AVAILABILITY STATEMENT
Approved for Public Release; Distribution Unlimited

13. SUPPLEMENTARY NOTES

14. ABSTRACT

Evidence of loss or attenuation of the Bin1 gene in human breast cancers has implicated Bin1 as a tumor suppressor or negative modifier gene in mammary gland epithelial cells. We have discovered that Bin1 loss can promote tumorigenesis through an immune escape mechanism and that this correlated with the negative regulatory impact that we showed Bin1 can exert on the important immunomodulatory enzyme indoleamine 2,3-dioxygenase (IDO). Previously we have demonstrated that, in combination with certain chemotherapeutic agents, inhibitors of IDO can be employed in a non-obvious therapeutic regimen to successfully treat pre-established, autochthonous breast tumors in MMTV-Neu transgenic mice. During this reporting period, we have obtained direct evidence in the MMTV-Neu model that, in the context of breast cancer, IDO activity in plasmacytoid dendritic cells from the tumor draining lymph nodes may be more relevant than in the tumor cells themselves. Furthermore, we have found that 1-methyl-D-tryptophan (D-1MT), the presumptive IDO inhibitor which is in early phase clinical trials may instead be directly targeting IDO2, a related enzyme that we discovered. Our data argue that genetic evaluation of patients for known IDO2 polymorphisms may be critically important to interpreting trial outcomes with D-1MT.

15. SUBJECT TERMS
Bin1, IDO, indoleamine 2,3-dioxygenase, tryptophan, 1-methyl-tryptophan, immune escape, tolerance, transgenic mice

16. SECURITY CLASSIFICATION OF:			17. LIMITATION OF ABSTRACT	18. NUMBER OF PAGES	19a. NAME OF RESPONSIBLE PERSON USAMRMC
a. REPORT U	b. ABSTRACT U	c. THIS PAGE U	UU	74	19b. TELEPHONE NUMBER *(include area code)*

Table of Contents

Muller, Alexander J. DOD 07-08 Annual Report

INTRODUCTION

Loss or attenuation of expression of the *Bin1* anti-cancer gene in patient biopsies has been associated with malignant breast carcinoma [1] as well as other prevalent cancers. Our previous studies have indicated that *Bin1* loss can have a striking effect in promoting tumoral immune escape and that this can be more important to tumor formation than the impact of *Bin1* loss on intrinsic growth properties [2]. We have identified the immunomodulatory gene *IDO* as a negatively-regulated downstream target of Bin1. *IDO* encodes indoleamine 2,3-dioxygenase, a tryptophan catabolizing enzyme that has been demonstrated to play a physiologically essential role in protecting the allogeneic fetus during pregnancy by suppressing T cell activation. Our work is the first to connect the *IDO* gene to a known cancer suppression pathway, and dovetails with the observation of increased IDO-mediated tryptophan catabolism that has been frequently reported in cancer patients. In a well-established transgenic mouse model for breast cancer, the MMTV-*Neu* mouse, we have demonstrated that IDO inhibitors can exhibit impressive therapeutic cooperativity when used in combination with specific chemotherapeutic agents [2]. Identification of this non-obvious combination of immunotherapeutic and chemotherapeutic-based regimens presents a clear path forward for translational development. Based on this knowledge, our proposed studies were aimed at addressing the links between *Bin1* loss, *IDO* dysregulation, and host immunity in mouse breast cancer models.

BODY

Task 1. Examine Bin1 and IDO expression in autochthonous MMTV-*Neu* tumors

Previously, we reported evidence that Bin1 function in MMTV-*Neu* tumors may be attenuated both through decreased expression and mislocalization during the process of malignant transformation. Technical difficulties had precluded similar evaluation of IDO levels in these tumors. We have overcome this roadblock through the establishment of a collaboration with Dr. David Munn at the Medical College of Georgia. His laboratory has successfully performed immunohistochemical analysis of IDO expressed in mouse tissues [3] and they have been willing to evaluate tissues from our breast tumor-bearing mice. In a preliminary experiment, reported last year on the evaluation of IDO in tumors formed by 4T1 breast carcinoma isografts implanted ectopically into the mammary fatpad, no evidence of IDO expression was observed in the actual tumor but rather was observed in tumor draining lymph nodes. We now have successfully stained specimens from tumor-bearing MMTV-*Neu* mice and a similar staining pattern has emerged (**Fig. 1**). Again, although there was no evidence of IDO expression in the tumor, IDO expression was detected in the tumor draining lymph node in what appear morphologically to be plasmacytoid dendritic cells. This is the same sort of staining pattern that the Munn group previously reported in a melanoma isograft model [4], which has led to the hypothesis that, in the case of some tumors, immune escape can be mediated by IDO expression in the tumor draining lymph node. Data from human breast cancer patients, which Dr, Munn's group has collected, is

consistent with this being the more common mechanism of immune escape for breast cancer and we are now writing up these findings for publication.

Task 2. Directly determine the impact of *Bin1* loss on tumor development

We previously reported that, although *Bin1* gene expression is not essential for mammary gland development, it does facilitate lobular development prior to and during pregnancy but that compensatory development apparently minimizes this difference following parturition. We also reported last year that mammary gland targeted Bin1 loss does not significantly impact the frequency or latency of carcinogen-induced breast cancer, but does consistently result in disease that scores as histopathologically more aggressive. These data were published in *Cancer Research* [5]. To address the goal of investigating how *Bin1* loss affects tumorigenesis driven by lactation-dependent expression of the c-*Neu* proto-oncogene in the mammary gland, we previously reported crossing the MMTV-*Neu* transgene onto the Wap-*Cre*$^{+/-}$*Bin1*$^{\text{flox/KO}}$ background, in which the *Bin1* gene undergoes tissue targeted disruption in the mammary epithelial cells of parous female mice. Experimental and control groups were evaluated under conditions that we had previously found to result in nearly 100% of MMTV-*Neu* transgenic female mice on the FVB strain background developing mammary gland tumors by 8 months. However, we were unable to obtain interpretable data in the targeted Bin1 loss studies because tumor formation was dramatically suppressed as a consequence of the mixed non-FVB strain background in which these experiments were conducted. In order to circumvent this problem, we have performed the necessary breeding to make it possible to perform the same experiment on an FVB strain background as described in the Potential Pitfalls and Alternative Approaches section of Task 2. This required backcrossing three different transgenic lines to FVB for at least 5 generations each (to bring the genetic background to > 95% FVB) and then performing a relatively complex breeding strategy (diagrammed in **Fig. 2**) to produce mice with all of the requisite genetic elements in place. We have since generated the necessary cohorts of FVB-strain MMTV-*Neu*$^{+/-}$Wap*Cre*$^{+/-}$ *Bin1*$^{\text{flox/KO}}$ experimental mice and MMTV-*Neu*$^{+/-}$Wap*Cre*$^{+/-}$*Bin1*$^{\text{flox/wt}}$ control mice to perform the study. Preliminary outcome analysis indicates that mammary gland targeted Bin1 loss does not demonstrably affect either tumor multiplicity or latency in this model. So far these data are consistent with outcomes from the carcinogenesis studies and we are currently waiting for histopathological analysis of these samples to determine if Bin1 loss promotes malignant progression in a similar manner as well. Because Bin1 loss in this model is targeted to the mammary gland epithelium and IDO appears to be expressed in dendritic in the tumor draining lymph node, we no longer expect there to be a direct connection between Bin1 loss and a contribution of IDO to tumor development in the breast cancer context.

Task 3. Investigate the chemopreventative activity of IDO inhibitor treatment in relation to *Bin1* status
AND
Task 4. Profile tumor-associated immune cell populations and functionally characterize the involvement of specific T cell populations.

The rationale for these final two Tasks was predicated on the prediction that loss of Bin1 in developing tumors of MMTV-*Neu* mice would promote tumor development through dysregulated elevation of IDO directly in the breast cancer cells. Data obtained in the course of this project has now led us to call this particular model into question. Since beginning work on this project, we are becoming increasingly convinced that the relative importance of tumor-expressed IDO may be contextual and that breast cancer may instead be a tumor type in which IDO activity in the normal stroma, particularly in antigen presenting dendritic cells (DCs) in the tumor draining lymph nodes (TDLN), is most relevant to tumor outgrowth. This idea is based on our findings in the MMTV-Neu model that IDO inhibition cooperates with chemotherapy to produce regression of primary tumors [2] even though no evidence of IDO expression in the primary tumor is apparent. As described below, this new way of thinking about IDO in breast cancer has been further corroborated in studies using the highly metastatic 4T1 breast carcinoma cell line [6], which forms progressively growing primary tumors and that spontaneously metastasize to the lungs, liver, blood, lymph nodes, brain, and bone marrow within two weeks after an initial orthotopic injection [7].

Interestingly, we have discovered that the particular compartment in which IDO activity is relevant, be it tumor or stroma, may have significant bearing on the development of potential therapeutic agents targeting IDO. Specifically, the two different stereoisomers of the IDO inhibitor 1MT appear to behave quite differently when targeting tumoral versus stromal IDO activity. The D isomer of 1MT, currently being developed by NewLink Genetics Corp. in conjunction with the National Cancer Institute (NCI), has received Investigational New Drug (IND) approval from the Food and Drug Administration (FDA) and has recently entered into early phase clinical testing. Therefore it is particularly critical to be cognizant of how this specific inhibitor may be predicted to behave in a particular therapeutic context. We have pursued this question as part of the collaboration established with Drs. David Munn and Andrew Mellor, who initiated the preclinical testing of D-1MT through the NCI RAID program. Initially we became interested in the discrepancy between *in vitro* and *in vivo* findings with the two different isomers of 1MT (D and L), where L is in the same conformation as the naturally occurring form of the amino acid tryptophan. Based on published reports, we had expected that the L isomer of 1MT would be a more potent IDO inhibitor than the D isomer and thus would show greater cooperativity against tumors. In order to directly examine this issue biochemically, we tested the ability of the different 1MT isomers to inhibit IDO activity in a cell-free, purified enzyme assay as well as in cancer cells induced to express IDO. As has been previously reported, the L isomer had a substantially lower Ki for inhibiting activity of the purified IDO enzyme than did the D isomer (**Fig. 3**). Likewise, when IDO was induced in the HeLa human cervical cancer cell line by interferon-γ treatment, EC50 determinations again revealed L-1MT to be a more potent inhibitor than D-1MT (**Fig. 4**). However, Dr. David Munn's laboratory has found that, in the case of toleragenic dendritic cells (DCs), D-1MT is at least as good an inhibitor of cellular IDO activity as L-1MT [8]. Furthermore, when tested for their ability to relieve IDO-mediated suppression of T cell activation in a mixed lymphocyte response (MLR) assay, D-1MT was found to be superior to L-1MT as well as DL-1MT [8]. It has been proposed that, for at least some types of cancer, IDO activity associated with toleragenic DCs in the tumor draining lymph nodes may be particularly relevant to immune escape by the tumor. Data from Dr. Munn's laboratory demonstrating D-1MT efficacy in targeting IDO-dependent, DC-mediated immune tolerance and our own data showing the superiority of D-1MT in cooperating with

6

chemotherapeutic agents in two mouse models of breast cancer, the MMTV-Neu transgenic model and the 4T1 mammary carcinoma isograft model (**Fig. 5 A,B**), are consistent with this idea of IDO-expressing, toleragenic DCs being important to tumoral immune escape in the context of breast cancers. A manuscript incorporating these findings has now been published in the journal *Cancer Research* [8].

Our recent work has gone on to uncover a possible explanation for the conundrum surrounding the 1MT stereoisomers in the discovery of a second IDO related enzyme that is specifically inhibited by D-1MT. BLAST searches of the publicly available human genome database for *INDO*-related sequences, led us to come across a second predicted gene directly adjacent to *INDO* at 8p12. Identified by the locus designator *LOC169355*, (which has since been changed to *INDOL1* (*INDO-like-1*)), the predicted gene sequence corresponded to only a fragment of the *INDO* gene. This, however, turned out to be a misannotation. Searching the human genomic sequence identified a complete set of putative exons encoding a full length gene, termed here *IDO2*, and a complete set of exons could be found in the syntenic region of the mouse genome as well. By RT-PCR, we have confirmed expression of the predicted full length human *IDO2* transcript as well as at least four truncated splice variants [9]. The full-length *IDO2* transcript is comprised of 11 exons (**Fig. 6**). An additional exon 1a in humans, encoding 8 N-terminal amino acids, has not yet been found in the mouse. The human and mouse IDO2 proteins are more highly conserved (72% identical) than their IDO counterparts (62% identical). Although the IDO and IDO2 proteins do not share a high degree of homology (43% identical), amino acids determined by crystallographic analysis and mutagenesis studies to be critical for IDO to catabolize tryptophan are highly conserved in IDO2 suggesting that it may be catalytically active as well. Indeed, the ability of IDO2 to catabolize tryptophan was confirmed using recombinant V5 epitope-tagged IDO2 ectopically expressed in a human embryonic kidney cell line (**Fig. 7**). Of particular interest, however, was the finding that in contrast to IDO, IDO2 was preferentially inhibited by the D isomer of 1MT. The differential was quite striking, with no evidence of inhibition by the L isomer at 50 µM at which concentration the maximal inhibition of kynurenine production by the D isomer had been achieved (**Fig. 7**). A manuscript incorporating these findings has now been published in the journal *Cancer Research* [9].

Two single nucleotide polymorphisms (SNPs) producing non-synonymous codon changes within the coding sequence for the *IDO2* gene, which are predicted to severely impact enzymatic function, have been identified through evaluation of the public human NCBI SNP database (**Fig. 8**). One, a T to A transition in exon 10, changes a tyrosine at position 359 to a stop codon. This results in premature termination of the protein immediately prior to a conserved histidine residue that in IDO is essential for catalytic activity [10]. The other, a C to T transversion in exon 8, changes an arginine at position 248 to a tyrosine. This residue is located at a position equivalent to R231 in IDO, which has been demonstrated by site directed mutagenesis to be critical for catalytic activity and, from the crystal structure, is postulated to be involved in substrate recognition through hydrophobic interactions [11]. This residue is predicted to reside near the entrance to the active site and the presence of the bulky tryptophan side chain may hinder substrate access as well (J. Lalonde, personal communication). Both polymorphisms have been confirmed by site directed mutagenesis to reduce the activity of ectopically expressed IDO2 to undetectable levels. In both cases, the protein product was found to be destabilized in the cells (unpublished results), and so the actual impact of these polymorphisms on enzymatic activity as

opposed to expression still remains to be formally evaluated. Remarkably, both of these inactivating polymorphisms are highly represented in the general population. Data from 339 individuals in the public database suggests that there may be some ethnic variation in the frequency of occurrence of these polymorphisms with the R248W most prevalent in individuals of European descent, the Y359Stop most prevalent in individuals of Asian descent, and a lower frequency both inactivating alleles in individuals of African descent. This evaluation is based on relatively small groups and the numbers should be expanded to confirm any trends, but still, the overall frequency at which both *IDO2* alleles are potentially inactivated appears to be remarkably high, ranging from up to 25% of individuals of African descent to possibly as high as 50% of individuals of either European or Asian descent (**Fig. 8**). This raises questions regarding how important the functional role of IDO2 actually is and whether there might be counterbalancing selective pressures on its expression due to both advantages and disadvantages that it might provide the host. IDO, for instance, has been implicated as being both protective against inflammatory pathology associated with infection as well as promoting tumoral immune escape. Along these lines, an interesting question to explore will be how these *IDO2* polymorphisms track with susceptibility and outcomes for different types of cancers. NewLink Genetics Corp. has initiated Phase-I clinical trials of the presumptive IDO inhibitor, 1-methyl-D-tryptophan (D-1MT), with breast cancer as a lead indication. Our recently published finding of the previously unrecognized IDO2 gene product being the preferential target for D-1MT, rather than IDO, has clear ramifications for genetic screening of individuals enrolled in such a trial due to loss-of-function polymorphisms in the *IDO2* gene that are present in the general population [9]. Therefore, future studies of the role of IDO2 in breast cancer development will have immediate bearing on how data from current clinical trials of D-1MT are interpreted as well as on how new inhibitors are designed (specifically targeting IDO2, IDO or both enzymes) in order to achieve maximum therapeutic benefit.

4T1 is an aggressively metastatic breast cancer model. Mortality in this model results from the development of disseminated metastases, particularly pulmonary metastases. The increased survival achieved with combination therapy data in the 4T1 model (**Fig. 5A**) suggested to us the possibility that IDO might be important to the establishment of metastases in this model. Because no detectable IDO expression was observed in 4T1 tumors, it also seemed likely that the relevant compartment for IDO expression was in the stroma. As indicated in the Potential Pitfalls and Alternate Approaches section to Task 3, we were clearly cognizant that this sort of question could be ideally addressed using an IDO knockout mouse, but we deemed creation of such a mouse to be beyond the scope of the project. We did not, however, anticipate at the time that we would be able to obtain the IDO knockout mice through the establishment of a collaboration with Drs. David Munn and Andrew Mellor. Acquiring their IDO knockout mouse line has allowed us to perform experiments aimed at dissecting the role of IDO in tumor development more directly than would be possible with just the use of small molecule IDO inhibitors as we had originally proposed. Based on our IDO inhibitor treatment data, we anticipated that we would have to provide chemotherapy to IDO knockout mice challenged with 4T1 tumor cells in order to produce a survival benefit. Instead we found that the IDO knockout mice, without any additional treatment, showed significantly improved survival over wild type mice that was comparable to what was achieved with the combination of 1MT + cyclophosphamide in the wild type mice even though primary tumor outgrowth was unaffected (**Fig. 9A,B**). A dramatic reduction in lung nodules, (indicative of pulmonary metastases), was observed in lungs from IDO knockout mice

as compared to lungs from wild type mice (**Fig. 9C**). The impact of IDO loss on metastasis was quantitatively assessed using a colony formation assay to compare tumor burden in the lungs. At 5 weeks post-challenge wild type mice had, on average, a 10-fold higher tumor burden in their lungs than did IDO knockout mice (**Fig. 9D**). This was not due to an intrinsic difference in the ability of metastatic 4T1 cells to escape from the site of the primary tumor in the context of the IDO knockout host as the number of 4T1 cells found in the bloodstream was equivalent between the wild type and IDO knockout mice. Metastatic disease is the primary cause of mortality in cancer patients and these are the first data to demonstrate that IDO may be an important therapeutic target to interfere with this critical aspect of breast cancer development.

KEY RESEARCH ACCOMPLISHMENTS

− Collaborated with Drs. David Munn and Andrew Mellor to evaluate IDO staining in MMTV-*Neu* mouse mammary gland tumors and tumor draining lymph nodes as part of a larger project to evaluate the relevance to breast cancer of IDO expression in these two compartments. Have obtained immunohistochemical staining data consistent with IDO expression being predominantly associated with plasmacytoid dendritic cells in the tumor draining lymph node rather than in the tumor itself.

− Backcrossed all of the necessary genetic elements onto the FVB strain background and performed all of the subsequent crosses needed to evaluate the impact of mammary gland targeted deletion of the Bin1 gene on MMTV-*Neu* driven breast cancer. Outcomes data from this experiment, consistent with previously reported carcinogenesis results, have been collected and we are currently awaiting histopathological analysis.

− Demonstrated that the D isoform of the IDO inhibitor 1-methyl-tryptophan, which selectively targets stromal rather than tumoral IDO activity, effectively combines with chemotherapy in two different mouse breast cancer models. These data were published in *Cancer Research*.

− Discovered a new IDO-related gene product, IDO2, that is specifically inhibited by the D isomer of 1MT, providing a possible explanation for the biological activity attributable to this compound. These data were also published in *Cancer Research*.

− Utilized an IDO knockout mouse, provided through our ongoing collaboration with Drs. David Munn and Andrew Mellor, to demonstrate that the absence of stromal IDO is sufficient to effectively delay the development of pulmonary metastases in an orthotopic breast carcinoma isograft model.

REPORTABLE OUTCOMES

• **Manuscripts**

Metz, R., J.B. DuHadaway, U. Kamasani, L.L. Kleintop, **A.J. Muller**, and G.C. Prendergast. Novel tryptophan catabolic enzyme IDO2 is the preferred biochemical target of the antitumor IDO inhibitory compound D-1MT. *Cancer Res.* **67**:7082-7087 (2007).

Chang, M.Y., J. Boulden, J.B. Katz, L. Wang, T.J. Meyer, A.P. Soler, **A.J. Muller**, and G.C. Prendergast. Bin1 ablation increases susceptibility to cancer during aging, particularly lung cancer. *Cancer Res*. **67**:7605-7612 (2007).

Banerjee, T., J.B. DuHadaway, P. Gaspari, E. Sutanto-Ward, D.H. Munn, A.L. Mellor, W.P. Malachowski, G.C. Prendergast and **A.J. Muller**. A key *in vivo* antitumor mechanism of action of natural product-based brassinins is inhibition of indoleamine 2,3-dioxygenase. *Oncogene* epub ahead of press, doi:10.1038/sj.onc.1210939 (2007).

Muller, A.J., R. Metz, and G.C. Prendergast. Differential targeting of tryptophan catabolism in tumors and in tumor-draining lymph nodes by stereoisomers of the IDO inhibitor 1-methyl-tryptophan. *International Congress Series* 1304C pp. 250-261 (2007).

Kumar, S., W.P. Malachowski, J.B. DuHadaway, J.M. LaLonde, P.J. Carroll, D. Jaller, R. Metz, G.C. Prendergast, and **A. J. Muller**. Indoleamine 2,3-dioxygenase is the anticancer target for a novel series of potent naphthoquinone-based inhibitors. *J. Med. Chem.* epub ahead of press, doi:10.1021/jm7014155 (2008)

Ramalingam, A., J.B. Duhadaway, E. Sutanto-Ward, Y. Wang, J. Dinchuk, M. Huang, P.S. Donover, J. Boulden, L.M. McNally, A.P. Soler, **A.J. Muller**, M.K. Duncan, and G.C. Prendergast. Bin3 deletion causes cataracts and increased susceptibility to lymphoma during aging. *Cancer Res*. **68:**1683-1690 (2008).

- **Abstracts/Presentations**

Centro Nacional de Investgaciones Oncologicas/Nature. Madrid, Spain. October 3-6, 2007.
Abstract presented: "IDO inhibition: an emerging therapeutic strategy targeting immune escape by tumors"
(Poster)

American Association for Cancer Research 98th Annual Meeting. Los Angeles, CA. April 14-18, 2006.
Abstract presented: "Brassinin compounds exhibit anti-cancer activity mediated through inhibition of the immunotolerogenic enzyme Indoleamine 2,3-dioxygenase"
(Poster)

NewLink Genetics Corporation, Ames, IA. January 10, 2007
"Evaluation And Development Of IDO Inhibitors To Defeat Tumoral Immune Tolerance"
(Invited Speaker)

29th Annual Induction Ceremony of Sigma Xi
Saint Joseph's University, Philadelphia, Pa. April 25, 2007
"Turning the Immune System Against Cancer: New Developments on an Old Idea"
(Keynote Speaker)

Farmingdale State College Campus-Wide Bioscience Seminar Series
Farmingdale State College, Farmingdale, NY. September 17, 2007
"Development of Small Molecule Inhibitors to Defeat Tumoral Immune Tolerance by Targeting IDO"
(Invited Speaker)

CONCLUSION

Our ongoing studies in mouse breast cancer models have helped to establish a case for this particular tumor type being more dependent on IDO-activity expressed in the stroma for mediating tumoral immune escape than on IDO-activity directly expressed in the tumor cells. This is consistent with observations made by Drs. David Munn and Andrew Mellor in the B16-F10 melanoma isograft tumor model. In particular, our IDO staining data indicate that, similar to the melanoma studies, the accumulation of plasmacytoid dendritic cell with elevated IDO in the tumor draining lymph node appears to be associated with the outgrowth of autochthonous MMTV-*Neu* breast carcinomas as well as orthotopic breast carcinoma isografts as we had shown previously.

The observation that IDO-activity is differentially targeted by the two isoforms of the IDO inhibitor 1-methlyl-tryptophan (1MT), so that the L form is more effective against IDO-activity expressed in tumors while the D form is more effective against IDO-activity expressed in the stroma, is interesting from both a basic research as well as a clinical development perspective. From a basic research perspective, this brings up the obvious question of what is different between IDO in these two compartments; a question that may be answered by our discovery of a novel IDO related enzyme, IDO2, that is specifically inhibited by D-1MT. D-1MT has just entered into early phase clinical trials, so it is imperative to acquire as much information as possible regarding the tumor settings in which this compound may most likely be efficacious as well as where it may not. The data we have generated point to breast cancer as potentially being a clinically relevant tumor type in which to evaluate D-1MT because it appears to be more dependent on the activity of stromal expressed IDO2 where D-1MT is active rather than tumor expressed IDO where it is not . Furthermore, our data suggest that targeting IDO/IDO2 may be an effective approach to impair breast cancer metastasis. Our studies are the first to demonstrate that IDO/IDO2 inhibition can be effective against tumor metastasis, and clinically this may be even more relevant than the data that have been generated regarding the activity of IDO/IDO2 inhibitory compounds against primary tumors.

REFERENCES

[1]   K. Ge, J. Duhadaway, D. Sakamuro, R. Wechsler-Reya, C. Reynolds, G.C. Prendergast. Losses of the tumor suppressor BIN1 in breast carcinoma are frequent and reflect deficits in programmed cell death capacity. Int J Cancer. 2000;85(3):376-83.

[2]   A.J. Muller, J.B. Duhadaway, P.S. Donover, E. Sutanto-Ward, G.C. Prendergast. Inhibition of indoleamine 2,3-dioxygenase, an immunoregulatory target of the cancer suppression gene Bin1, potentiates cancer chemotherapy. Nat Med. 2005;11(3):312-9.

[3]   M. Friberg, R. Jennings, M. Alsarraj, S. Dessureault, A. Cantor, M. Extermann, et al. Indoleamine 2,3-dioxygenase contributes to tumor cell evasion of T cell-mediated rejection. Int J Cancer. 2002;101(2):151-5.

[4]   D.H. Munn, M.D. Sharma, D. Hou, B. Baban, J.R. Lee, S.J. Antonia, et al. Expression of indoleamine 2,3-dioxygenase by plasmacytoid dendritic cells in tumor-draining lymph nodes. J Clin Invest. 2004;114(2):280-90.

[5]   M.Y. Chang, J. Boulden, E. Sutanto-Ward, J.B. Duhadaway, A.P. Soler, A.J. Muller, et al. Bin1 ablation in mammary gland delays tissue remodeling and drives cancer progression. Cancer Res. 2007;67(1):100-7.

[6]   C.J. Aslakson, F.R. Miller. Selective events in the metastatic process defined by analysis of the sequential dissemination of subpopulations of a mouse mammary tumor. Cancer Res. 1992;52(6):1399-405.

[7]   B.A. Pulaski, S. Ostrand-Rosenberg. Reduction of established spontaneous mammary carcinoma metastases following immunotherapy with major histocompatibility complex class II and B7.1 cell-based tumor vaccines. Cancer Res. 1998;58(7):1486-93.

[8]   D.Y. Hou, A.J. Muller, M.D. Sharma, J. DuHadaway, T. Banerjee, M. Johnson, et al. Inhibition of indoleamine 2,3-dioxygenase in dendritic cells by stereoisomers of 1-methyl-tryptophan correlates with antitumor responses. Cancer Res. 2007;67(2):792-801.

[9]   R. Metz, J.B. Duhadaway, U. Kamasani, L. Laury-Kleintop, A.J. Muller, G.C. Prendergast. Novel tryptophan catabolic enzyme IDO2 is the preferred biochemical target of the antitumor indoleamine 2,3-dioxygenase inhibitory compound D-1-methyl-tryptophan. Cancer Res. 2007;67(15):7082-7.

[10]   T.K. Littlejohn, O. Takikawa, R.J. Truscott, M.J. Walker. Asp^{274} and His^{346} are essential for heme binding and catalytic function of human indoleamine 2,3-dioxygenase. J Biol Chem. 2003;278(32):29525-31.

[11]   H. Sugimoto, S.I. Oda, T. Otsuki, T. Hino, T. Yoshida, Y. Shiro. Crystal structure of human indoleamine 2,3-dioxygenase: Catalytic mechanism of O2 incorporation by a heme-containing dioxygenase. Proc Natl Acad Sci USA. 2006;103(8):2611-6.

Novel Tryptophan Catabolic Enzyme IDO2 Is the Preferred Biochemical Target of the Antitumor Indoleamine 2,3-Dioxygenase Inhibitory Compound D-1-Methyl-Tryptophan

Richard Metz,[1] James B. DuHadaway,[1] Uma Kamasani,[1] Lisa Laury-Kleintop,[1] Alexander J. Muller,[1,2] and George C. Prendergast[1,2]

[1]Lankenau Institute for Medical Research, Wynnewood, Pennsylvania and [2]Kimmel Cancer Center, Thomas Jefferson University, Philadelphia, Pennsylvania

Abstract

Small-molecule inhibitors of indoleamine 2,3-dioxygenase (IDO) are currently being translated to clinic for evaluation as cancer therapeutics. One issue related to trials of the clinical lead inhibitor, D-1-methyl-tryptophan (D-1MT), concerns the extent of its biochemical specificity for IDO. Here, we report the discovery of a novel IDO-related tryptophan catabolic enzyme termed IDO2 that is preferentially inhibited by D-1MT. IDO2 is not as widely expressed as IDO but like its relative is also expressed in antigen-presenting dendritic cells where tryptophan catabolism drives immune tolerance. We identified two common genetic polymorphisms in the human gene encoding IDO2 that ablate its enzymatic activity. Like IDO, IDO2 catabolizes tryptophan, triggers phosphorylation of the translation initiation factor eIF2α, and (reported here for the first time) mobilizes translation of LIP, an inhibitory isoform of the immune regulatory transcription factor NF-IL6. Tryptophan restoration switches off this signaling pathway when activated by IDO, but not IDO2, arguing that IDO2 has a distinct signaling role. Our findings have implications for understanding the evolution of tumoral immune tolerance and for interpreting preclinical and clinical responses to D-1MT or other IDO inhibitors being developed to treat cancer, chronic infection, and other diseases. [Cancer Res 2007;67(15):7082–7]

Introduction

Tryptophan catabolism by indoleamine 2,3-dioxygenase (IDO) mediates a protolerogenic mechanism that suppresses T cells, providing balance or feedback control in immune reactions (1, 2). This role for IDO was first established with the demonstration that the specific bioactive IDO inhibitor 1-methyl-tryptophan (1MT; 3) can trigger T cell–mediated rejection of allogeneic mouse concepti (4, 5). More recently, IDO has become recognized as a central mediator of immune tolerance in many settings. In cancer, IDO expression in tumor cells and antigen-presenting cells present in tumor-draining lymph nodes mediates an important mechanism of immune escape (6). IDO inhibitors trigger antitumor immunity (7, 8) and act synergistically with conventional or experimental chemotherapies (9, 10). Based on preclinical efficacy studies, the D stereoisomer of 1MT has emerged as a clinical lead inhibitor that is entering human trials. D-1MT has superior antitumor activity relative to the L stereoisomer in most preclinical models, and IDO is genetically required for the activity of D-1MT (11). However, at the level of biochemical specificity, the distinction between the two isomers is complicated, with the D isomer exhibiting little biochemical activity as an IDO inhibitor relative to L isomer (11). In dendritic cells, both isomers block tryptophan catabolism comparably but the D isomer is again relatively more active biologically (11). Two possible resolutions to this disparity in results are that D-1MT targets either an undefined cellular isoform of IDO, for example, an alternate spliced or modified isoform, or a different target. Here, we corroborate the latter possibility with the discovery of a novel IDO-related enzyme that is a preferential target for biochemical inhibition by D-1MT.

Materials and Methods

All materials and methods are included as online Supplementary Material.

Results

IDO2 is a novel tryptophan-catabolizing enzyme that is preferentially inhibited by D-1MT. We discovered IDO2 by Basic Local Alignment Search Tool searches of the human genome using IDO sequences as probes, identifying a new gene on chromosome 8p12 just downstream of the IDO gene *INDO*. At the time of discovery, genome annotation in this region referred to an anonymous gene termed LOC169355 that was changed later to a misannotated partial gene termed *INDOL1* (IDO like-1; Hs.122077). By trial and error, we identified exons permitting assembly of a full-length IDO-related gene termed *IDO2*. This nomenclature was chosen to distinguish it from *INDOL1*, which remains misannotated as incomplete gene in the database. By homology searching, we also identified the mouse orthologue *Ido2*.

Oligonucleotide primers specific to murine and human coding regions were used to amplify cDNAs by reverse transcription-PCR (RT-PCR) from total RNA isolated from various tissues (Supplementary Figs. S1 and S2). In this manner, we obtained full-length cDNAs with complete coding regions including four alternatively spliced variants of each gene. The primary human transcript is derived from 11 exons encompassing a 74 kb region of chromosome 8p12 (Fig. 1*A* and Supplementary Fig. S3). In three of the five splice isoforms of *IDO2* mRNA we identified, introduction of an out-of-frame stop codon causes a premature truncation of IDO2 protein. Transcripts are initiated only 5 to 7 kb
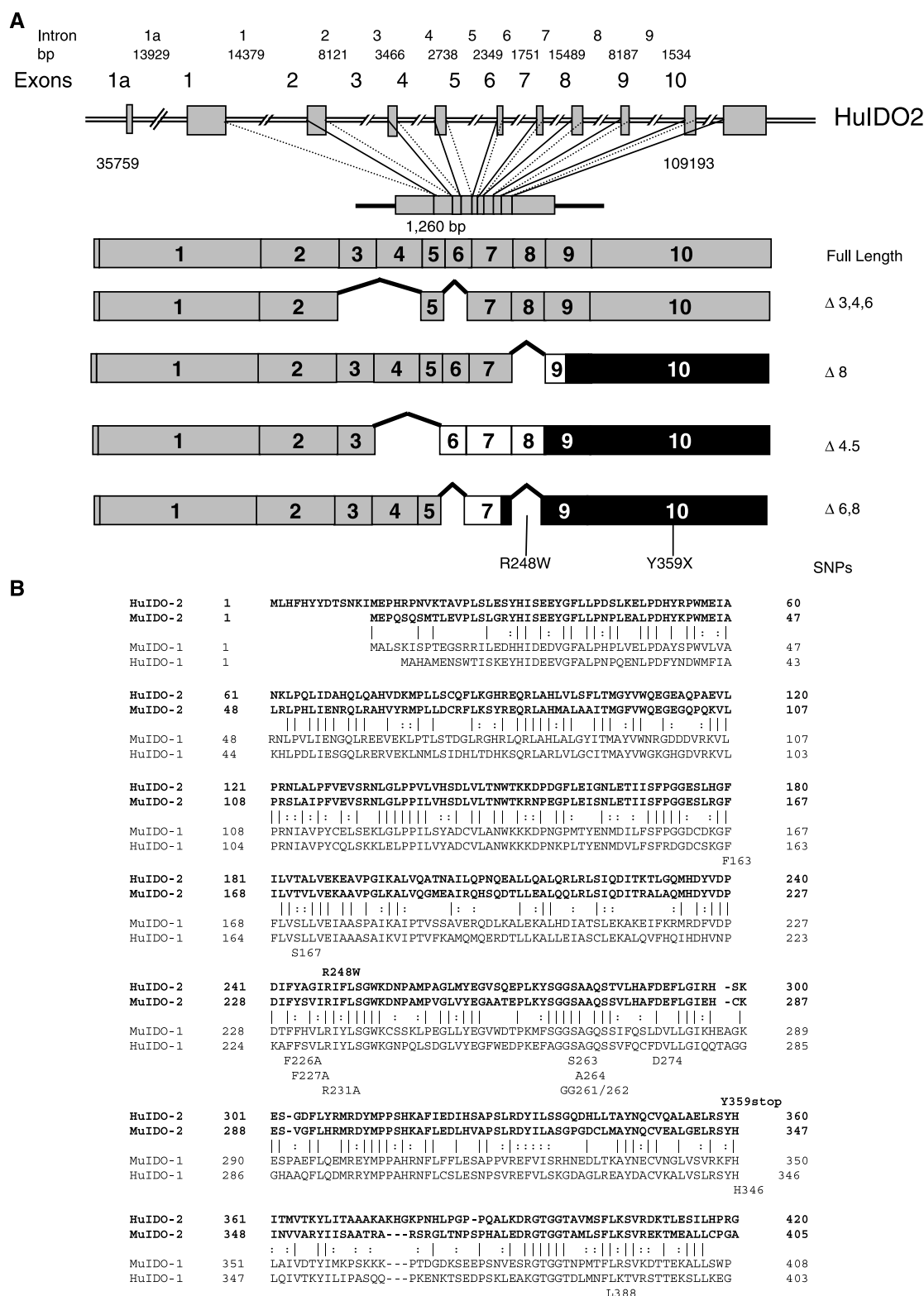
Figure 1. IDO2 structure and similarities to IDO. *A,* structure of human *IDO2* gene and transcripts. Complete coding region is 1,260 bp encoding a 420-amino-acid polypeptide. Alternate splice isoforms lacking the exons indicated are noted. *White boxes,* a frameshift in the coding region to an alternate reading frame leading to termination. *Black boxes,* 3′ untranslated regions. Nucleotide numbers, intron sizes, and positioning are based on IDO sequence files NW_923907.1 and GI:89028628 in the Genbank database. *B,* amino acid alignment of IDO and IDO2. Amino acids determined by mutagenesis and the crystal structure of IDO that are critical for catalytic activity are positioned below the human IDO sequence. Two commonly occurring SNPs identified in the coding region of human IDO2 are shown above the sequence that alter a critical amino acid (R248W) or introduce a premature termination codon (Y359stop).

downstream of the *INDO* gene. The mouse gene seems to differ in its lack of the alternate exon 1a found in the human gene; otherwise, exon positions are conserved, indicating gene duplication during evolution of this region of the genome. Human and mouse IDO2 proteins are 420 and 405 amino acids, respectively, and are more conserved (72% identical, 84% similar) than IDO proteins (62% identical, 77% similar). Alignments between IDO and IDO2 sequence reveal highly conserved features that mediate heme and substrate binding (Fig. 1*B*), although the overall level of sequence conservation is not particularly high (43% identical, 63% similar for human). Significantly, residues determined by IDO mutagenesis and crystallographic analysis to be critically important for catalytic activity are highly conserved in IDO2 (Fig. 1*B*).
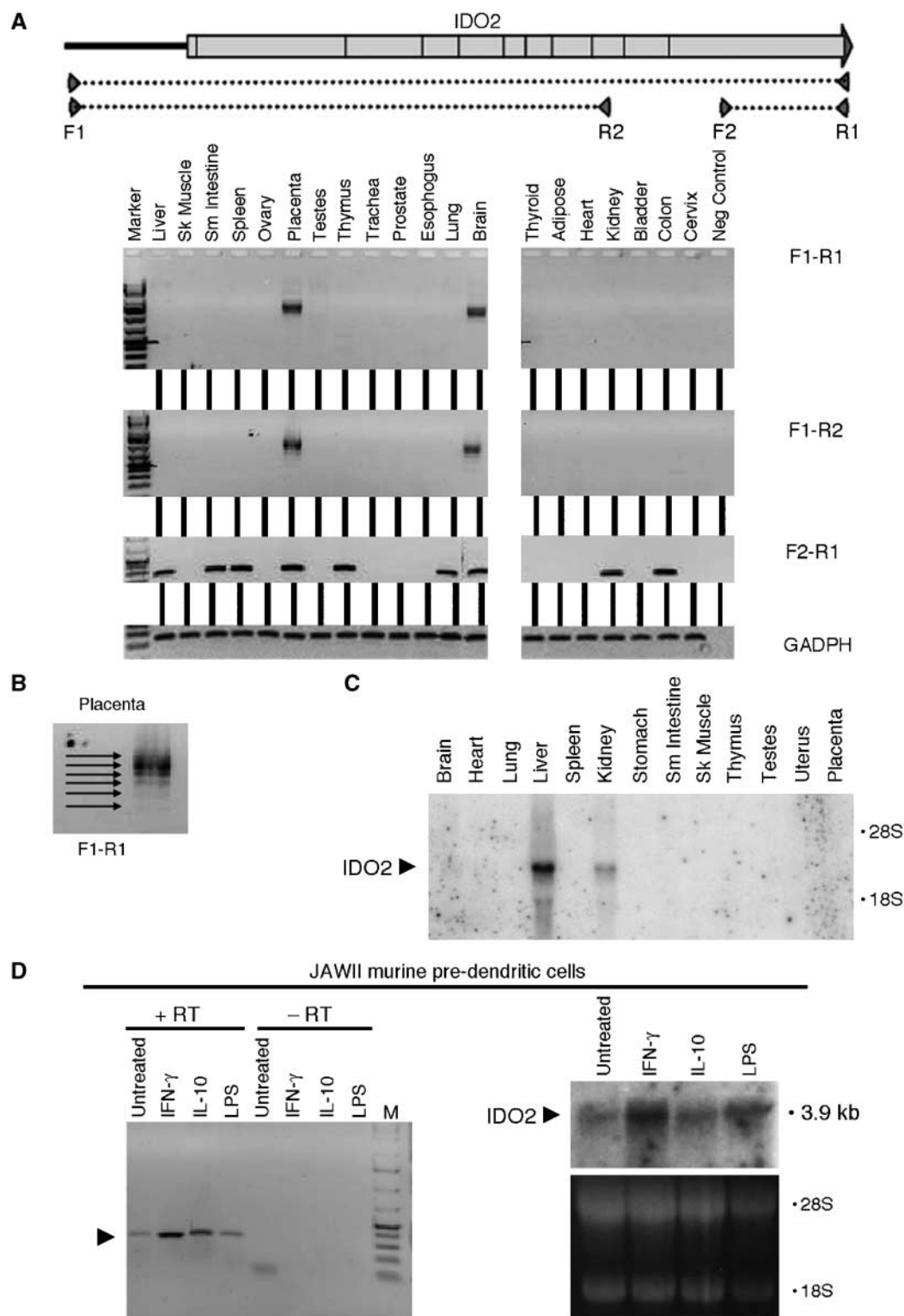
To confirm the expectation that IDO2 catabolizes tryptophan, we expressed it in a doxycycline-regulated T-REX cell system where formation of the enzymatic product *N*-formyl-kynurenine (Kyn) was monitored. Stable cell lines expressing V5 epitope–tagged or untagged proteins with similar levels of doxycycline-induced expression were used for analysis (Fig. 2*A*; Supplementary Fig. S4). As expected, both human and murine IDO2 catabolized tryptophan effectively as measured by Kyn production (Fig. 2*B*). Based on IDO-IDO2 similarity, we compared the ability of known IDO

inhibitors to block the activity of IDO2 in T-REX cells. For reasons mentioned above, the IDO inhibitor D-1MT was of particular interest based on uncertainties about its biochemical target (9, 11). Therefore, we evaluated how IDO1 or IDO2 activity was affected by the D or L stereoisomers of 1MT, or by a third inhibitor MTH-trp (9). Consistent with previous observations (11), we found that IDO activity was modestly inhibited by L-1MT but not D-1MT. In contrast, IDO2 activity was inhibited by D-1MT but not L-1MT. This pattern of inhibition was specific to these 1MT isomers insofar as MTH-trp inhibited the activity of both enzymes (Fig. 2*C*). These results identify IDO2 as a relevant target for biochemical inhibition by D-1MT, which may explain its well-documented antitumor effects.

IDO2 expression is more restricted than IDO but includes dendritic cells. By RT-PCR analysis, we found *IDO2* is expressed in a subset of tissues expressing IDO. Primers spanning the complete human coding region detected full-length mRNAs only in placenta and brain, whereas primers specific to exon 10 (found to be common to all human *IDO2* cDNAs) detected *IDO2* mRNAs in human liver, small intestine, spleen, placenta, thymus, lung, brain, kidney, and colon (Fig. 3*A* and *B*). Although RT-PCR reactions spanning exons 1 to 8 might not have been sensitive enough to detect low-level transcripts, exon 1a–specific primers gave similar results (data not shown), implying that other transcription start
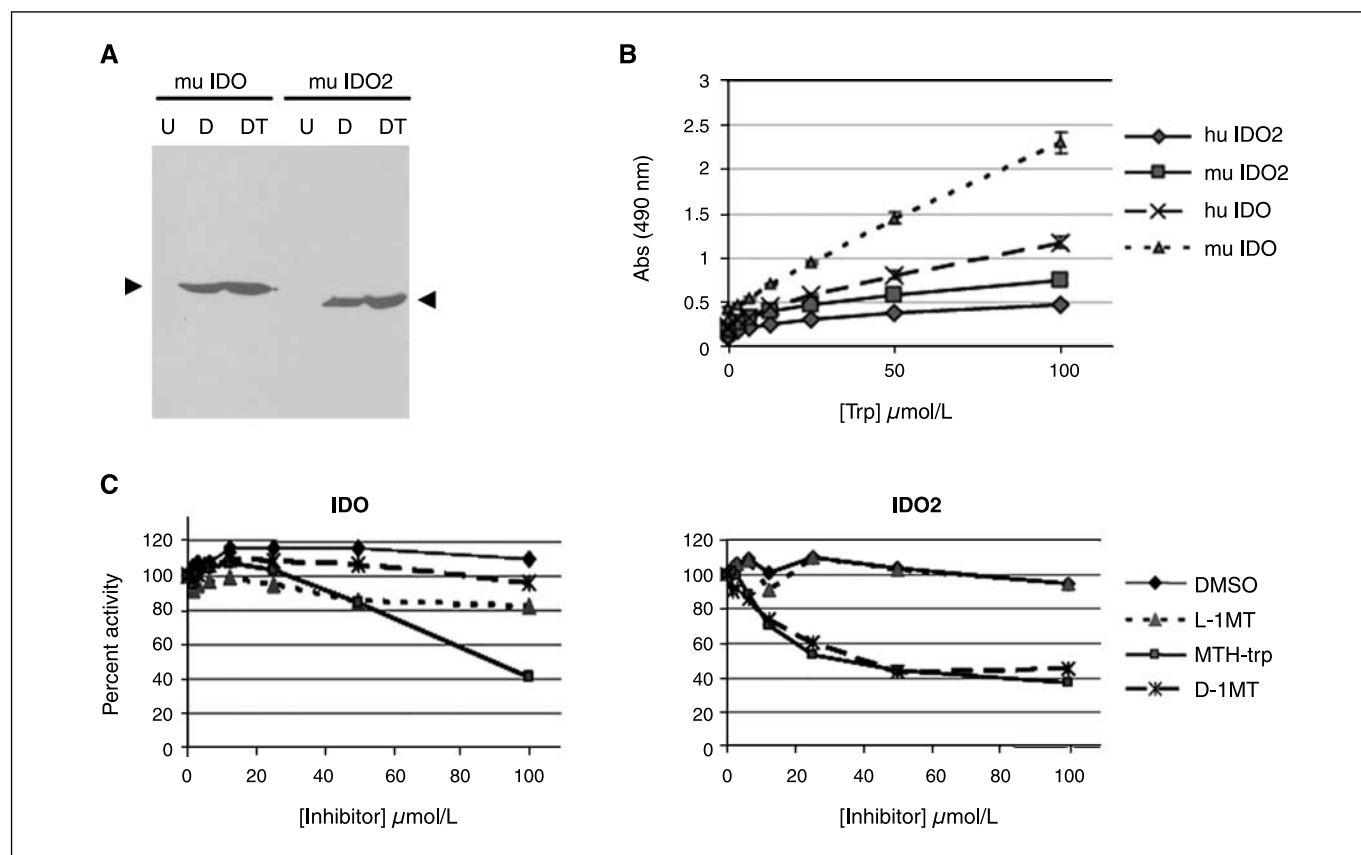
Figure 2. Tryptophan catabolic activity of IDO2 and inhibition by D-1MT. *A,* inducible expression of IDO and IDO2 in representative T-REX cells. Western blot analysis of the V5 epitope–tagged proteins indicated was done with a horseradish peroxidase–conjugated anti-V5 antibody (Invitrogen) in cells that were untreated (*U*), treated with 20 ng/mL doxycycline (*D*), or treated with doxycycline and 100 μmol/L tryptophan (*DT*). *B,* tryptophan catabolism. T-REX cells were seeded at 60% to 70% confluence in 96-well dishes in medium supplemented with 0 to 100 μmol/L tryptophan. Kyn production was determined 48 h later and normalized to protein levels as determined by sulforhodamine B assay. Each enzyme was catalytically active, based on increased Kyn levels with increasing substrate concentrations, although IDO2 seemed to be 2- to 4-fold less active than IDO when normalized to protein levels as determined by sulforhodamine B assay. *Points,* mean of values determined in triplicate and normalized to cellular protein levels. *Abs,* absorbance. *C,* effect of IDO inhibitors on IDO2 catalytic activity. T-REX cells were seeded and processed as above except for the addition to the medium of 0 to 100 μmol/L of the IDO inhibitors MTH-trp, L-1MT, D-1MT, or vehicle control (DMSO). *Points,* mean of values determined in triplicate and normalized to cellular protein levels as before.

Figure 3. Tissue-specific and dendritic cell expression of IDO2. *A,* human tissues. A panel of total RNAs (Ambion) was analyzed by RT-PCR and agarose gel electrophoresis. *Cartoon above the figure,* location of primer pairs used for RT-PCR as indicated next to the gel photos. Glyceraldehyde-3-phosphate dehydrogenase was used as a positive control. *B,* human placenta. Expression of splice variants characterized as detected by the F1-R1 primer pair spanning the full-length cDNA. A similar pattern of expression was observed with primers extending through exons 8 to 10 as F2-R1. *C,* murine tissues. A commercial Northern blot (Seegene) was hybridized to murine IDO2 cDNA probe before washing and autoradiography using standard methods. *D,* murine JAWII predendritic cells. *Top,* RT-PCR analysis. Total RNA isolated from cells that were unstimulated or stimulated 24 h with IFN-γ, IL-10, or lipopolysaccharide was analyzed using primers F6 and R5 for murine IDO-2 (Supplementary Fig. S2). *Bottom,* Northern analysis. RNAs were fractionated on an agarose gel, blotted to nitrocellulose, and hybridized with a murine IDO2 cDNA probe. *Top,* ethidium-stained gel photograph showing intact 28S and 18S rRNAs. *LPS,* lipopolysaccharide.

sites may exist in human *IDO2*. Northern analysis of mouse tissue RNAs confirmed a more narrow range of expression, revealing detectable *IDO2* transcripts only in liver and kidney (Fig. 3C). In a query of the NCBI SAGEmap database with a sequence tag to *IDO2*, the top four hits in terms of tag count prevalence were all identified as bone marrow–derived dendritic cell libraries. Because D-1MT inhibits kynurenine production in dendritic cells and block their ability to activate T cells (11), we examined *IDO2* expression in an established predendritic mouse cell line (JAWII) that matures to dendritic cells after treatment with IFN-γ. *IDO2* mRNA was expressed in unstimulated JAWII cells, and IFN-γ treatment and, to a lesser extent, IL-10 or lipopolysaccharide treatment increased levels modestly (Fig. 3D). Using an IDO2-specific monoclonal antibody, we confirmed expression of IDO2 protein in JAWII cells by Western blotting and indirect immunofluorescence microscopy, the latter of which revealed a generally cytoplasmic pattern of expression like IDO (data not shown). Although we could not detect Kyn production in JAWII cells, we confirmed that full-length cDNAs cloned from these cells encoded a fully active enzyme in T-REX cells (data not shown). Together, these observations defined a pattern of expression for IDO2 that includes dendritic cells.

Common genetic polymorphisms in human IDO2 compromise or abolish enzymatic activity. During characterization of *IDO2* cDNAs, we identified two single nucleotide polymorphisms (SNP) that abolished enzymatic activity. One C-T SNP affecting R248 in human IDO2 was structurally analogous to R231 in human IDO, which makes a critical contact with the indole ring of tryptophan (12). The nonsynonymous substitution (R248W) reduced catalytic activity ∼ 90% in T-REX cells (Supplementary Fig. S5). A second T-A SNP affecting Y359 generated a premature stop codon (Y359X), which completely abolished activity (Supplementary Fig. S5). Strikingly, both SNPs were commonly found in human genomic DNAs in public databases, with the C-T SNP being highly represented in individuals of European descent, the T-A SNP being highly represented individuals of Asian descent, and neither SNP being as prevalent in individuals of African descent (Supplementary Fig. S6). Thus, as many as 50% of individuals of European or Asian descent and 25% of individuals of African descent may lack functional IDO2 alleles. This analysis implicates these SNPs as having a broad effect on IDO2 activity in human populations, which may have a significant bearing on the interpretation of clinical responses to drug-like inhibitors of IDO2 like D-1MT.

IDO2 and IDO each activate LIP, an inhibitory isoform of immune regulatory transcription factor NF-IL6, but IDO2

produces a tryptophan-independent signal. Tryptophan catabolism by IDO triggers GCN2-dependent phosphorylation of the translation initiation factor eIF-2α (13). Activation of this pathway inhibits translation of most messages with the exception of certain messages essential for stress-related functions. Additional contributions of IDO to tolerogenesis are imparted by Kyn and other downstream catabolites (14–16). We evaluated the ability of IDO2 to activate this pathway in T-REX cells. In IDO-expressing cells, Kyn production was constant for 4 days postinduction after which cell growth rate slowed appreciably. This effect related to tryptophan depletion rather than Kyn elevation, because supplementing the culture medium with tryptophan rescued the effect (Supplementary Fig. S7). In IDO2-expressing cells, tryptophan consumption was slower such that cell growth was not affected (Supplementary Fig. S7). Nevertheless, induction of IDO2 caused GCN2-dependent phosphorylation of eIF-2α like IDO (data not shown). To compare downstream effects, we examined how IDO or IDO2 activation affected translation of LIP, an inhibitory isoform of the transcription factor NF-IL6/CEPBβ that is up-regulated by amino acid deprivation by a switch to an alternate translational start site (17). Both enzymes up-regulated LIP strongly, however, restoring tryptophan to culture medium reversed LIP induction only when stimulated by IDO (Fig. 4). Thus, IDO2 produced a distinct signal for LIP activation that was independent of tryptophan availability. This signal required catalytic activity because it was inhibited by D-1MT (Fig. 4). These findings implied that IDO2 has a distinct signaling role in cells compared with IDO.

Discussion

The findings of this study are significant and timely regarding how tryptophan catabolism suppresses T-cell immunity, how immune escape evolves during cancer progression, and how the D stereoisomer of the widely studied IDO inhibitor 1MT, presently entering phase I clinical trials, acts to elicit antitumor responses in animals. Given the striking therapeutic effects of D-1MT in preclinical models of cancer and other diseases (6), our findings point to IDO2 as an important therapeutic target and genetic modifier for understanding disease susceptibility. The existence of widely dispersed genetic polymorphisms in human populations that ablate catalytic activity argues that knowing the genetic status of IDO2 of individuals enrolled in D-1MT trials may be important for understanding clinical responses. Given the likelihood that IDO2 may contribute to immune tolerance, two implications are that individuals heterozygous or homozygous for catalytically inactive alleles may be (*a*) less susceptible to developing diseases driven by immune suppression, and (*b*) less susceptible to manifesting clinical responses to D-1MT or other IDO2 inhibitory compounds. Due to deficiencies in IDO2 activity, such individuals may be relatively less prone to immune escape and malignant progression of oncogenically initiated lesions, but relatively more prone to autoimmune disorders. Given differences in the antitumor responses seen in various preclinical cancer models to L-1MT versus D-1MT (11), it may also be interesting to evaluate the murine *IDO2* gene for related polymorphisms.

In LIP, we have defined a novel component of the tryptophan catabolism signaling pathway triggered by IDO or IDO2, using it here to reveal a mechanistic difference in how translational control by these enzymes may modulate immune tolerance. As a downstream reporter, LIP could provide a useful biomarker for genetic and biochemical pathways activated by IDO1 or IDO2 in cells that express

Figure 4. Distinct role of IDO2 in tryptophan catabolic signaling to transcription factor LIP. Western analysis of LIP and LAP isoforms of NF-IL6/CEBPβ was done using lysates isolated from T-REX cells seeded into 12-well dishes that were uninduced (*UI*), treated with 20 ng/mL doxycycline (*Dox*), or treated with doxycycline and 100 μmol/L tryptophan (*Tryp*). In the lanes indicated, cells were also treated with 100 μmol/L L-1MT or D-1MT.

NF-IL6 (also known as CEBPβ). In essence, LIP is a dominant inhibitory isoform composed of only the DNA binding region of NF-IL6 (17). By interfering with target genes that control stress signaling, cell growth, and immune modulation, LIP is well positioned to mediate stable effects of IDO or IDO2 on immune tolerance generated by antigen-presenting cells or other cell types. Using LIP, we found that transient activation of IDO2 generates a stable signal that persists independently of tryptophan availability. The potential significance of this mechanism is that it could be used to propagate tolerance from a local to a peripheral immune environment, away from an initial site of tryptophan catabolism (18), for example, to support cancer metastasis. Differences in LIP response argue that the functions of IDO and IDO2 may be distinct, even if outcomes for eliciting immune tolerance are similar.

IDO2 may address key questions about how 1MT manifests its antitumor activity. Previous studies indicated that D-1MT can inhibit tryptophan catabolism in human dendritic cells and that the *IDO* gene is needed for antitumor activity, implicating IDO in the D-1MT mechanism at some level (11). Our findings do not rule out the possibility that 1MT may target an endogenous IDO protein differing at some level, for example, due to posttranslational modification (11); however, identifying IDO2 addresses a key gap in knowledge concerning the biochemical target of D-1MT. In most models, D-1MT displays much better antitumor activity than L-1MT prompting the choice made for clinical development. One implication is that compounds with dual specificity for IDO and IDO2 may exert more potent antitumor efficacy, and MTH-trp fulfills this expectation (9). Based on genetic knockout studies supporting a role for IDO in the response to D-1MT at some level (11), our findings strongly suggest cross-talk or cooperation between the functions of IDO and IDO2 in immune regulation. Consistent with this idea, IDO activity may be supported by other elements involved in tryptophan catabolism (16, 19). In future work, it will be important to examine IDO-IDO2 cooperation as well as how catabolites of tryptophan catabolism may figure into IDO2 action.

Addendum

Recently we became aware of another group reporting the identification of this gene (20).

Acknowledgments

References

1. Mellor AL, Munn DH. IDO expression by dendritic cells: tolerance and tryptophan catabolism. Nat Rev Immunol 2004;4:762–74.
2. Puccetti P. On watching the watchers: IDO and type I/II IFN. Eur J Immunol 2007;37:876–9.
3. Cady SG, Sono M. 1-Methyl-DL-tryptophan, β-(3-benzofuranyl)-DL-alanine (the oxygen analog of tryptophan), and β-[3-benzo(*b*)thienyl]-DL-alanine (the sulfur analog of tryptophan) are competitive inhibitors for indoleamine 2,3-dioxygenase. Arch Biochem Biophys 1991;291:326–33.
4. Munn DH, Zhou M, Attwood JT, et al. Prevention of allogeneic fetal rejection by tryptophan catabolism. Science 1998;281:1191–3.
5. Mellor AL, Sivakumar J, Chandler PKS, Molina H, Mao D, Munn DH. Prevention of T cell-driven complement activation and inflammation by tryptophan catabolism during pregnancy. Nat Immunol 2001;2:64–8.
6. Munn DH, Mellor AL. Indoleamine 2,3-dioxygenase and tumor-induced tolerance. J Clin Invest 2007;117:1147–54.
7. Friberg M, Jennings R, Alsarraj M, et al. Indoleamine 2,3-dioxygenase contributes to tumor cell evasion of T cell-mediated rejection. Int J Cancer 2002;101:151–5.

8. Uyttenhove C, Pilotte L, Theate I, et al. Evidence for a tumoral immune resistance mechanism based on tryptophan degradation by indoleamine 2,3-dioxygenase. Nat Med 2003;9:1269–74.
9. Muller AJ, DuHadaway JB, Sutanto-Ward E, Donover PS, Prendergast GC. Inhibition of indoleamine 2,3-dioxygenase, an immunomodulatory target of the tumor suppressor gene Bin1, potentiates cancer chemotherapy. Nat Med 2005;11:312–9.
10. Muller AJ, Prendergast GC. Indoleamine 2,3-dioxygenase in immune suppression and cancer. Curr Cancer Drug Targets 2007;7:31–40.
11. Hou DY, Muller AJ, Sharma MD, et al. Inhibition of indoleamine 2,3-dioxygenase in dendritic cells by stereoisomers of 1-methyl-tryptophan correlates with antitumor responses. Cancer Res 2007;67:792–801.
12. Sugimoto H, Oda SI, Otsuki T, Hino T, Yoshida T, Shiro Y. Crystal structure of human indoleamine 2,3-dioxygenase: Catalytic mechanism of O_2 incorporation by a heme-containing dioxygenase. Proc Natl Acad Sci U S A 2006;103:2311–6.
13. Munn DH, Sharma MD, Baban B, et al. GCN2 kinase in T cells mediates proliferative arrest and anergy induction in response to indoleamine 2,3-dioxygenase. Immunity 2005;22:633–42.
14. Fallarino F, Grohmann U, Vacca C, et al. T cell

apoptosis by tryptophan catabolism. Cell Death Diff 2002;9:1069–77.
15. Fallarino F, Grohmann U, You S, et al. The combined effects of tryptophan starvation and tryptophan catabolites down-regulate T cell receptor ζ-chain and induce a regulatory phenotype in naive T cells. J Immunol 2006; 176:6752–61.
16. Belladonna ML, Grohmann U, Guidetti P, et al. Kynurenine pathway enzymes in dendritic cells initiate tolerogenesis in the absence of functional IDO. J Immunol 2006;177:130–7.
17. Descombes P, Schibler U. A liver-enriched transcriptional activator protein, LAP, a transcriptional inhibitory protein, LIP, are translated from the same mRNA. Cell 1991;67:569–79.
18. Grohmann U, Bianchi R, Belladonna ML, et al. IFN-γ inhibits presentation of a tumor/self peptide by CD8α⁻ dendritic cells via potentiation of the CD8α⁺ subset. J Immunol 2000;165:1357–63.
19. Manlapat AK, Kahler DJ, Chandler PR, Munn DH, Mellor AL. Cell-autonomous control of interferon type I expression by indoleamine 2,3-dioxygenase in regulatory CD19⁺ dendritic cells. Eur J Immunol 2007;37:1064–71.
20. Ball HJ, Sanchez-Perez A, Weiser S, et al. Characterization of an indoleamine 2,3-dioxygenase-like protein found in humans and mice. Gene 2007;396:203–13.

Bin1 Ablation Increases Susceptibility to Cancer during Aging, Particularly Lung Cancer

Mee Young Chang,[1] Janette Boulden,[1] Jessica B. Katz,[1] Liwei Wang,[3] Thomas J. Meyer,[2] Alejandro Peralta Soler,[1,4] Alexander J. Muller,[1] and George C. Prendergast[1,5]

[1]Lankenau Institute for Medical Research, and [2]Lung Cancer Program, Lankenau Hospital, Wynnewood, Pennsylvania; [3]Department of Gastrointestinal Medical Oncology, M. D. Anderson Cancer Center, Houston, Texas; [4]Department of Pathology, Duke University Medical Center, Durham, North Carolina; and [5]Department of Pathology, Anatomy and Cell Biology, Jefferson Medical College, Thomas Jefferson University, Philadelphia, Pennsylvania

Abstract

Age is the major risk factor for cancer, but few genetic pathways that modify cancer incidence during aging have been described. *Bin1* is a prototypic member of the BAR adapter gene family that functions in vesicle dynamics and nuclear processes. *Bin1* limits oncogenesis and is often attenuated in human cancers, but its role in cancer suppression has yet to be evaluated fully *in vivo*. In the mouse, homozygous deletion of *Bin1* causes developmental lethality, so to assess this role, we examined cancer incidence in mosaic null mice generated by a modified Cre-lox technology. During study of these animals, one notable phenotype was an extended period of female fecundity during aging, with mosaic null animals retaining reproductive capability until the age of 17.3 ± 1.1 months. Through 1 year of age, cancer incidence was unaffected by *Bin1* ablation; however, by 18 to 20 months of age, ~50% of mosaic mice presented with lung adenocarcinoma and ~10% with hepatocarcinoma. Aging mosaic mice also displayed a higher incidence of inflammation and/or premalignant lesions, especially in the heart and prostate. In mice where colon tumors were initiated by a *ras*-activating carcinogen, *Bin1* ablation facilitated progression to more aggressive invasive status. In cases of human lung and colon cancers, immunohistochemical analyses evidenced frequent attenuation of *Bin1* expression, paralleling observations in other solid tumors. Taken together, our findings highlight an important role for *Bin1* as a negative modifier of inflammation and cancer susceptibility during aging. [Cancer Res 2007;67(16):7605–12]

Introduction

Aging is the major risk factor for cancer. Nevertheless, most preclinical models of cancer employ young animals that are unlikely to fully recapitulate the participation of the inflammatory tissue microenvironment, immune senescence, or other age-associated factors. Insights into the cause and treatment of cancer might therefore benefit from studies of genetic pathways that modify cancer incidence during aging. However, few such pathways have been defined.

Bin1 encodes a nucleocytosolic BAR adapter protein that can interact with the c-Myc oncoprotein and inhibit its cell transforming activity (1–3). c-Myc is involved in the development of many human cancers where its overexpression is associated with poor prognosis (4). Multiple splice isoforms of Bin1 exist with diverse patterns of tissue distribution, subcellular localization, and protein interactions (5–8). Although BAR adapter proteins share canonical functions in membrane dynamics (9), certain BAR proteins, such as those encoded by the *Bin1* and *APPL* genes, may also have functions in transcriptional control (2, 3, 10). Notably, only nuclear-localizing isoforms of Bin1 can restrict proliferation, survival, and immune escape of oncogenically transformed cells (1, 2, 11–17). Bin1 is widely inactivated in human cancers by attenuation or mis-splicing (1, 12–14, 18–20). However, the consequences of *Bin1* loss to cancer susceptibility in an animal has not been fully evaluated to date.

Homozygous inactivation of *Bin1* causes perinatal lethality associated with severe cardiac hypertrophy (21). Therefore, to assess roles of this gene beyond cardiac development, we generated mosaic null mice using a recently constructed "floxed" conditional mutant (22). In mosaic animals, recombination is distributed throughout the animal, offering several inherent advantages for investigating the impact of gene loss on diverse processes including tumorigenesis. First, null cells are distributed throughout every tissue, so the impact of gene loss in different organs can be evaluated without having to generate multiple independent lines harboring different tissue-specific Cre-expressing alleles. Second, each mouse is internally controlled, provided that the gene of interest is haplosufficient, because tissues include cells that are both null (recombined) and expressing (non-recombined). Third, mosaic analysis is useful in mixed genetic backgrounds because the paired control is derived from the same animal rather than from a different littermate with a different distribution of parental alleles. Fourth, Cre expression is restricted to early embryogenesis, alleviating the concern that contemporaneous Cre activity may influence phenotype, a common concern in tissue-specific knock-outs. Lastly, a mosaic model allows one to gauge the impact of field effects by allowing one to vary the extent of gene loss in a tissue. In this study, we employed a mosaic model to evaluate the contribution of *Bin1* to cancer suppression in mammals. Our findings suggest that *Bin1* limits age-associated inflammation and cancer.

Materials and Methods

Generation and characterization of transgenic mouse strains. We modified the standard design for Cre-mediated gene targeting by introducing a point mutation into the 3′-most loxP site, which we found to (*a*) confer a selective advantage to Cre-mediated excision of the marker

in vitro while maintaining Cre-mediated excision of the target sequence *in vivo*; and (*b*) favor the production of mosaic null animals relative to the standard technology, which was desired for this project. The targeting plasmid has been described previously in a study of tissue-specific gene deletion (22). Briefly, a neomycin resistance gene (neo) cassette flanked by wild-type (wt) loxP sites was inserted into a genomic targeting vector spanning introns 2 to 5 of the mouse *Bin1* gene (23). ES cells with the desired homologous recombination event were infected with a recombinant Cre adenovirus and subcloned to identify cell colonies that had selectively lost the neo marker, leaving intact the targeted exon 3 segment. Correctly targeted ES cell lines were microinjected into C57BL/6J blastocysts, and chimeric mice exhibiting germ line transmission were interbred to produce strains that included the wt allele (+), floxed knock-out allele (flox), and a previously constructed straight knock-out allele (KO; ref. 21). *Bin1* is known to be haplosufficient for viability (21). Therefore, to establish the most efficient system for producing Bin1-expressing or nonexpressing cells by a single Cre-mediated excision event, we crossed the floxed allele (flox) onto a strain with the "straight" knock-out allele (KO; ref. 21). To mediate recombination of the flox allele, *Cre* alleles were introduced by crosses to the transgenic mouse strains FVB-TgN (EIIa-cre) C5379Lmgd/J (EIIa-Cre mice).

Crossing female rather than male EIIa-Cre mice produced higher rates of mosaic offspring (67% versus 42%).[6] Therefore, female EIIa-Cre mice were used to generate more Bin1 mosaic −/− mice and Bin1 heterozygote mice, and male EIIa-Cre mice were used to generate more Bin1+/+ mice. Tumor formation was monitored in mice up to 18 to 21 months of age, after which animals were euthanized and tissues were isolated and fixed in 10% neutral buffered formalin, sectioned, and stained for histopathologic analysis with H&E using standard methods. To monitor fecundity, if no evidence of pregnancy was observed within 4 weeks of housing male and female mice together, the male mice were replaced. Where offspring emerged, litter size was recorded, and the age of the mother was calculated from the date of coitus based on the appearance of a vaginal plug.

Genotype analysis. PCR was used to genotype mice as follows. Mouse tissue samples were digested overnight at 60°C in lysis buffer [50 mmol/L Tris-HCl (pH, 8.0), 100 mmol/L EDTA, 100 mmol/L NaCl, 1% SDS, 30 mg/mL proteinase K]. DNA-containing supernatant was diluted 1/50 in 10 mmol/L Tris-Cl (pH, 8.0), and 2 μL of diluted supernatant was used for PCR in a final volume of 20 μL in a PTC-2000 Peltier Thermal Cycler (MJ Research). Amplification products were separated by electroporation on 2% agarose gels prestained with ethidium bromide using *Hae*III-digested φX174 phage DNA (Fisher) as a molecular size marker. The primers used to monitor the Bin1flox allele were LoxP1 5′-TGGAGTCTGCCACCTTCTATCC-3′ and loxP2 5′-GCTCATACACCTCCTGAAGACAC-3′, with expected sizes of 0.9, 1.07, and 0.31 kb for wt, flox, and recombined flox (floxΔ) alleles, respectively. Following a 4-min denaturation at 94°C, 35 cycles of PCR were done at 94°C for 20 s, 58°C for 1 min, and 72°C for 1 min, with the addition of a 10- min final elongation step at 72°C. The primers and PCR conditions used to monitor the Bin1 KO allele have been described (21). The primers used to monitor the EIIa-Cre gene were Cre1 5′-AGGTTCGTTCACT-CATGGA-3′ and Cre2 5′-GCCACCAGCTTGCATGATC-3′ with allele-positive mice identified by a single 512-bp agarose gel band. PCR conditions for the Cre gene were 2 min denaturation at 94°C followed by 29 cycles of PCR at 94°C for 15 s, 53°C for 30 s, and 72°C for 1 min, with a final 10-min elongation step at 72°C.

Colon carcinogenesis. 1,2-Dimethylhydrazine (DMH) was administered on a traditional protocol as described previously (24). Briefly, mice 6 to 8 weeks old were injected i.p. with DMH each week for 20 weeks at a dose of 30 mg/kg in 10 mmol/L sodium bicarbonate/10 mmol/L EDTA (pH, 8.0). Animals were euthanized 27 weeks after the initial injection, and intestinal tissues that included visible tumors at necropsy were harvested and fixed in 10% neutral buffered formalin for histopathologic analysis using standard methods.

---

[6] M.Y. Chang, unpublished observations.

Results

Generation and validation of *Bin1* mosaic mice. Homozygous deletion of *Bin1* in mice causes perinatal lethality associated with a severe hypertrophic cardiomyopathy (21). Therefore, to bypass lethality, we generated mosaic mice using a conditional floxed knock-out of *Bin1* that we have described recently (22). The scheme is illustrated in Fig. 1*A*. Briefly, deletion of exon 3 leads to exon 2 to 4 splicing that produces out-of-frame stop codon in exon 4. Our design incorporated a mutant loxP site containing a T→C mutation at the 3′-most loxP site in the construct, which confers a selective advantage to *in vitro* excision of the neo cassette without overly compromising *in vivo* excision of the target sequences.[6] To generate mosaic mice, we employed EIIa-Cre transgenic mice where Cre recombinase expression is controlled by the EIIa promoter. In the absence of adenovirus E1A coactivator, expression driven by the EIIa promoter is restricted to mouse oocytes and preimplantation embryos including the one-cell stage zygote (25, 26). EIIa-Cre and Bin1KO/+ mice were interbred to obtain Bin1KO/+;EIIa-Cre(+/+) offspring. These offspring were then crossed with Bin1flox/flox mice to obtain Bin1KO/floxΔ;EIIa-Cre(+/−) mice (Bin1 mosaic nulls), Bin1+/floxΔ;EIIa-Cre(+/−) mice (Bin1 mosaic heterozygotes), and Bin1+/flox;EIIa-Cre(+/−) mice (Bin1 non-recombined controls). For simplicity, these strains are referred in the text below as Bin1 mosaic −/−, Bin1 mosaic +/−, and Bin1+/+. Genotype was defined by the wt, flox, and floxΔ alleles, which generated specific PCR products of 0.90, 1.07, and 0.31 kb, respectively (Fig. 1*B*). Although recombination frequency varied between individual mosaic mice, the proportion of cells harboring recombined to non-recombined alleles was consistent across multiple tissues (Fig. 1*C*). Because the proportion of recombined to non-recombined alleles in all tissues could be predicted by noninvasive genotypic analysis of a standard tail biopsy, to approach the nullizygous state, we selected viable Bin1 mosaic −/− mice with the highest proportion of recombined alleles as reported by PCR analysis (e.g., as illustrated by animal A in Fig. 1*D*). In contrast to designs using wt loxP sites, where EIIa-Cre targeting produces ~50% systemic knock-outs and ~50% mosaic knock-outs (25), we found that our design using the variant 3′ loxP site produced 63% mosaic knock-outs, 6% systemic knock-outs, and 31% non-recombinant animals among progeny from multiple matings (Fig. 1*A*). These results showed that using the variant 3′ loxP site increased the efficiency of producing mosaic mice.

To confirm that the floxΔ allele was a true functional knock-out, we determined whether complete systemic recombinants phenocopied the myocardial hypertrophy and perinatal lethality of the straight KO/KO mouse (21). Progeny from five independent litters were examined after crossing Bin1KO/+ mice with Bin1floxΔ/+ mice that had been defined as germ line recombinants by genotype analysis and progeny testing. Of the neonates obtained from the litters, 11/52 (21%) were unhealthy, died shortly after birth, and were determined to have inherited the KO/floxΔ genotype. Histologic analysis of the hearts from pups that died confirmed that they had a severe myocardial hypertrophy indistinguishable from that characterized previously in KO/KO neonates (Fig. 1*E*). We concluded that Cre-mediated recombination of the flox allele could produce a functional knock-out of *Bin1*.

While breeding heterozygous Bin1+/KO mice over a period of several years, we noticed no apparent phenotypes except that females remained reproductively fertile until well past 1 year of age.
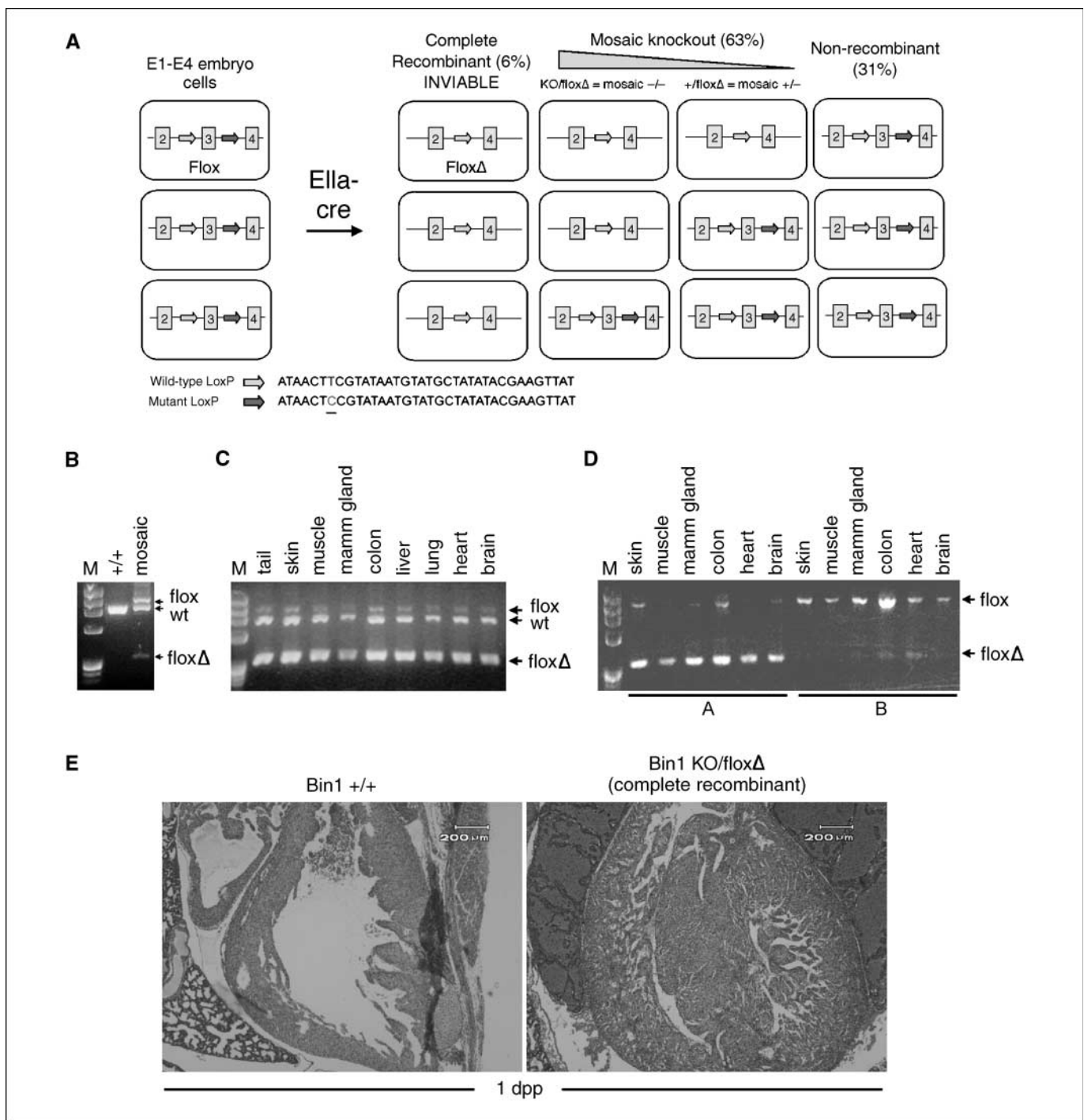
Figure 1. Generation and validation of a conditional allele of the murine *Bin1* gene. *A,* scheme used to produce mosaic mice (see text for details). *B,* variant loxP site produces complete or mosaic gene knock-out. Tail genomic DNA from offspring of *Bin1* flox/+ and EIIa-Cre transgenic was evaluated by PCR for Cre-mediated recombination. The wt, flox, and floxΔ alleles yield products of 0.90, 1.07, and 0.31 kb, respectively. Both recombined and intact flox alleles are present in tail DNA from mosaic mice. *Marker, Hae*III-digested φX174 phage DNA. *C,* Cre-mediated recombination occurs with consistent efficiency across different tissues. Tissues from a single animal were examined. *D,* the extent of cre-mediated recombination varies in individual mosaic mice. Two mice exhibiting a high or low degree of conversion of the flox allele to the floxΔ allele are shown (*A* and *B*). In six tissues examined, the proportion of cells with a recombined allele is consistent with prior analysis of tail biopsies. *E,* the floxΔ allele is a functional knock-out. Histologic analysis of the heart from Bin1(KO)/(floxΔ) pups that expired at birth revealed severe myocardial hypertrophy indistinguishable from that seen in *Bin1* null mice (21). *dpp,* days postpartum.

Breeders in the mouse colony at our institute are typically retired by 8 months due to poor reproductive capability, so this phenotype was unusual. An examination of the breeding history of 23 female Bin1+/KO mice collected over 2 years indicated that the mean age

at the last recorded litter was 14.1 ± 0.5 months (Supplementary Table S1). In contrast, an explicit measurement of the mean age of the last litter in Bin1+/+ females was 11.3 ± 1.2 months, consistent with observations in aged C57BL/10Sn mice that have been

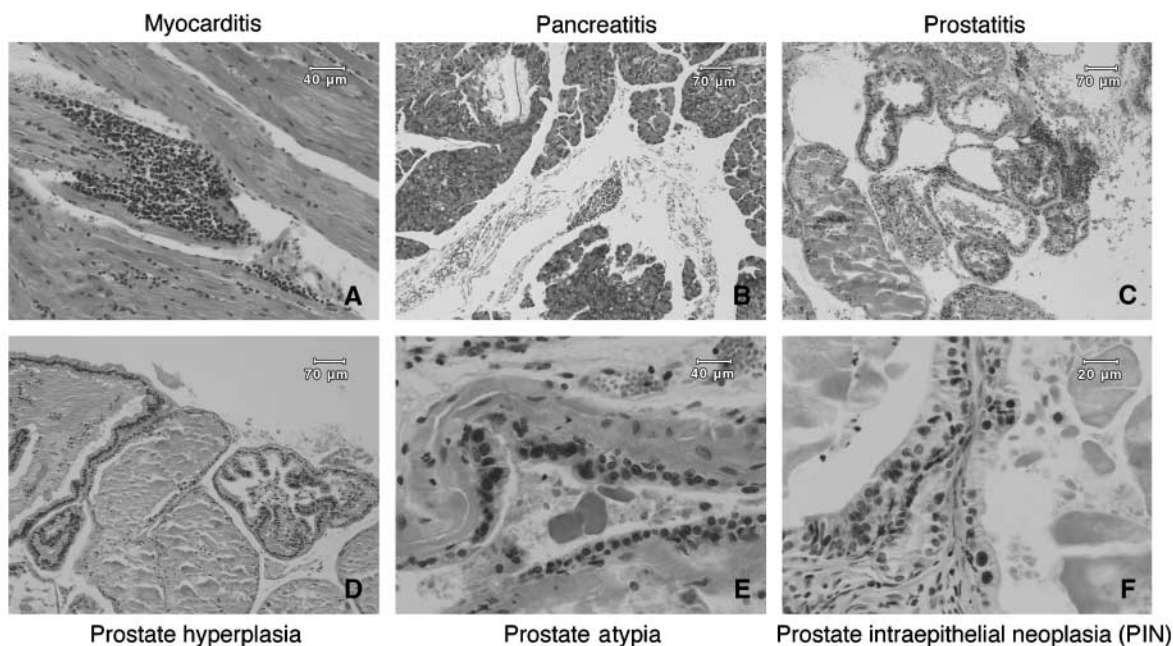**Table 1.** Inflammation and premalignant lesions in *Bin1* mosaic mice

Tissue and abnormality	Bin1 mosaic −/− (N = 19)	Bin1 mosaic +/− (N = 32)	Bin1+/+ (N = 12)
Heart			
Myocarditis	3/19 (16%)	6/32 (19%)	0/12 (0%)
Liver			
Fatty metamorphosis	3/19 (16%)	6/32 (19%)	5/12 (42%)
Adenoma	0/19 (0%)	2/32 (6%)	1/12 (8%)
Pancreas			
Pancreatitis	1/19 (5%)	2/32 (6%)	0/12 (0%)
Prostate			
Prostatitis	4/19 (21%)	6/32 (19%)	0/12 (0%)
Prostate hyperplasia	10/19 (53%)	23/32 (72%)	1/12 (8%)
Prostate atypia	4/19 (21%)	5/32 (16%)	0/12 (0%)
Prostate intraepithelial neoplasia	1/19 (5%)	1/32 (3%)	0/12 (0%)
Seminal vesicle			
Inflammation	6/19 (32%)	9/32 (28%)	3/12 (25%)

NOTE: Major organs were collected at necropsy from mice of 18 to 20 mo of age and processed for histologic examination.

reported previously (27). Our findings were extended in the Bin1 mosaic model, particularly in null mosaic females whose last litters were at an unusually old age of 17.3 ± 1.1 months (Supplementary Table S1). This striking effect suggested that *Bin1* negatively modified some aspect of reproductive physiology during aging.

Bin1 inhibits inflammation and premalignant lesions in the heart and prostate during aging. No effects of *Bin1* attenuation were seen in any mice through 1 year of age; however, we observed a markedly increased incidence of inflammatory conditions and/or premalignant lesions in more elderly animals (Table 1). By 18 to 20 months of age, 16% to 29% of mosaic mice displayed myocarditis, an inflammatory condition in the heart (Fig. 2A). Additionally, several mosaic mice displayed evidence of pancreatitis (inflammation of the pancreas; Fig. 2B). These conditions are rare in naïve laboratory mice and were not seen in any of the control animals examined. More dramatically, there was evidence of widespread inflammation and/or premalignant lesions in the prostates of mosaic mice (Fig. 2C–F). Prostatitis (inflammation of the prostate) was observed in ∼20% of mosaic mice but no animal in the control group. Hyperplasia was evident in 53% to 72% of the mosaic

Figure 2. Inflammation and premalignant lesions in *Bin1* mosaic mice at 18 to 20 mo of age. Representative histologies are shown.

mice in comparison to only a single case in the control group. Prostate atypia and prostate intraepithelial neoplasia, both frank premalignant lesions, were detected in 16% to 21% and ~4% of mosaic mice, respectively, but not in any control animal. These findings were specific to prostate insofar as we saw a similar incidence of seminal vesicle inflammation in each cohort (Table 1). Furthermore, in mosaic animals, we observed an opposite trend in the incidence of fatty metamorphosis of the liver, a lesion documented in both mosaic and control cohorts (Table 1). Together, these observations argued that *Bin1* acted to limit the development of inflammation and premalignant lesions during aging.

Bin1 inhibits the development of lung adenocarcinoma and hepatocarcinoma during aging. We previously noted a modest hyperplasia in lungs of Bin1KO/KO embryos harboring a complete gene knock-out (Supplementary Fig. S1). This phenotype was not seen in the Bin1 mosaic knock-out mice, which preserved sufficient Bin1 function to complete development and which lacked any apparent phenotype through ~1 year of age. In contrast, in older mice of 18 to 20 months of age, there was a striking increase in the incidence of lung tumors, with 47% of mosaic mice presenting with tumors at this time compared with a single case seen in the control group (Table 2 and Fig. 3A). This observation suggested that the hyperplasia in KO/KO embryonic lung may represent a premalignant lesion possibly controlled in the mosaic setting until older age. The lung tumors that arose were histopathologically defined as intrabronchial *in situ* papillary carcinoma (A.P. Soler, data not shown), establishing that they were of lung epithelial origin. Background issues that defeat the use of Bin1 antibodies in staining mouse tissues prevented us from performing an immunohistologic analysis of Bin1 in normal or tumor lung tissues; however, Northern and quantitative reverse transcription-PCR analyses confirmed a relative reduction in Bin1 RNA levels in tumors arising in mosaic animals compared with normal tissues (Supplementary Fig. S2). In human tissues where Bin1 antibodies are fully validated for immunohistochemical analysis (28), we were able to examine immunohistochemical status in lung and lung adenocarcinoma. In normal bronchial epithelia and stage I tumors (localized disease), we documented strong Bin1 expression, whereas in cases of stage II to IV lung adenocarcinoma reduced expression was apparent (Supplementary Fig. S3). The patterns of normal expression and immunohistochemical losses in tumors was reminiscent of that seen in other epithelial tumors such as breast and prostate tumors (13, 14, 28). Taken together, these findings were internally

consistent in suggesting a role for *Bin1* in the suppression of lung carcinoma during aging.

In mice of 18 to 20 months of age, we also observed a smaller but significant increase in the incidence of hepatocellular carcinoma (HCC), with 6% to 11% of mosaic mice but no control mice exhibiting tumors (Table 2 and Fig. 3B). As noted above, fatty metamorphosis of the liver was documented in all animals but was slightly reduced in mosaic animals (Table 2). Clinical studies indicate that this lesion can be a precursor to cirrhosis and HCC, but typically in association with alcohol abuse or obesity (29). Further studies may reveal greater insight into the relationship between *Bin1* ablation and the incidence of fatty metamorphosis as a possible precursor to HCC.

The effects of *Bin1* ablation on cancer incidence during aging were selective, insofar as mosaic and control mice displayed a relatively similar incidence of lymphoma, a cancer that arises commonly in old mice (Table 2). Taken together with the above findings, we concluded that *Bin1* acted as a negative modifier that suppresses hepatocarcinoma and lung adenocarcinoma during aging.

Bin1 inhibits colon carcinogenesis. We reasoned that a modifier effect of *Bin1* on spontaneous cancers arising in older mice might also be manifested in carcinogen-induced cancers in younger animals. To examine this possibility, we compared the response of mosaic and control animals to i.p. administration with DMH, a *ras*-activating carcinogen that induces gastrointestinal cancers. In the protocol used, weekly treatment with DMH induced mainly colon tumors. All animals in the mosaic group and all but one animal in the control group presented with colon tumors at the experimental endpoint of 27 weeks. However, invasive tumors were displayed in 33% of the mosaic mice but none of the control animals. Moreover, tumor multiplicity was greater, and mouse weight was reduced at the experimental endpoint, consistent with a more progressive status of tumors in the *Bin1* mosaic mice (Table 3 and Supplementary Fig. S4). Support for the clinical relevance of these observations were provided by the results of a pilot immunohistochemical study of Bin1 status in 30 cases of human colon carcinoma. In normal colonic epithelia, strong progressive staining of villus cells was observed, similar to that documented previously (28), whereas >50% of the carcinomas examined showed strongly reduced expression of Bin1 (Supplementary Fig. S5). Taken together, these observations reinforced and extended the conclusion that *Bin1* acts to suppress the development and/or progression of epithelial cancers of the colon, lung, and liver.

Table 2. Tumors arising in aging *Bin1* mosaic mice

Tissue	Bin1 mosaic −/− (*N* = 19)	Bin1 mosaic +/− (*N* = 32)	Bin1+/+ (*N* = 12)
Lung			
Adenocarcinoma	9/19 (47%)	15/32 (47%)	1/12 (8%)
Liver			
HCC	2/19 (11%)	2/32 (6%)	0/12 (0%)
Lymph node			
Lymphoma	2/19 (11%)	5/32 (16%)	1/12 (8%)

NOTE: Tumors were scored macroscopically in animals of 18 to 20 mo of age at necropsy and subsequently verified by histologic examination. If less than two events of an abnormality were scored in the mosaic cohort, they are not listed, based on a lack of significance; but for abnormalities noted in the table, all the events are noted for the corresponding control group.
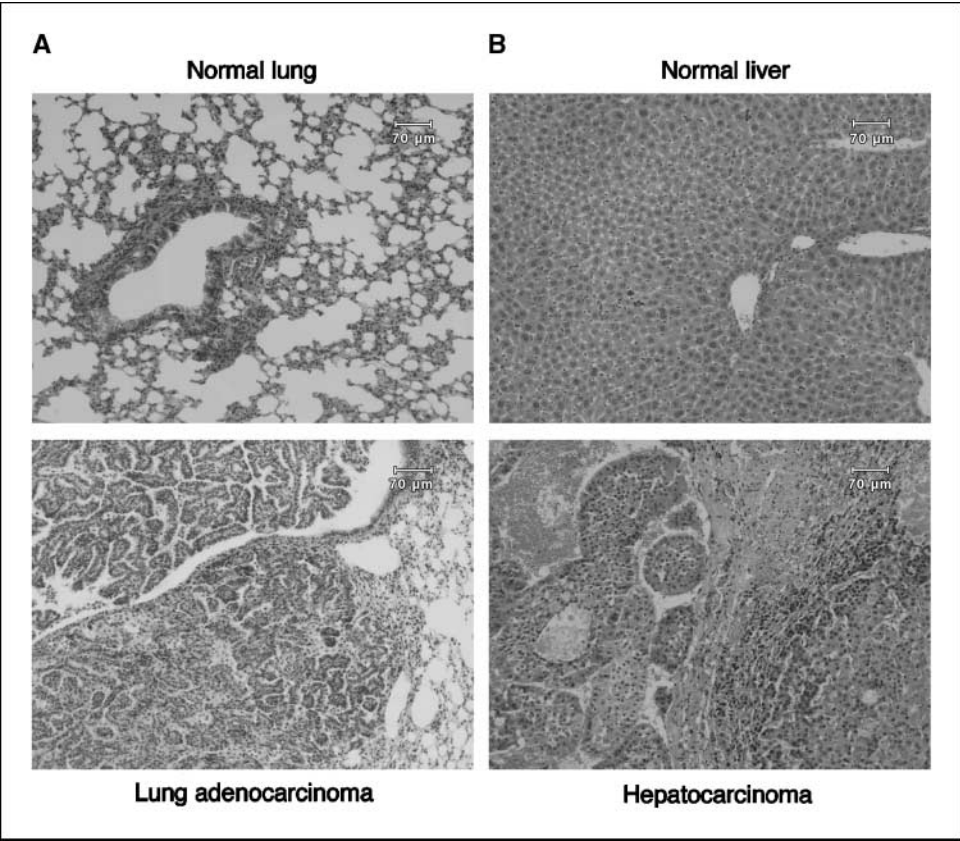
Figure 3. Lung and liver tumors in *Bin1* mosaic mice at 18 to 20 mo of age. Normal tissues from age-matched control animals are shown, along with histologies of representative tumors from mosaic animals.

Discussion

Genetic modifier pathways dramatically influence rates of cancer initiation and progression (30, 31). Using a genetically mosaic mouse model that bypasses perinatal lethality associated with systemic inactivation of *Bin1*, we have identified physiologic roles for this gene as a negative modifier of fecundity and cancer susceptibility during aging. Genetic mosaics have been used widely to study otherwise lethal mutations in *Drosophila* (32), but this approach has been used little in mice despite its ability to successfully rescue embryonic lethal phenotypes (33). Our strategy using a mutated loxP site proved advantageous in several ways. First, it eased production of the desired ES cell line by facilitating

selective *in vitro* deletion of the neo marker while leaving the targeted sequences intact (34). At this stage in strain construction, the desired partial recombination event in a "tri-lox" ES allele usually occurs rarely, sometimes preventing the ability to obtain the desired cell clone for chimera generation. Thus, introducing a point mutation into the 3′-most loxP site conferred a selective advantage to achieve Cre-mediated excision of the marker *in vitro* within a tri-lox allele without abolishing Cre-mediated excision of the floxed target sequences *in vivo*. Second, the presence of the mutated loxP site elevated the efficiency of mosaic animal generation by skewing the recombination pattern from complete recombinants occurring at the one-cell stage of development to

Table 3. *Bin1* ablation drives progression during colon carcinogenesis

Genotype	Tumor incidence	n*	Mouse weight at endpoint (g)	Early [†]	Noninvasive [‡]	Invasive [§]
Bin1+/+	9/10	1.8 ± 0.4	30.2 ± 1.7	1/9	8/9	0/9
Bin1 mosaic −/−	10/10	2.3 ± 0.5	26.5 ± 0.6	0/9	6/9	3/9

NOTE: Mice in mosaic and control groups (*n* = 10) were treated with DMH to induce colon tumors as described in the Materials and Methods. Tumors were harvested from euthanized animals at necropsy and processed for histology. Age at euthanasia was 7.8 to 8.0 mo for all DMH-treated mice. Representative examples of tumor histologies are presented in Supplementary Fig. S3.

*Number of tumors per colon scored (multiplicity).

[†]Submucosal tumors.

[‡]Mucosal tumors, no muscle invasion apparent.

[§]Muscle-invasive tumors.

mosaic recombinants occurring after oocyte division had begun. Lastly, using this strategy, we learned that delivering the *cre* allele through the father recombination occurs with much lower efficiency when than through the mother. Thus, we were able to develop breeding strategies to allow efficient generation of mosaic animals and non-recombinant control animals, despite the common presence of the EIIa transgene.

Although the systemic disruption of *Bin1* causes ventricular hypertrophic cardiomyopathy and perinatal lethality (21), mosaic animals readily survived to adulthood even in situations where there was a significant nullizygosity in all organs including the heart. This result indicates that the presence of a subset of wt cells in the animal is sufficient to compensate for the developmental defect associated with *Bin1* loss. However, with regard to its role as a suppressor gene, our findings suggested that *Bin1* may be haploinsufficient in its ability to fully limit the development of premalignant lesions and certain cancers during aging. This finding may explain why in human cancers, one usually see attenuations rather than homozygous deletions of *Bin1,* because partial losses may be sufficient to functionally abrogate its tumor suppressor activity.

We found that *Bin1* attenuation increased fecundity during aging, but at the cost of elevating age-associated inflammation and cancer. Recent studies suggest that *Bin1* helps coordinate normal stress responses, and that it supports mammary gland remodeling during pregnancy (16, 22, 35). These roles are compatible with a tumor suppressor function, but how they may relate to effects on the period of female fecundity during aging is not yet known. Some tumor suppressor genes exhibit antagonistic pleiotropy, supporting fitness early in life but at a later cost to aging that exerts little evolutionary impact because the deficits accrue after reproduction is complete (36). Because the benefits of increased fecundity seemed to accrue in *Bin1* mosaic mice before cancers were detected, it is uncertain whether *Bin1* fits this model. In any case, it is tempting to speculate that these disparate phenotypes may be linked by previously documented effects of *Bin1* loss on elevating expression of the enzyme indoleamine 2,3-dioxygenase (IDO), a potent regulator of T cell immunity (37). In cancer cells, IDO elevation caused by *Bin1* attenuation can drive tumoral immune escape and progression (17). In pregnancy, IDO elevation in the placenta limits T cell activation by foreign paternal antigens, stabilizing pregnancies by preventing conceptus rejection (38). In future work, it will be important to determine whether the two phenotypic manifestations associated with *Bin1* loss during aging in the mouse are causally related to dysregulation of IDO activity.

We noted an increased incidence of inflammation and/or premalignant lesions in the heart, pancreas, liver, and prostate of *Bin1* mosaic mice during aging. Myocarditis was an interesting phenotype given that systemic inactivation *Bin1* causes cardiomyopathy during development (21), and that the human *Bin1* gene maps to a susceptibility locus for the development of dilated cardiomyopathy (39). Our observations suggest that *Bin1* might modify disease in this setting by influencing cardiac inflammation during aging. In *Bin1* mosaic mice, we also observed a modest increase in the incidence of pancreatitis, a known risk factor for pancreatic cancer. More dramatically, aging mosaic mice displayed an increase in prostatitis and prostate hyperplasia and in the frank premalignant lesions of prostate atypia and intraepithelial neoplasia. These findings were particularly notable given the evidence that loss of heterozygosity and expression of *Bin1* occur

often in human cases of metastatic prostate cancer (14). Thus, by promoting inflammation, our findings suggest that *Bin1* attenuation might contribute to prostate tumorigenesis during aging or in settings where appropriate initiating lesion(s) are present.

We found that *Bin1* ablation greatly increased the incidence of lung adenocarcinoma during aging, with a lesser increase in HCC also evident. Tumor susceptibility varies widely among laboratory mouse strains, but lung and liver cancers occur rarely even in elderly mice. For example, with regard to lung tumors in strains relevant to this study, a lifetime incidence of lung tumors of 1% to 3% has been reported for C57BL/6 (Mouse Genome Informatics) and of 7.7% with a latency of ∼21 months has been reported for FVB-N (40). In our work, aged-matched Bin1+/+ control mice on the same mixed strain background exhibited only one case of lung cancer consistent with the published low rate of incidence. Further evidence that *Bin1* suppresses cancer was provided by the finding that *Bin1* mosaic mice were more susceptible to colon carcinogenesis, where *Bin1* ablation heightened the progression status of arising tumors. This finding corroborates and extends a recent study showing that mammary gland–specific deletion of *Bin1* is insufficient to initiate tumor formation, but sufficient to drive tumor progression (22). Here, we emphasize that the findings of both studies are consistent: breast cancers were not expected to arise in mosaic mice, because mammary gland–specific deletion of *Bin1* is insufficient for development of breast cancer during a similar 2-year period which is sufficient to yield development of lung and liver cancers in mosaic mice where *Bin1* was more widely inactivated. Consistent with previous findings (22), we found that mosaic mice exhibit a heightened progression status (more advanced histology) following the induction of 7,12-dimethylbenz(*a*)anthracene (DMBA)–induced breast cancers.[6] In summary, *Bin1* can limit cancer incidence or progression in different settings, perhaps related to the extent to which its role in limiting inflammation may be important at different stages of tumor development in those settings.

Because *Bin1* suppresses tumor formation in part by cell nonautonomous mechanisms that support immune surveillance (17), our findings prompt further study of the effects of tissue-specific ablation of *Bin1* in lung, liver, and colon epithelial cells. In humans, cancers of the lung, liver, colon, and prostate occur usually in elderly individuals. Given evidence of frequent immunohistochemical losses of Bin1 in human lung and colon cancers, paralleling related findings in breast and prostate cancers (1, 13, 14, 28, 41), the striking age-associated cancer phenotypes in the *Bin1* mosaic mice argues that such losses may be clinically relevant. In this regard, further studies of the mosaic model may permit new insights into cancer pathophysiologies associated with immune escape, inflammation, and aging.

Acknowledgments

References

1. Sakamuro D, Elliott K, Wechsler-Reya R, Prendergast GC. BIN1 is a novel MYC-interacting protein with features of a tumor suppressor. Nat Genet 1996;14:69–77.

2. Elliott K, Sakamuro D, Basu A, et al. Bin1 functionally interacts with Myc in cells and inhibits cell proliferation by multiple mechanisms. Oncogene 1999;18:3564–73.

3. Pineda-Lucena A, Ho CS, Mao DY, et al. A structure-based model of the c-Myc/Bin1 protein interaction shows alternative splicing of Bin1 and c-Myc phosphorylation are key binding determinants. J Mol Biol 2005; 351:182–94.

4. Deming SL, Nass SJ, Dickson RB, Trock BJ. C-myc amplification in breast cancer: a meta-analysis of its occurrence and prognostic relevance. Br J Cancer 2000; 83:1688–95.

5. Butler MH, David C, Ochoa G-C, et al. Amphiphysin II (SH3P9; BIN1), a member of the amphiphysin/RVS family, is concentrated in the cortical cytomatrix of axon initial segments and nodes of Ravier in brain and around T tubules in skeletal muscle. J Cell Biol 1997;137:1355–67.

6. Ramjaun AR, Micheva KD, Bouchelet I, McPherson PS. Identification and characterization of a nerve terminal-enriched amphiphysin isoform. J Biol Chem 1997;272:16700–6.

7. Tsutsui K, Maeda Y, Tsutsui K, Seki S, Tokunaga A. cDNA cloning of a novel amphiphysin isoform and tissue-specific expression of its multiple splice variants. Biochem Biophys Res Commun 1997;236:178–83.

8. Wechsler-Reya R, Sakamuro D, Zhang J, Duhadaway J, Prendergast GC. Structural analysis of the human BIN1 gene: evidence for tissue-specific transcriptional regulation and alternate RNA splicing. J Biol Chem 1997;272:31453–8.

9. Ren G, Vajjhala P, Lee JS, Winsor B, Munn AL. The BAR domain proteins: molding membranes in fission, fusion, and phagy. Microbiol Mol Biol Rev 2006;70:37–120.

10. Miaczynska M, Christoforidis S, Giner A, et al. APPL proteins link Rab5 to nuclear signal transduction via an endosomal compartment. Cell 2004;116:445–56.

11. Elliott K, Ge K, Du W, Prendergast GC. The c-Myc–interacting adapter protein Bin1 activates a caspase-independent cell death program. Oncogene 2000;19:4669–84.

12. Ge K, DuHadaway J, Du W, Herlyn M, Rodeck U, Prendergast GC. Mechanism for elimination of a tumor suppressor: aberrant splicing of a brain-specific exon causes loss of function of Bin1 in melanoma. Proc Natl Acad Sci U S A 1999;96:9689–94.

13. Ge K, DuHadaway J, Sakamuro D, Wechsler-Reya R, Reynolds C, Prendergast GC. Losses of the tumor suppressor Bin1 in breast carcinoma are frequent and reflect deficits in a programmed cell death capacity. Int J Cancer 2000;85:376–83.

14. Ge K, Minhas F, DuHadaway J, et al. Loss of heterozygosity and tumor suppressor activity of Bin1 in prostate carcinoma. Int J Cancer 2000;86:155–61.

15. DuHadaway JB, Sakamuro D, Ewert DL, Prendergast GC. Bin1 mediates apoptosis by c-Myc in transformed primary cells. Cancer Res 2001;16:3151–6.

16. Muller AJ, DuHadaway JB, Donover PS, Sutanto-Ward E, Prendergast GC. Targeted deletion of the suppressor gene Bin1/amphiphysin 2 enhances the malignant character of transformed cells. Cancer Biol Ther 2004; 3:1236–42.

17. Muller AJ, DuHadaway JB, Sutanto-Ward E, Donover PS, Prendergast GC. Inhibition of indoleamine 2,3-dioxygenase, an immunomodulatory target of the tumor suppressor gene Bin1, potentiates cancer chemotherapy. Nat Med 2005;11:312–9.

18. Tajiri T, Liu X, Thompson PM, et al. Expression of a MYCN-interacting isoform of the tumor suppressor BIN1 is reduced in neuroblastomas with unfavorable biological features. Clin Cancer Res 2003;9:3345–55.

19. Xu Q, Lee C. Discovery of novel splice forms and functional analysis of cancer-specific alternative splicing in human expressed sequences. Nucleic Acids Res 2003; 31:5635–43.

20. Karni R, de Stanchina E, Lowe SW, Sinha R, Mu D, Krainer AR. The gene encoding the splicing factor SF2/ASF is a proto-oncogene. Nat Struct Mol Biol 2007;14:185–93.

21. Muller AJ, Baker JF, DuHadaway JB, et al. Targeted disruption of the murine Bin1/amphiphysin II gene does not disable endocytosis but results in embryonic cardiomyopathy with aberrant myofibril formation. Mol Cell Biol 2003;23:4295–306.

22. Chang MY, Boulden J, Sutanto-Ward E, et al. Bin1 ablation in mammary gland delays tissue remodeling and drives cancer progression. Cancer Res 2007;67:100–7.

23. Mao NC, Steingrimsson E, DuHadaway J, et al. The murine Bin1 gene functions early in myogenesis and defines a new region of synteny between mouse chromosome 18 and human chromosome 2. Genomics 1999;56:51–8.

24. Jackson PE, Cooper DP, O'Connor PJ, Povey AC. The relationship between 1,2-dimethylhydrazine dose and the induction of colon tumours: tumour development in female SWR mice does not require a K-ras mutational event. Carcinogenesis 1999;20:509–13.

25. Lakso M, Pichel JG, Gorman JR, et al. Efficient *in vivo* manipulation of mouse genomic sequences at the zygote stage. Proc Natl Acad Sci U S A 1996;93:5860–5.

26. Dooley TP, Miranda M, Jones NC, DePamphilis ML. Transactivation of the adenovirus EIIa promoter in the absence of adenovirus E1A protein is restricted to mouse oocytes and preimplantation embryos. Development 1989;107:945–56.

27. Lerner SP, Anderson CP, Walford RL, Finch CE. Genotypic influences on reproducing aging of inbred female mice: effects of H-2 and non–H2 alleles. Biol Reprod 1988;38:1035–43.

28. DuHadaway JB, Lynch FJ, Brisbay S, et al. Immuno-histochemical analysis of Bin1/amphiphysin II in human tissues: diverse sites of nuclear expression and losses in prostate cancer. J Cell Biochem 2003;88:635–42.

29. Reddy JK, Rao MS. Lipid metabolism and liver inflammation. II. Fatty liver disease and fatty acid oxidation. Am J Physiol Gastrointest Liver Physiol 2006; 290:G852–8.

30. Jackson-Grusby L. Modeling cancer in mice. Oncogene 2002;21:5504–14.

31. Dragani TA. 10 years of mouse cancer modifier loci: human relevance. Cancer Res 2003;63:3011–8.

32. Perrimon N. Creating mosaics in *Drosophila*. Int J Dev Biol 1998;42:243–7.

33. Betz UA, Vosshenrich CA, Rajewsky K, Muller W. Bypass of lethality with mosaic mice generated by Cre-loxP–mediated recombination. Curr Biol 1996;6:1307–16.

34. Kwan KM. Conditional alleles in mice: practical considerations for tissue-specific knockouts. Genesis 2002;32:49–62.

35. Routhier EL, Donover PS, Prendergast GC. hob1+, the homolog of Bin1 in fission yeast, is dispensable for endocytosis but required for the response to starvation or genotoxic stress. Oncogene 2003;22:637–48.

36. Campisi J. Cancer and ageing: rival demons? Nat Rev Cancer 2003;3:339–49.

37. Munn DH, Mellor AL. Indoleamine 2,3-dioxygenase and tumor-induced tolerance. J Clin Invest 2007;117:1147–54.

38. Munn DH, Zhou M, Attwood JT, et al. Prevention of allogeneic fetal rejection by tryptophan catabolism. Science 1998;281:1191–3.

39. Jung M, Poepping I, Perrot A, et al. Investigation of a family with autosomal dominant dilated cardiomyopathy defines a novel locus on chromosome 2q14-22. Am J Hum Genet 1999;65:1068–77.

40. Zhou H, Liu L, Lee K, et al. Lung tumorigenesis associated with erb-B-2 and erb-B-3 overexpression in human erb-B-3 transgenic mice is enhanced by methylnitrosourea. Oncogene 2002;21:8732–40.

41. Ghaneie A, Zemba-Palko V, Itoh H, et al. Bin1 attenuation in breast cancer is correlated to nodal metastasis and reduced survival. Cancer Biol Ther 2007;6:192–4.

npg

ORIGINAL ARTICLE

A key *in vivo* antitumor mechanism of action of natural product-based brassinins is inhibition of indoleamine 2,3-dioxygenase

T Banerjee[1,10], JB DuHadaway[2,10], P Gaspari[3], E Sutanto-Ward[2], DH Munn[4,5], AL Mellor[4,6], WP Malachowski[3], GC Prendergast[2,7,8] and AJ Muller[2,8,9]

[1]NewLink Genetics Corporation, Ames, IA, USA; [2]Lankenau Institute for Medical Research, Wynnewood, PA, USA; [3]Department of Chemistry, Bryn Mawr College, Bryn Mawr, PA, USA; [4]Immunotherapy Center, Medical College of Georgia, Augusta, GA, USA; [5]Department of Pediatrics, Medical College of Georgia, Augusta, GA, USA; [6]Department of Medicine, Medical College of Georgia, Augusta, GA, USA; [7]Department of Pathology, Anatomy, and Cell Biology, Jefferson Medical College, Thomas Jefferson University, Philadelphia, PA, USA; [8]Kimmel Cancer Center, Thomas Jefferson University, Philadelphia, PA, USA and [9]Department of Microbiology and Immunology, Jefferson Medical College, Thomas Jefferson University, Philadelphia, PA, USA

Agents that interfere with tumoral immune tolerance may be useful to prevent or treat cancer. Brassinin is a phytoalexin, a class of natural products derived from plants that includes the widely known compound resveratrol. Brassinin has been demonstrated to have chemopreventive activity in preclinical models but the mechanisms underlying its anticancer properties are unknown. Here, we show that brassinin and a synthetic derivative 5-bromo-brassinin (5-Br-brassinin) are bioavailable inhibitors of indoleamine 2,3-dioxygenase (IDO), a pro-toleragenic enzyme that drives immune escape in cancer. Like other known IDO inhibitors, both of these compounds combined with chemotherapy to elicit regression of autochthonous mammary gland tumors in MMTV-*Neu* mice. Furthermore, growth of highly aggressive melanoma isograft tumors was suppressed by single agent treatment with 5-Br-brassinin. This response to treatment was lost in athymic mice, indicating a requirement for active host T-cell immunity, and in IDO-null knockout mice, providing direct genetic evidence that IDO inhibition is essential to the antitumor mechanism of action of 5-Br-brassinin. The natural product brassinin thus provides the structural basis for a new class of compounds with *in vivo* anticancer activity that is mediated through the inhibition of IDO.
Oncogene advance online publication, 19 November 2007; doi:10.1038/sj.onc.1210939

Keywords: IDO; *INDO*; tumoral immune tolerance; immunotherapy; targeted therapeutics; tryptophan

Introduction

Indoleamine 2,3-dioxygenase (IDO) is a monomeric, heme-containing enzyme that catabolizes the essential amino acid tryptophan (Hayaishi *et al.*, 1984). Whereas a second liver-specific enzyme, tryptophan dioxygenase (TDO2), is responsible for maintaining tryptophan homeostasis, IDO has an immunomodulatory role that is mediated through effects of tryptophan catabolism on T cells (Mellor and Munn, 2004). An interferon-inducible enzyme, IDO is elevated at sites of inflammation and immune privilege. IDO was first established as an important pro-toleragenic enzyme in a seminal *in vivo* study that utilized the bioavailable IDO inhibitor 1-methyl-tryptophan (1MT) to elicit immune rejection of allogenic concepti during pregnancy (Munn *et al.*, 1998). Significantly, IDO plays a similar pro-toleragenic role in the pathophysiological context of tumors. The IDO enzyme was first identified, in part, through findings of elevated tryptophan catabolism in cancer patients that could not be ascribed to TDO2 (Hayaishi *et al.*, 1984) and recent reports have associated IDO elevation with less favorable outcomes in certain cancers (Okamoto *et al.*, 2005; Brandacher *et al.*, 2006; Ino *et al.*, 2006). Pharmacological intervention in tumoral immune escape is a novel concept for which IDO is a leading target (Muller and Scherle, 2006) based on preclinical evidence that small molecule inhibitors of IDO can effectively cooperate with chemotherapy to elicit regression of established tumors in mice (Muller *et al.*, 2005).

Plants produce a vast array of chemically complex compounds that have been a valuable source for the discovery of novel chemotherapeutic agents and currently there is particular interest in the development of botanicals for chemoprevention (Chemoprevention Working Group, 1999; Park and Pezzuto, 2002). Among the potentially active components identified, some of the most promising are phytoalexins. Resveratrol is perhaps the best known of this class of anti-microbial compounds, which are synthesized by plants in response to various stresses (Muller, 1958). Brassinin ([3-(*S*-methyl-dithiocarbamoyl)aminomethyl indole]), first isolated from Chinese cabbage inoculated with *Pseudomonas chichorii* (Takasugi *et al.*, 1986, 1988), belongs to a group of sulfur-containing, tryptophan-derived phytoalexins that are unique to crucifers (Mezencev *et al.*,

---

2003). Brassinin has been shown to inhibit the formation of carcinogen-induced preneoplastic lesions in mouse mammary gland organ culture and to suppress papilloma formation in the classical two-stage DMBA/TPA skin carcinogenesis model (Mehta et al., 1995). Recently, we have shown that brassinin is a micromolar inhibitor of the IDO enzyme and have evaluated the IDO inhibitory activity of a large set of derivatized variations of the brassinin core structure in order to investigate structure–activity relationships (Gaspari et al., 2006). In this study, we provide direct in vivo evidence that brassinin-based compounds can act as anticancer agents through their ability to inhibit IDO.

Results

IDO has wide substrate specificity for compounds containing an indole structure (Malachowski et al., 2005). Evaluating commercially available indole-containing compounds, we have identified several molecules with IDO inhibitory potencies of less than $100 \mu M$ (Figure 1), including a methylthiohydantoin derivative of tryptophan that has been described previously (Muller et al., 2005). Of particular interest among these molecules were two natural products with chemopreventive properties—3,3'-diindolylmethane, the primary metabolic product of indole-3-carbinol and brassinin (Figure 1). Based on its superior potency, specificity and bioavailability, we focused work in this study on brassinin and a synthetic derivative, 5-bromo-brassinin (5-Br-brassinin; Figure 1).

Brassinin and 5-Br-brassinin both behaved as competitive inhibitors of the tryptophan catabolic activity of recombinant human IDO enzyme in a cell-free enzyme assay, with K_i values (Table 1) below the $35 \mu M$ value obtained for the widely used IDO inhibitor D,L-1MT (Hou et al., 2007). The potency of 1MT is substantially attenuated in cell-based assays, with EC_{50} values in the $100 \mu M$ range (Hou et al., 2007), but this was not a significant issue for the two brassinin compounds. Tryptophan catabolism by both human and mouse IDO expressed ectopically in the COS-1 cell line was inhibited by both compounds with EC_{50} values in the $25–35 \mu M$ range (Table 1). In this same cell-based assay, activity of recombinant human tryptophan 2,3-dioxygenase (TDO2), the hepatic enzyme which catabolizes tryptophan in the same manner as IDO, was not significantly affected at concentrations of either compound up to $100 \mu M$ (data not shown). Cell viability profiles for both COS-1 cells, used to perform the cell-based enzyme assay, and B16-F10 mouse melanoma-derived cells, used in tumor experiments described below, indicated no evidence of cytotoxicity or growth suppression associated with exposure up to $100 \mu M$ of brassinin or 5-Br-brassinin (Figure 2).

Serum analysis from mice indicated that both brassinin and 5-Br-brassinin are orally bioavailable. When formulated for oral gavage in 50% hydroxypropyl β-cyclodextran (HPBCD), an excipient that can improve drug delivery (Davis and Brewster, 2004), 5-Br-brassinin was found to have a superior pharmacologic profile (Figure 3), exhibiting sustained levels in serum for up to 8 h while brassinin was essentially cleared by 3 h.

In mouse mammary tumor virus (MMTV)-Neu transgenic mice, HER2/Neu expression controlled by the MMTV promoter drives the development of focal mammary gland carcinomas (Guy et al., 1992) which histopathologically resemble human ductal carcinoma in situ (Cardiff and Wellings, 1999). We have previously reported that continuous administration of IDO inhibitory compounds, delivered by subcutaneously


Reference Compound	Structure
1-Methyl-DL-Tryptophan	

New Compounds	Structure
MTH-DL-Tryptophan	
Indole-3-Carbinol	
3-3' Diindoylmethane	
Brassinin	
5-Bromo-Brassinin	

Figure 1 Indole-containing natural products and derivatives that scored positive in a screen for IDO inhibitors.

Table 1 IDO inhibitory activity in cell-free and cell-based enzyme assays

Compound	$K_i\ (\mu M)$[a] (human)	$EC_{50}\ (\mu M)$[b] (human)	$EC_{50}\ (\mu M)$[b] (mouse)
Brassinin	27.9	37.9	31.1
5-Br-Brassinin	24.5	24.0	26.1

Abbreviations: 5-Br-Brassinin, 5-bromo-brassinin; IDO, indoleamine 2,3-dioxygenase. [a]K_i values were determined by global nonlinear regression analysis of enzyme kinetic data obtained using purified recombinant human his$_6$-IDO. [b]EC_{50} values for inhibition of both human and mouse IDO enzymes expressed ectopically in COS-1 cells were determined by nonlinear regression analysis of compound dose escalation data.
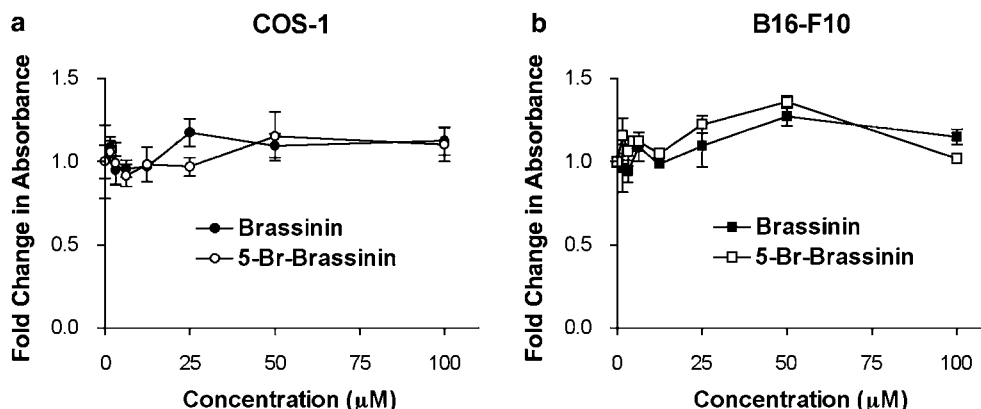
Figure 2 Brassinin and 5-bromo-brassinin (5-Br-brassinin) do not significantly compromise cell viability at concentrations sufficient to inhibit IDO. (**a**) COS-1 and (**b**) B16-F10 cells were exposed for 72 h to a range of compound concentrations up to 100 μM after which total cellular protein in each well was assessed using the sulforhodamine B assay. The fold change in absorbance is indicative of the percent viable cells relative to untreated controls that were present following treatment. Each assay was performed in triplicate and graphed as the mean ± s.d.
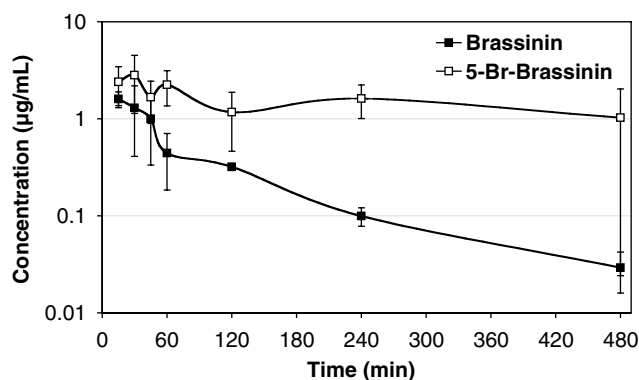
Pharmacokinetic Parameters		Brassinin	5-Br-Brassinin
C_{max}	μg/mL	1.6	2.8
T_{max}	min	15.0	30.0
$T_{1/2}$	min	105.1	526.3
AUC_∞	μg-min/mL	129.7	1485

C_{max} is the maximum observed concentration
T_{max} is the time at maximum observed concentration
$T_{1/2}$ is the time for concentration to diminish by one-half in the elimination phase
AUC_∞ is the total area under the curve calculated using observed data points combined with an extrapolated value

Figure 3 5-Bromo-brassinin (5-Br-brassinin) is cleared less rapidly from serum than brassinin. HPLC-based pharmacokinetic analysis was performed following administration of a single bolus dose of either brassinin or 5-Br-brassinin by oral gavage at 400 mg kg⁻¹ in 50% hydroxypropyl β-cyclodextran excipient. Three mice were evaluated per time point for serum levels of the administered compound and the results graphed as the mean ± s.d. Pharmacokinetic parameters shown in the accompanying table were calculated from the data by using PK Solutions 2.0 software (Summit Research Services, Montrose, CO, USA).

implanted time-release pellets, can cooperate with paclitaxel as well as other cytotoxic chemotherapeutic agents to elicit regression of established mammary gland tumors in this very stringent autochthonous tumor model (Muller et al., 2005). More recently, we have demonstrated that bolus oral delivery of the IDO inhibitor 1MT on a twice a day (b.i.d.) schedule can also cooperate with paclitaxel to regress these tumors

(Hou et al., 2007). Based on their oral bioavailability in HPBCD, we evaluated brassinin and 5-Br-brassinin administered by oral bolus dosing at 400 mg kg⁻¹ twice a day, a treatment regimen that likely approached the maximum tolerated dose as the mice exhibited clear evidence of compound-related toxicity which manifested outwardly as the development of a scruffy appearance. Delivered in this manner, neither compound alone demonstrated significant single agent activity. Brassinin in combination with paclitaxel did produce tumor regressions; however, the effect was not of sufficient magnitude to infer a statistically significant benefit relative to paclitaxel treatment alone with the number of tumors evaluated (Figure 4b). Rapid clearance of this compound following bolus dose delivery may account for this rather limited response relative to our previous experience with other IDO inhibitory compounds (Muller et al., 2005). In contrast, the more pharmacologically stable compound 5-Br-brassinin in combination with paclitaxel did produce an effect that was significantly better than paclitaxel treatment alone (Figure 4b). Collectively, these data are consistent with the conclusion that these brassinin-based compounds are able to target IDO effectively in vivo and add to the number of structurally distinct compounds with IDO inhibitory activity that can cooperate with the cytotoxic chemotherapeutic drug paclitaxel to regress autochthonous mammary carcinomas in this mouse breast cancer model.

To directly test the antitumor mechanism of action of the brassinin compounds in vivo, we have conducted studies using B16-F10 melanoma isografts which do not express IDO directly in the tumor but rather accumulate IDO-expressing, toleragenic plasmacytoid DCs in the tumor draining lymph node (Munn et al., 2004). The IDO inhibitor 1MT, although lacking significant single agent activity, cooperatively suppressed growth of B16-F10 tumors in combination with chemotherapeutic agents or tumor irradiation (Hou et al., 2007), consistent with IDO-expression in host stromal cells being the
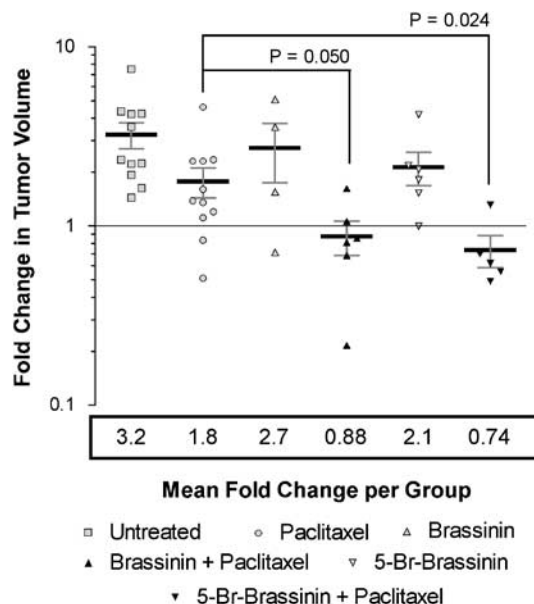
Figure 4 Brassinin and 5-bromo-brassinin (5-Br-brassinin) combine with paclitaxel chemotherapy to regress established breast tumors. Parous MMTV-*Neu* mice with 0.5–1.0 cm mammary gland tumors were randomly enrolled for 2-week treatment studies. Tumor volume determinations were made at the beginning and end of the treatment period. Cohorts receiving brassinin or 5-Br-brassinin were administered compound p.o. at $400 \, mg \, kg^{-1}$ b.i.d. in 50% hydroxypropyl β-cyclodextran for 5 consecutive days during the first week of treatment. Paclitaxel was administered to the indicated cohorts i.v. at $13.3 \, mg \, kg^{-1}$ q.i.d. $3 \times$ per week over the entire course of the 2-week treatment period. Each point represents the fold change in volume for an individual tumor with the mean ± s.e.m. indicated for each group. *P*-values for the differences in outcome between groups receiving paclitaxel and combination treatments were determined using a nonparametric, two-tailed Mann–Whitney test.

relevant target in this tumor model. We confirmed that IDO expression was undetectable in the B16-F10 cell line (Figure 5a). Neither the D nor L isomer of 1MT produced significant growth inhibition when administered as single agents and a similar outcome was obtained with brassinin (data not shown). On the other hand, 5-Br-brassinin treatment produced significant suppression of B16-F10 tumor outgrowth (Figure 5b). This effect of 5-Br-brassinin treatment on tumor outgrowth was not evident in athymic nude mice (Figure 5c), indicating that its mechanism of action requires T cell-based immunity and is not mediated through a direct cytotoxic effect on the tumor. Because B16-F10 tumors do not express any detectable IDO, such that the stromal compartment is the only source of IDO activity (Munn *et al.*, 2004), it was possible also to directly test the relevance of IDO as a target by performing the experiment in genetically modified, syngeneic mice in which both alleles of the *Indo* gene were functionally disrupted (IDO-null). In the context of the IDO-null host, 5-Br-brassinin had no impact on tumor growth (Figure 5d). The results of this experiment, therefore, genetically define IDO as a therapeutically essential molecular target of 5-Br-brassinin in this *in vivo* tumor model.

Discussion

In this study, we have shown that, as with other IDO inhibitory compounds, brassinins can be delivered *in vivo* to leverage the effectiveness of chemotherapy against established tumors in an autochthonous mouse model of breast cancer. Moreover, we have directly demonstrated that the brassinin-based compound 5-Br-brassinin can suppress tumor outgrowth through a T cell-dependent mechanism that obligately involves IDO. Cruciferous vegetables have garnered a great deal of attention due to their anticancer properties (Murillo and Mehta, 2001), and brassinin is a constituent of crucifers with demonstrated anticancer activity in mouse tumor models. While a variety of possible molecular mechanisms have been proposed to explain this activity, none has been directly validated *in vivo*. In particular, brassinin is cited as an inducer of quinone reductase (QR) based on data from a mouse mammary gland organ culture model in which incubation with $220 \, \mu M$ brassinin for 3 days resulted in a fourfold increase in QR activity (Mehta *et al.*, 1995). QR is a phase II enzyme that detoxifies mutagenic carcinogens, and as an inducer of this enzyme, brassinin would be predicted to act as an 'anti-initiator'. However, the same study found that, in the two stage DMBA/TPA skin carcinogenesis model, brassinin acted instead as an 'anti-promoter' with no apparent impact on the initiation stage of carcinogenesis (Mehta *et al.*, 1995). Unlike QR, IDO is likely to affect the promotional stage of carcinogenesis and, indeed, TPA is a powerful proinflammatory contact-sensitizer that would be expected to substantially elevate levels of IFNγ, the principle cytokine inducer of IDO, in the draining lymph nodes (Thomson *et al.*, 1993).

The B16-F10 tumor isograft data reported here clearly indicate that inhibition of host IDO activity is essential for the single agent suppression of tumor outgrowth by 5-Br-brassinin. This degree of efficacy is rather remarkable when compared with other agents that target immune-based pathways. For example, the costimulatory molecule CTLA4 is a powerful antagonist of T-cell activation that may act, at least in part, by elevating IDO (Grohmann *et al.*, 2002). However, in the B16-F10 tumor model, CTLA4 monoclonal antibody blockade failed to elicit a single agent response, (although it produced significant autoimmunity), effecting tumor growth suppression only when administered in conjunction with a granulocyte-macrophage colony-stimulating factor transduced tumor cell vaccine (GVAX) (Quezada *et al.*, 2006).

Administration of brassinin, unlike 5-Br-brassinin, did not significantly impact B16-F10 tumor growth, perhaps simply reflecting inferior pharmacokinetics. However, since the IDO inhibitor 1MT also does not show single agent activity in the B16-F10 tumor model either, it is also possible that IDO inhibition may be necessary but not sufficient to account for the ability of 5-Br-brassinin to suppress B16-F10 tumor growth. Previously, 1MT has been shown to cooperate with various cytotoxic agents (cyclophosphamide, gemcitabine,
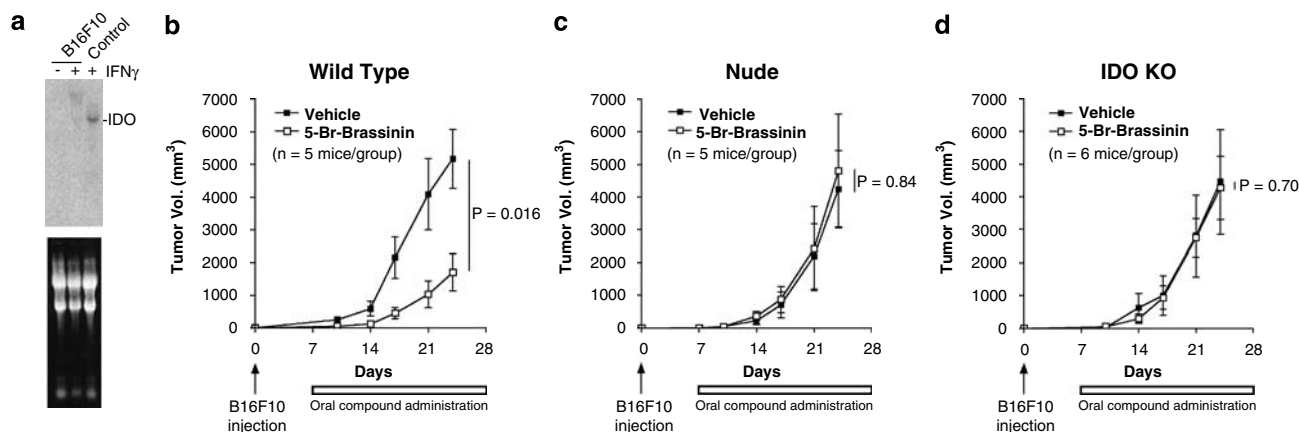
Figure 5 5-Bromo-brassinin (5-Br-brassinin) treatment elicits T cell-dependent suppression of B16-F10 tumors through inhibition of host indoleamine 2,3-dioxygenase (IDO). (**a**) Absence of detectable IDO expression in B16F10 cells. Northern blot analysis of total RNA from B16-F10 cells, untreated and following 24 h exposure to 100 ng ml^{-1} interferon-γ (IFNγ). Total RNA from 4T1 cells stimulated with IFNγ, which produces a modest elevation in IDO message level, was used as the positive control. (**b**) 5-Br-brassinin exhibits single agent activity to suppress the outgrowth of B16-F10 tumors. 5-Br-brassinin treatment was initiated 7 days following subcutaneous challenge of C57BL/6 mice with 1×10^5 B16-F10 melanoma-derived cells. Compound in 50% HPBCD was administered p.o. at 400 mg kg^{-1} b.i.d. 5 days a week until termination of the experiment. Caliper measurements of tumors were recorded biweekly. The mean $\pm$ s.e.m. from these measurements is plotted for each group. To compare the two groups at the 4-week end point of the study, a nonparametric, two-tailed Mann–Whitney test was performed to generate the P-value shown. (**c**) Suppression of B16-F10 tumor outgrowth by 5-Br-brassinin is dependent on T-cell immunity. Athymic NCr-nu/nu mice were challenged with B16-F10 and treated with 5-Br-brassinin as in (**b**). (**d**) 5-Br-brassinin targets host IDO to suppress B16-F10 tumor outgrowth. IDO knockout mice were challenged with B16-F10 and treated with 5-Br-brassinin as in (**b**).

IR) to suppress B16-F10 tumor growth (Hou et al., 2007). Analogous to these agents, 5-Br-brassinin may have an intrinsic cytotoxic effect that enhances its antitumor activity. Although we observed no discernable impact of brassinin or 5-Br-brassinin at concentrations up to 100 μM on the viability of either B16-F10 or COS-1 cells, other groups have reported that at similar concentrations brassinin can reduce the number of viable cells in a 72 h assay by 25–50% relative to controls among different cancer cell lines tested including B16-F10 (Sabol et al., 2000; Pilatova et al., 2005; Csomos et al., 2006). While our finding that 5-Br-brassinin treatment had no significant impact on B16-F10 tumor growth in athymic nude mice clearly indicates that any direct cytotoxic effect that this compound may have is not sufficient to account for its antitumor activity in vivo, these data do not rule out that mild cytotoxicity might contribute to therapeutic efficacy. It will be important to further explore such mechanistic questions to fully understand how to best develop the antitumor mechanism of action associated with brassinin-based compounds.

A key finding of this study is that 5-Br-brassinin treatment substantially suppressed B16-F10 tumor growth in wild-type mice but not IDO-null mice. However, these data also apparently indicate that a complete absence of IDO in the host is irrelevant to tumor outgrowth since comparable growth rates were observed in IDO-null and wild-type mice in the absence of compound treatment. These results recapitulate observations made in pregnancy studies in which acute exposure to the IDO inhibitor 1MT resulted in immune rejection of allogeneic concepti while the viability of allogeneic concepti was normal in genetic knockout mice but was no longer affected by 1MT

treatment (Munn et al., 1998; Baban et al., 2004). One possible explanation given for these apparently dichotomous results is that compensatory mechanisms may come into play in the knockout mice (Baban et al., 2004). In the context of cancer, these data suggest that, while IDO may not be the only possible immune escape mechanism, when IDO is available to tumors they may preferentially become dependent on it for continued growth in what might be termed 'tolerance addiction'.

Because targeting tumoral immune tolerance is a unique approach to cancer treatment, the use of IDO inhibitors in combination with other types of agents may represent the best opportunity to simultaneously attack tumors on multiple fronts. Evidence from mouse tumor models already supports the possible use of IDO inhibitors with certain chemotherapeutic drugs (Muller et al., 2005; Hou et al., 2007) and it seems likely that IDO inhibitors will enhance cancer vaccines and other approaches that aim at stimulating immune effector function as well. IDO inhibitors might also be used to intervene earlier in the process of immune editing when the nascent tumor is not as plastic. For this sort of chemopreventive strategy, administration of IDO inhibitors through dietary uptake would be a particularly attractive means of delivery, and further study of the pharmacodynamic impact of cruciferous vegetable consumption on IDO activity should be pursued.

Materials and methods

Chemical compounds
Brassinin was synthesized as described (Gaspari et al., 2006). 5-Br-brassinin was synthesized by the Advanced Synthesis

Group (Newark, DE, USA). HPBCD was purchased from Cargill Inc. (Cedar Rapids, IA, USA).

Cell culture

COS-1 monkey cells and B16-F10 mouse melanoma cells (ATCC, Manassas, VA, USA) were cultured with Dulbecco's modified Eagle's medium (DMEM) (Invitrogen Corporation, Carlsbad, CA, USA) supplemented with 10% fetal bovine serum (FBS) (Hyclone, Logan, UT, USA) and 1% penicillin-streptomycin (Invitrogen) at 37 °C in 5% CO_2.

Mice

C57BL/6 and FVB-strain MMTV-*Neu* transgenic mice were obtained from the Jackson Laboratory. Athymic NCr-*nu/nu* (nude mice) were obtained from NCI-Frederick. IDO knock-out mice have previously been described (Baban *et al.*, 2004). Studies involving mice were approved by the institutional animal use committee of the Lankenau Institute for Medical Research.

IDO enzyme assays

The cell-free IDO enzyme assay was performed in a 96-well microtiter plate with active recombinant human his6-IDO enzyme purified by sequential chromatography over phospho-cellulose and Ni-NTA agarose columns from *E.coli* strain BL21DE3pLysS transformed with pet5Ahis6huIDO as described (Gaspari *et al.*, 2006). The reaction mixture for carrying out the enzyme assay contained 50 mM potassium phosphate buffer (pH 6.5), 40 mM ascorbic acid, 400 µg ml^{-1} catalase, 20 µM methylene blue. Enzyme activity was assessed for each IDO preparation and the amount of enzyme used in the assay was based on this determination. The substrate L-tryptophan (100 mM stock in 0.1 N HCl) was serially diluted from 200 to 25 µM. Inhibitors were dissolved in DMSO to make 100 mM stock solutions and assessed at final concentrations of 100 and 50 µM in a total reaction volume of 200 µl. Reactions were carried out at 37 °C for 60 min, stopped by adding 30% (w/v) trichloroacetic acid, and then heated at 65 °C for 15 min to convert kynurenine to *N*-formyl-kynurenine. Plates were then spun at 6000 g for 5 min, 100 µl supernatant from each well was transferred to a new 96-well plate and mixed with 2% (w/v) *p*-dimethyl benzaldehyde (Sigma-Aldrich, St Louis, MO, USA) in acetic acid. The yellow color generated from the reaction with *N*-formyl-kynurenine was quantitated at 490 nm using a Synergy HT microtiter plate reader (Bio-Tek, Winnooski, VT, USA). The data were analysed by using Prism 4 software (Graph Pad software, Inc., San Diego, CA, USA).

Cellular activity of selected compounds was assessed against both the human and mouse IDO enzymes transiently expressed in COS-1 monkey cells in a 96-well assay as described (Muller *et al.*, 2005). COS-1 cells at 2.5×10^4 cells per well were transfected overnight with pcDNA3.1-based expression plasmids in Opti-MEM I media (Invitrogen) using polyethylenei-mine (Sigma-Aldrich), replaced the next day with standard growth medium (DMEM supplemented with 10% FBS and antibiotics). The following day, compounds solubilized in DMSO were serially diluted into plate wells (final DMSO concentration was no more than 1:1000). Plates were sealed in plastic wrap and incubated 16 h at 37 °C in a humified CO_2 incubator. Reactions were terminated by withdrawing 140 µl media per well and mixing thoroughly into 10 µl 26% trichloroacetic acid (TCA) in wells of a new plate. Stopped reactions were heated at 65 °C for 15 min to convert kynurenine to *N*-formyl-kynurenine, which was processed

and quantitated as above. The data were analysed by using Prism 4 software.

In vitro cytotoxicity assay

Compound cytotoxicity was assessed using the sulforhodamine B (SRB) viable cell assay (Skehan *et al.*, 1990). Cells were seeded into 96-well tissue culture plates at densities (2000 cells per well) which allowed untreated cells to reach a nearly confluent state after 4 days. Cells were treated with serial dilutions of brassinin and its 5-Br analogue 24 h after seeding. The SRB cytotoxicity assay was performed following 72 h of compound exposure. Cells were fixed with 50% trichloroacetic acid and stained with 0.4% (w/v) SRB (Sigma-Aldrich) dissolved in 1% acetic acid. Unbound dye was removed by four washes with 1% acetic acid, and protein bound dye was extracted with 10 mM unbuffered Tris base (pH 10.5) for 5 min. Optical density was read at 570 nm using a Synergy HT microtiter plate reader.

Pharmacokinetic studies

MMTV-*Neu* mice were orally gavaged with 0.1 ml of a sonicated suspension of the desired compound (400 mg kg^{-1}) in 50% HPBCD. Blood was collected at different intervals and serum prepared using the Stat Sampler Kit (Statspin, Norwood, MA, USA) following the vendor's instructions. Serum samples were stored at −80 °C. Samples were processed by extracting twice with 300 µl of *tert*-butyl methyl ether (Sigma-Aldrich) per 100 µl of serum. Organic and aqueous phases were separated by centrifugation (2800 g for 10 min), transferred to a fresh microfuge tube, and evaporated to dryness in the presence of 15 µl DMSO. Extracted samples in DMSO were diluted to 110 µl with 1:4 mixture of acetonitrile:-water and then analysed by high-pressure liquid chromato-graphy on a 250 × 4.5 mm Luna 5u C18 column (Phenomenex, Torrance, CA, USA). The mobile phase consisting of acetonitrile-water and solutes was eluted at a flow rate of 1.0 ml per minute in a 0–90% acetonitrile gradient for the first 7 min and in 90% acetonitrile for an additional 8 min. Columns were re-equilibrated with water for 20 min between samples. Serially diluted solutions of brassinin and 5-Br brassinin in 1:4 acetonitrile:water served as standards. The analyte was detected by UV detector at 278 nm and the peak area was quantified using Windaq software (DataQ Instrument, Akron, OH, USA).

Tumor formation and drug response

For autochthonous mammary gland tumor treatment studies, parous, FVB-strain MMTV-*Neu* mice expressing the wild-type form of the rat *HER2/Neu* proto-oncogene were used as described (Muller *et al.*, 2005). When subjected to two rounds of pregnancy and lactation, the incidence of palpable tumors in this model is ∼80% by 7 months of age and increases to nearly 95% by 8 months. Tumor-bearing animals were enrolled randomly in control and experimental groups when tumors reached 0.5–1.0 cm in diameter for 2-week treatment response studies. Brassinin compounds were delivered for the first five consecutive days in 50% HPBCD excipient by oral gavage b.i.d. at 400 mg kg^{-1} while control animals received vehicle only. For those animals receiving paclitaxel, treatment was initiated concurrent with the administration of brassinin compounds and delivered by bolus i.v. injection into the tail vein on a schedule of 3 × per week. At the end of the 2-week treatment period, tumors were excised from euthanized animals and volumes were determined. Graphing and statis-tical analysis of the data was performed by using Prism 4 software.

B16-F10 melanoma-derived cell line isograft tumor challenge experiments were carried out as described (Hou et al., 2007). 1×10^5 cells were injected subcutaneously into mice at day 0 of the experiment, and treatment was initiated at day 7 following initial tumor cell engraftment. Tumor growth was monitored by performing caliper measurements of orthogonal diameters and the estimated tumor volume was calculated based on the formula for determining a prolapsed elliptoid ($d^2 \times l/0.52$) where d is the shorter of the two orthogonal measurements. Graphing and statistical analysis of the data was performed by using Prism 4 software.

References

Baban B, Chandler P, McCool D, Marshall B, Munn DH, Mellor AL. (2004). Indoleamine 2,3-dioxygenase expression is restricted to fetal trophoblast giant cells during murine gestation and is maternal genome specific. J Reprod Immunol 61: 67–77.

Brandacher G, Perathoner A, Ladurner R, Schneeberger S, Obrist P, Winkler C et al. (2006). Prognostic value of indoleamine 2,3-dioxygenase expression in colorectal cancer: effect on tumor-infiltrating T cells. Clin Cancer Res 12: 1144–1151.

Cardiff RD, Wellings SR. (1999). The comparative pathology of human and mouse mammary glands. J Mammary Gland Biol Neoplasia 4: 105–122.

Chemoprevention Working Group (1999). Prevention of cancer in the next millennium: Report of the Chemoprevention Working Group to the American Association for Cancer Research. Cancer Res 59: 4743–4758.

Csomos P, Zupko I, Rethy B, Fodor L, Falkay G, Bernath G. (2006). Isobrassinin and its analogues: novel types of antiproliferative agents. Bioorg Med Chem Lett 16: 6273–6276.

Davis ME, Brewster ME. (2004). Cyclodextrin-based pharmaceutics: past, present and future. Nat Rev Drug Discov 3: 1023–1035.

Gaspari P, Banerjee T, Malachowski WP, Muller AJ, Prendergast GC, Duhadaway J et al. (2006). Structure–activity study of brassinin derivatives as indoleamine 2,3-dioxygenase inhibitors. J Med Chem 49: 684–692.

Grohmann U, Orabona C, Fallarino F, Vacca C, Calcinaro F, Falorni A et al. (2002). CTLA-4-Ig regulates tryptophan catabolism in vivo. Nat Immunol 3: 1097–1101.

Guy CT, Webster MA, Schaller M, Parsons TJ, Cardiff RD, Muller WJ. (1992). Expression of the neu protooncogene in the mammary epithelium of transgenic mice induces metastatic disease. Proc Natl Acad Sci USA 89: 10578–10582.

Hayaishi O, Ryotaro Y, Takikawa O, Yasui H. (1984). Indoleamine-dioxygenase—a possible biological function. Progress in Tryptophan and Serotonin Research. Walter De Gruyter and Co.: Berlin. pp 33–42.

Hou DY, Muller AJ, Sharma MD, DuHadaway J, Banerjee T, Johnson M et al. (2007). Inhibition of indoleamine 2,3-dioxygenase in dendritic cells by stereoisomers of 1-methyl-tryptophan correlates with antitumor responses. Cancer Res 67: 792–801.

Ino K, Yoshida N, Kajiyama H, Shibata K, Yamamoto E, Kidokoro K et al. (2006). Indoleamine 2,3-dioxygenase is a novel prognostic indicator for endometrial cancer. Br J Cancer 95: 1555–1561.

Malachowski WP, Metz R, Prendergast GC, Muller AJ. (2005). A new cancer immunosuppression target: indoleamine 2,3-dioxygenase (IDO). A review of the IDO mechanism, inhibition and therapeutic applications. Drugs Fut 30: 897.

Mehta RG, Liu J, Constantinou A, Thomas CF, Hawthorne M, You M et al. (1995). Cancer chemopreventive activity of brassinin, a phytoalexin from cabbage. Carcinogenesis 16: 399–404.

Mellor AL, Munn DH. (2004). IDO expression by dendritic cells: tolerance and tryptophan catabolism. Nat Rev Immunol 4: 762–774.

Mezencev R, Mojzis J, Pilatova M, Kutschy P. (2003). Antiproliferative and cancer chemopreventive activity of phytoalexins: focus on indole phytoalexins from crucifers. Neoplasma 50: 239–245.

Muller AJ, Duhadaway JB, Donover PS, Sutanto-Ward E, Prendergast GC. (2005). Inhibition of indoleamine 2,3-dioxygenase, an immunoregulatory target of the cancer suppression gene Bin1, potentiates cancer chemotherapy. Nat Med 11: 312–319.

Muller AJ, Scherle PA. (2006). Targeting the mechanisms of tumoral immune tolerance with small-molecule inhibitors. Nat Rev Cancer 6: 613–625.

Muller KO. (1958). Studies on phytoalexins. Aust J Biol Sci 11: 275–330.

Munn DH, Sharma MD, Hou D, Baban B, Lee JR, Antonia SJ et al. (2004). Expression of indoleamine 2,3-dioxygenase by plasmacytoid dendritic cells in tumor-draining lymph nodes. J Clin Invest 114: 280–290.

Munn DH, Zhou M, Attwood JT, Bondarev I, Conway SJ, Marshall B et al. (1998). Prevention of allogeneic fetal rejection by tryptophan catabolism. Science 281: 1191–1193.

Murillo G, Mehta RG. (2001). Cruciferous vegetables and cancer prevention. Nutr Cancer 41: 17–28.

Okamoto A, Nikaido T, Ochiai K, Takakura S, Saito M, Aoki Y et al. (2005). Indoleamine 2,3-dioxygenase serves as a marker of poor prognosis in gene expression profiles of serous ovarian cancer cells. Clin Cancer Res 11: 6030–6039.

Park EJ, Pezzuto JM. (2002). Botanicals in cancer chemoprevention. Cancer Metastasis Rev 21: 231–255.

Pilatova M, Sarissky M, Kutschy P, Mirossay A, Mezencev R, Curillova Z et al. (2005). Cruciferous phytoalexins: antiproliferative effects in T-Jurkat leukemic cells. Leuk Res 29: 415–421.

Quezada SA, Peggs KS, Curran MA, Allison JP. (2006). CTLA4 blockade and GM-CSF combination immunotherapy alters the intratumor balance of effector and regulatory T cells. J Clin Invest 116: 1935–1945.

Sabol M, Kutschy P, Siegfried L, Mirossay A, Suchy M, Hrbkova H et al. (2000). Cytotoxic effect of cruciferous phytoalexins against murine L1210 leukemia. Biologia, Bratislava 55: 701–707.

Skehan P, Storeng R, Scudiero D, Monks A, McMahon J, Vistica D et al. (1990). New colorimetric cytotoxicity assay for anticancer-drug screening. J Natl Cancer Inst 82: 1107–1112.

Takasugi M, Monde K, Nobukatsu K, Shirata A. (1988). Novel sulfur-containing phytoalexins from the Chinese cabbage Brassica campestris L. ssp. pekinesis (Cruciferae). Bull Chem Soc Jpn 61: 285–289.

Takasugi M, Nobukatsu K, Shirata A. (1986). Isolation of three novel sulphur-containing phytoalexins from the Chinese cabbage Brassica campestris L. ssp. pekinesis (Cruciferae). J Chem Soc Chem Commun, 1077–1078.

Thomson JA, Troutt AB, Kelso A. (1993). Contact sensitization to oxazolone: involvement of both interferon-gamma and interleukin-4 in oxazolone-specific Ig and T-cell responses. Immunology 78: 185–192.

Differential targeting of tryptophan catabolism in ₂
tumors and in tumor-draining lymph nodes ₃
by stereoisomers of the IDO inhibitor ₄
1-methyl-tryptophan ₅

Alexander J. Muller [a,b,*], Richard Metz [a], George C. Prendergast [a,c] 6

[a] *Lankenau Institute for Medical Research, Wynnewood PA, USA* 7
[b] *Departments of Microbiology and Immunology, Jefferson Medical College and Kimmel Cancer Center,* 8
Thomas Jefferson University, Philadelphia PA, USA 9
[c] *Departments of Pathology, Anatomy & Cell Biology, Jefferson Medical College and Kimmel Cancer Center,* 10
Thomas Jefferson University, Philadelphia PA, USA 11

Abstract. Increased activity of the tryptophan-catabolizing enzyme indoleamine 2.3-dioxygenase 12
(IDO), encoded by the *INDO* gene, has been associated with a broad spectrum of cancers and is 13
implicated in the pathophysiological process of tumoral immune escape. Our interest in IDO grew 14
out of the finding that disruption of the *Bin1* anti-cancer gene in oncogenically transformed mouse 15
cells can lead to elevated interferon-γ mediated induction of *Indo* gene expression that is associated 16
with immune escape. Using the prototypical IDO inhibitor 1-methyl-tryptophan (1MT), we 17
demonstrated synergistic cooperativity with cytotoxic chemotherapy in an autochthonous mouse 18
breast cancer model. Of the two stereoisomers of 1MT, the D isomer has been demonstrated to be a 19
substantially less potent inhibitor of the IDO enzyme. However, in tolerogenic, IDO-expressing 20
dendritic cells (DCs), D-1MT is as effective as L-1MT at blocking tryptophan catabolism and is 21
actually superior at abrogating T cell suppression. This is consistent with data obtained in two mouse 22
breast cancer models in which IDO is predominantly expressed in DCs within the tumor-draining 23
lymph nodes. In both of these models D-1MT was more effective than L-1MT as an anti-tumor 24
agent. We have recently discovered that a previously undocumented, IDO-related enzyme, referred 25
to here as IDO2, is preferentially inhibited by D-1MT. The relative importance of targeting IDO 26

* Corresponding author. 100 Lancaster Avenue, Wynnewood PA 19096, USA. Tel.: +1 610 645 8034; fax: +1
610 645 2095.
E-mail address: mullera@mlhs.org (A.J. Muller).

versus IDO2 with inhibitory compounds and the possibility of cross-talk between these two enzymes is currently being evaluated. © 2007 Published by Elsevier B.V.

1. Introduction

The interactions that occur at the host tumor interface are complex and dynamic, but, fundamentally, tumors are dependent on the host environment for their survival and growth. It should therefore be possible to target vulnerabilities at the host/tumor interface as a therapeutic strategy. This general idea has recently received some degree of validation with the approval of angiogenesis inhibitors for clinical use. Cancer and inflammation have long been linked. The inflammatory environment is comprised of cytokines, chemokines and growth factors, activated stroma, and DNA damaging agents all of which can contribute to tumorigenesis [1], and the importance of inflammation for promoting and sustaining tumor growth is an area of active investigation. Chronic inflammatory diseases, such as inflammatory bowel disease, or agents that induce inflammation, such as TPA, greatly exacerbate local tumor susceptibility, while developing tumors typically promote a pro-inflammatory environment. Inflammation, however, is also a key step in activating both innate and adaptive immune responses, which should inherently increase the likelihood of immune-mediated tumor rejection. This dichotomy imparts a strong selective pressure on the tumor to overcome immune surveillance so as to maintain the benefits of an inflammatory milieu while minimizing the danger. Cancer cells might accomplish this by eliminating the external signals they present in order to evade anti-tumor immunity. Another option is for the tumor to create a tolerogenic environment that suppresses anti-tumor immunity. The former is passive, the latter is active, and while both these mechanisms may be positively selected during the immune editing process [2], growing evidence suggests that successful immune escape depends predominantly upon the establishment of active pathological immune tolerance [3].

Immunotherapeutic strategies such as cytokine and vaccine-based therapies have, to date, concentrated predominantly on developing approaches to promote immune effector functions. Overall these efforts have produced only a small proportion of positive clinical responses [4]. Dominant mechanisms of immune tolerance could account for the low success rate achieved with exogenous immune stimulation. The complexity of the inflammatory signaling networks may also lead to exogenous signals not eliciting the desired effect within the pathophysiological context of the tumor. For instance IL-2, one of the first cytokines to be used for immunotherapy, is clearly important for effector T cell activation but also promotes the differentiation and survival of immunosuppressive regulatory T cells (T_{regs}) [5]. As such, IL-2 may have a counterproductive role in promoting self-tolerance which has recently led to calls to rethink its widespread use in immunotherapeutic protocols in favor of other cytokines that might be more effective at preferentially promoting anti-tumor responses [6]. Other than IL-2, which has had some limited success, two other approaches to elicit immune responses against solid tumors have been reported to produce objective clinical responses. Breaking

immune tolerance is a key component to both of these approaches underscoring the notion that defeating pathological immune tolerance may be critical to mounting an effective anti-tumor immune response. CTLA-4 is a T cell surface molecule closely related to the costimulatory molecule CD28, but which antagonizes effector T cell responses. Unlike effector T cells, T_{regs} constitutively express CTLA-4 on their surface and CTLA-4 blockade with monoclonal antibody can reportedly abrogate T_{reg}-mediated suppression in humans [7]. In early clinical trials for melanoma, CTLA-4 blockade in combination with vaccine therapy produced an objective response rate of 13% [8]. Recent advances have been made in the approach of adoptive cell transfer so that objective responses approaching 50% have been reported out of early clinical trials. A key development for this procedure has been the incorporation of non-myeloablative, lymphoablative whole body irradiation, which has a pronounced impact on alleviating toleragenic mechanisms that have become established in conjunction with the tumor [9].

Small molecule drugs have a number of advantages relative to biologics in terms of production, delivery, titratability, and cost. However, the development of small molecule agonists of immune function tends to be conceptually problematic and immunotherapeutic approaches have instead focused on biologics, including cell, cytokine, and monoclonal-based therapies. Targeting key enzymes involved in maintaining immune tolerance with small molecule inhibitors should be more straightforward. As the mechanisms for tumoral immune tolerance are elucidated, several nodes for possible intervention with traditional small molecule inhibitors have become apparent [10]. One that has recently been garnering attention is the enzyme indoleamine 2,3-dioxygenase (IDO).

2. IDO in normal and pathological immune tolerance

IDO is an ubiquitously expressed enzyme, encoded by the *INDO* gene, which catalyzes the initial and rate limiting step in the degradation of tryptophan along a pathway which can lead to the biosynthesis of NAD^+ (nicotinamide adenine dinucleotide) [11,12]. IDO does not, however, handle dietary catabolism of tryptophan, which is instead the role of the structurally unrelated liver-specific enzyme tryptophan dioxygenase (TDO2), nor does it appear to be critical for maintaining NAD^+ levels, which in mammalian cells is predominantly the purview of salvage pathways. Instead, IDO is an interferon-γ (IFN-γ) inducible enzyme and its pattern of expression suggested early on that IDO might be somehow involved in inflammation. Detection of elevated levels of tryptophan catabolites in the urine of bladder cancer patients was first reported in the 1950s [13,14]. The determination that this could not be attributed to elevated activity of liver tryptophan oxygenase activity [15] led, in part, to the discovery of IDO from rabbit intestine as an alternative enzyme that also catalyzes the breakdown of tryptophan along the kynurenine pathway [11,16]. A general consensus was initially formed around the idea of IDO elevation being a tumoricidal effect of IFN-γ exposure that operates by starving the rapidly growing tumor cells of the essential amino acid tryptophan [17]. Recently, however, it has been demonstrated that IDO modulates immune function by suppressing cytotoxic T cell activation [18,19]. Because antigen presenting cells (APCs) can up-regulate IDO in response to interferon-γ (IFNγ?, which is produced by activated T cells), this suggests that IDO may participate in a negative regulatory feedback loop for T cell activation. The role of IDO in promoting immune tolerance was dramatically established by the

demonstration that administration of the specific, bioactive IDO inhibitor 1-methyl- 113
tryptophan (1MT) [20] could elicit MHC-restricted, T cell-mediated rejection of allogeneic 114
mouse concepti [21,22], a result we have corroborated [23]. This finding has produced a 115
radical rethinking of the consequences of elevated IDO activity to developing tumors by 116
suggesting that this might be a means by which tumors promote pathogenic tolerization to 117
overcome tumor immunosurveillance. 118

3. Dysregulated *Indo* expression in transformed *Bin1*-null cells is associated with 119 tumoral immune escape 120

Our interest in IDO as a potential therapeutic target originated from the finding that IDO 121
induction by interferon-γ (IFNγ) is moderated by the cancer suppression gene *Bin1*. Bin1 122
is a nuclocytosolic protein that was first identified in a two-hybrid screen for cMyc- 123
interacting proteins [24]. It belongs to a family of genes that is characterized by an 124
evolutionarily conserved N-terminal sequence of ~250 amino acids termed the BAR 125
domain, the crystal structure of which has been recently solved [25]. Frequent loss or 126
attenuation of *Bin1* gene expression has been observed in advanced breast cancer [26], 127
prostate cancer [27], melanoma [28], neuroblastoma [29], and lung cancer [30]. At least 128
seven different mammalian Bin1 splice isoforms have been reported. A subset of these Bin1 129
isoforms has been demonstrated to interact functionally with the proto-oncogenes cMyc 130
and cAbl, to suppress neoplastic transformation, and to induce programmed cell death in a 131
variety of malignant cell lines [24,31–34]. We have reported that *Bin1* loss significantly 132
augments the induction of IDO expression in response to IFNγ exposure by approximately 133
4–5 fold at 24 h [35]. This result was observed in the MR keratinocytes as well as in 134
macrophages, a cell type in which IDO expression and activity had been previously 135
documented [19]. The dysregulation of IDO expression as a result of Bin1 loss occurs 136
downstream of both the STAT1 and NF-κB pathways [35]. 137

Keratinocytes derived from constitutive *Bin1* knock-out embryos and transformed with a 138
combination of cMyc and H-Ras oncogenes (MR) were found to be much more tumorigenic 139
than their *Bin1* expressing counterparts. In syngeneic animals, the *Bin1*+/− MR KECs 140
formed only small, indolent nodules while the *Bin1*−/− cells formed large aggressive tumors 141
that were on average >30-fold larger than those formed by the *Bin1*+/− cells over the same 142
four-week period. In marked contrast to these results obtained in immunocompetent mice, 143
Bin1 loss conferred no significant advantage to tumor growth in T cell deficient mice. 144
These results indicated that *Bin1* loss could contribute to tumor formation in a cell-extrinsic 145
manner that is attributable to decreased T cell-mediated anti-tumor immunity. Consistent 146
with the hypothesis that IDO up-regulation promotes tumor outgrowth, we have shown that 147
treatment of mice with the bioavailable IDO inhibitory compound 1-methyl-tryptophan 148
(1MT) significantly impedes the outgrowth of *Bin1*−/− MR keratinocytes *in vivo* and that 149
this effect is dependent upon intact host T cell immunity [35]. 150

4. IDO inhibition cooperates with chemotherapy in mouse breast cancer models 151

The ability of IDO inhibitor treatment to suppress the outgrowth of transplanted tumors 152
raised for us the question of how effective targeting immune tolerance might be when 153

applied to autochthonous tumors. To evaluate this hypothesis in a less contrived system 154
than the Bin1−/− MR KECs cell isografts that we knew from the outset could overexpress 155
IDO, we began to explore this question in a well-accepted mouse model of breast cancer, 156
the MMTV-*Neu* 'oncomouse'. Autochthonous MMTV-*Neu* mammary gland tumors are 157
induced by the overexpression of the c-*Neu* proto-oncogene, which is also frequently 158
elevated in human breast cancer [36,37]. MMTV-*Neu* transgenic mice present with 159
spontaneous focal adenocarcinomas that are very similar, both histologically and 160
cytologically, to human ductal carcinoma-in situ (DCIS) [38]. Several other criteria were 161
factored into the decision to use this breast cancer model. MMTV-*Neu* transgenic mice are 162
tolerized to *Neu* overexpression in tumors thereby mimicking a condition that is observed 163
in patients [39], and the primary *Neu* epitope that is recognized by CTLs has been identified 164
[40] which will facilitate future studies on the role of IDO in immune tolerance. The model 165
is also relevant to clinical issues of chemotherapy resistance, since tumors that arise in 166
MMTV-*Neu* mice are aggressive and poorly differentiated [41], and are refractory to a 167
number of clinical chemotherapeutics (unpublished observations). We have investigated the 168
possible anti-tumor effects of the IDO inhibitor 1MT either alone or in combination with 169
other agents. 1MT treatment alone slowed tumor growth but did not reverse it, consistent 170
with other published observations [42,43]. This finding suggests that IDO inhibitor-based 171
immunotherapy may have limited anti-tumor efficacy when applied to established tumors 172
as a single-agent. 173

In contrast to these single agent results, treatment of tumor-bearing MMTV-*Neu* mice 174
with a combination of 1MT+paclitaxel, a first line chemotherapeutic agent for the 175
treatment of breast cancer, produced decreases in tumor volume by, on average, ~30% at 176
the two-week endpoint. Paclitaxel by itself produced only growth inhibition of MMTV-*Neu* 177
tumors, consistent with the reported finding that *Neu* overexpression can render cancer 178
cells paclitaxel resistant [44]. The impact of combination treatment was highly significant 179
when compared with untreated tumors (two-tailed t test, $p < 0.0001$) or with either 1MT 180
($p = 0.0010$) or (paclitaxel $p = 0.0011$) single agent treatments. Similar cooperativity was 181
observed with some but not all chemotherapeutic agents tested [35]. In summary, IDO 182
inhibition produced dramatic anti-tumor efficacy in the autochthonous MMTV-*Neu* tumor 183
model in combination with certain cytotoxic chemotherapeutic agents. This finding is 184
striking, as it suggests, perhaps counterintuitively, that combining immunomodulation with 185
chemotherapy might be an effective means to induce tumor regression. 186

In order to confirm the importance of T cell mediated immunity to the enhanced efficacy 187
achieved with the combination of 1MT+paclitaxel, monoclonal antibodies were used to 188
immunodeplete specific T cell populations from animals during tumor treatment by 189
targeting the surface markers CD4 (helper T cells) and CD8 (cytotoxic T cells). As 190
expected, immunodepletion of either the CD4$^+$ or CD8$^+$ populations abolished the ability 191
of combined 1MT+paclitaxel treatment to cooperatively elicit tumor regression despite 192
some dampening of tumor outgrowth associated with immunodepletion alone [35]. The 193
importance of intact T cell immunity to 1MT+paclitaxel cooperativity was further 194
validated using a transplantable MMTV-*Neu* tumor-derived cell line to compare the impact 195
of combination treatment on tumors established in syngeneic with athymic nude mice [35]. 196
These findings confirm the expected immunological basis for the impact of 1MT treatment 197
on tumor regression in response to combination therapy. 198

5. D and L stereoisomers of 1MT show differential IDO inhibitory activity 199

1MT, like the amino acid tryptophan that it resembles, can exist as either a D or L 200
stereoisomer. Tryptophan occurs naturally only in the L configuration and the K_m of human 201
IDO for D-tryptophan is substantially higher than for L-tryptophan [45]. Because 1MT is 202
such a close analog of tryptophan, it might be expected that the K_i would be higher for the 203
D-1MT relative to the L-1MT as well, and indeed this is consistent with published data [46]. 204
However, at least in some instances, the D isomer of 1MT has been reported to be the more 205
biologically active form [47]. We have collaborated with Drs. David Munn and Andrew 206
Mellor to further evaluate the basis for this dichotomy. To directly examine this issue 207
biochemically, the ability of the different 1MT isomers to inhibit IDO activity in a cell-free, 208
purified enzyme assay as well as in cancer cells induced to express IDO was evaluated. 209
Consistent with the anticipated outcome, the L isomer had a substantially lower K_i for 210
inhibiting activity of the purified IDO enzyme than did the D isomer [48]. Likewise, when 211
IDO was induced in the HeLa human cervical cancer cell line by IFNγ treatment, EC_{50} 212
determinations again revealed L-1MT to be a more potent IDO inhibitor than D-1MT [48]. 213
Similar outcomes were observed for mouse Ido. However, in the case of IDO-expressing, 214
toleragenic dendritic cells (DCs), D-1MT was found to be at least as effective an inhibitor of 215
cellular tryptophan catabolism as L-1MT [48]. Furthermore, when these compounds were 216
tested for their ability to relieve DC-mediated suppression of T cell activation in a mixed 217
lymphocyte response (MLR) assay, D-1MT was found to be superior to both L-1MT as well 218
as D,L-1MT [48]. This was true for DCs of both human and mouse origin. Importantly, in 219
terms of therapeutic efficacy, D-1MT was shown to effectively cooperate with 220
chemotherapy and radiation in a mouse melanoma model and to be superior to L-1MT 221
in combining with chemotherapy to elicit anti-tumor responses in two mouse breast cancer 222
models [48]. It has been proposed that, for at least some types of cancer, IDO activity 223
associated with toleragenic DCs in the tumor-draining lymph nodes may be particularly 224
relevant to immune escape by the tumor [49,50]. These data demonstrating the superiority 225
of D-1MT in selectively targeting IDO-dependent, DC-mediated immune tolerance in 226
conjunction with data demonstrating the superiority of D-1MT in cooperating with 227
chemotherapeutic agents in two mouse models of breast cancer [48], are consistent with this 228
idea of IDO-expressing, toleragenic DCs being important to tumoral immune escape in at 229
least certain contexts. Supporting this interpretation, immunohistochemical analysis has 230
revealed no evidence of significant IDO expression in the tumors obtained from the D-1MT 231
responsive mouse melanoma and breast cancer models but elevated IDO expression 232
within the tumor-draining lymph nodes discreetly localized to plasmacytoid dendritic cells 233
(pDCs; [50] and unpublished results). 234

6. A previously uncharacterized, IDO-related enzyme IDO2 is preferentially 235 targeted by D-1MT 236

BLAST searches of the publicly available human genome database for *INDO*-related 237
sequences, led us to come across a second predicted gene directly adjacent to *INDO* at 238
8p12. Identified by the locus designator *LOC169355*, (which has since been changed to 239
INDOL1 (*INDO-like-1*)), the predicted gene sequence corresponded to only a fragment 240

of the *INDO* gene. This, however, turned out to be a misannotation. Searching the human genomic sequence identified a complete set of putative exons for encoding a full length gene, termed here *IDO2*, and a complete set of exons could be found in the syntenic region of the mouse genome as well. Independent identification and characterization of this gene [51] was publicly reported at the ISTRY 2006 Conference by Dr. Nicholas Hunt. By RT-PCR, we have confirmed expression of the predicted full length human *IDO2* transcript as well as at least four truncated splice variants [52]. The full-length *IDO2* transcript is comprised of 11 exons. An additional exon 1a in humans, encoding 8 N-terminal amino acids, has not yet been found in the mouse. The human and mouse IDO2 proteins are more highly conserved (72% identical) than their IDO counterparts (62% identical). Although the IDO and IDO2 proteins do not share a high degree of homology (43% identical), amino acids determined by crystallographic analysis and mutagenesis studies to be critical for IDO to catabolize tryptophan are highly conserved in IDO2 suggesting that it may be catalytically active as well. Indeed, the ability of IDO2 to catabolize tryptophan was confirmed using recombinant V5 epitope-tagged IDO2 ectopically expressed in a human embryonic kidney cell line [52]. Of particular interest, however, was the finding that in contrast to IDO, IDO2 was preferentially inhibited by the D isomer of 1MT. The differential was quite striking, with no evidence of inhibition by the L isomer at 50 µM at which concentration the maximal inhibition of kynurenine production by the D isomer had been achieved [52]. In terms of tissue distribution, the range of expression of IDO2 appears to be more limited than that of IDO. Evaluation of the NCBI public SAGEmap database with a sequence tag to *IDO2* suggested that the gene is expressed in DCs, as the top 4 hits in which tag counts were most prevalent were identified as being from mouse bone marrow-derived dendritic cell libraries. Following up on this, expression of full length, IFNγ-inducible *IDO2* message has been confirmed in the pre-dendritic mouse cell line JAWII [52]. Further work to evaluate the functional relevance of IDO2 expression in DCs is underway.

   An important mechanism through which IDO activity in dendritic cells has been shown to exert biological effects on T cells is by signaling through GCN2 [53], a kinase that is activated by uncharged tRNA and is one of the kinases that initiates the integrated stress response (ISR) through phosphorylation of a common target, the alpha subunit of translation initiation factor 2 (eIF2α). One outcome of the ISR is a generalized suppression of mRNA translation. However, for a subset of genes, phosphorylated eIF2α has been shown to activate translation of mRNAs that contain an internal ribosomal entry site [54]. We have found that induction of IDO2 in a tetracycline-inducible cell system leads to eIF2α phosphorylation (unpublished results) and elevates the expression of LIP [52], an inhibitory isoform of the transcription factor NF-IL6-C/EBPβ that represents a truncated protein product produced as the result of a switch to an internal mRNA initiation codon [55]. Elevation of C/EBPζ (aka CHOP or GAD153), has been previously shown to occur as a result of IDO-mediated activation of GCN2 [53], but this is the first reported demonstration that LIP elevation is also a consequence of activating this signaling pathway. When IDO was induced in this system, there was clear evidence of tryptophan depletion in the cell culture medium and elevation of LIP expression could be blocked by increasing the level of tryptophan in the medium. When IDO2 was induced, on the other hand, no evidence of tryptophan depletion from the medium was evident, which might be expected from its lower level of activity. However, in direct contrast to the result

obtained with IDO, increasing the level of tryptophan had no impact on LIP elevation by 286
IDO2 [52]. This may be indicative of a fundamental difference in the mechanisms through 287
which these two enzymes signal to activate GCN2 kinase activity. Among its physiological 288
effects, C/EBPβ is involved in regulating immune function and defects in cytokine 289
production and T_H1 immune responsiveness are among the consequences associated with 290
C/EBPβ loss [56,57]. IFNγ signals through MAPK signaling pathways to positively 291
regulate C/EBPβ transcriptional activity [58]. The discovery that IDO and IDO2 elevate 292
LIP indicates that these enzymes may drive an IFNγ-driven negative feedback mechanism 293
that restrains C/EBPβ activity. Because of the integral involvement of C/EBPβ in immune 294
responsiveness, the ability of IDO to elevate the trans-dominant inhibitor LIP suggests that 295
this may be an additional mechanism through which elevated IDO activity can attenuate 296
immune responsiveness.   297

Two single nucleotide polymorphisms (SNPs) producing non-synonymous codon 298
changes within the coding sequence for the *IDO2* gene, which are predicted to severely 299
impact enzymatic function, have been identified through evaluation of the public human 300
NCBI SNP database [52]. One, a T to A transition in exon 10, changes a tyrosine at position 301
359 to a stop codon. This results in premature termination of the protein immediately prior 302
to a conserved histidine residue that in IDO is essential for catalytic activity [59]. The other, 303
a C to T transversion in exon 8, changes an arginine at position 248 to a tyrosine. This 304
residue is located at a position equivalent to R231 in IDO, which has been demonstrated by 305
site directed mutagenesis to be critical for catalytic activity and, from the crystal structure, is 306
postulated to be involved in substrate recognition through hydrophobic interactions [60]. 307
This residue is predicted to reside near the entrance to the active site and the presence of the 308
bulky tryptophan side chain may hinder substrate access as well (J. Lalonde, personal 309
communication). Both polymorphisms have been confirmed by site directed mutagenesis to 310
reduce the activity of ectopically expressed IDO2 to undetectable levels. In both cases, the 311
protein product was found to be destabilized in the cells (unpublished results), and so the 312
actual impact of these polymorphisms on enzymatic activity as opposed to expression still 313
remains to be formally evaluated. Remarkably, both of these inactivating polymorphisms 314
are highly penetrant in the general population. Data from 339 individuals in the public 315
database suggest that there may be some ethnic variation in the frequency of occurrence of 316
these polymorphisms with the R248W most prevalent in individuals of European descent, 317
the Y359Stop most prevalent in individuals of Asian descent, and a lower frequency both 318
inactivating alleles in individuals of African descent. This evaluation is based on relatively 319
small groups and the numbers should be expanded to confirm any trends, but still, the 320
overall frequency at which both *IDO2* alleles are potentially inactivated appears to be 321
remarkably high, ranging from up to 25% of individuals of African descent to possibly as 322
high as 50% of individuals of either European or Asian descent [52]. This raises questions 323
regarding how important the functional role of IDO2 actually is and whether there might be 324
counterbalancing selective pressures on its expression due to both advantages and 325
disadvantages that it might provide the host. IDO, for instance, has been implicated as being 326
both protective against inflammatory pathology associated with infection as well as 327
promoting tumoral immune escape. Along these lines, an interesting question to explore 328
will be how these *IDO2* polymorphisms track with susceptibility and outcomes for different 329
types of cancers.   330

7. Discussion

331

1MT has proved to be a very useful tool for investigating the role of IDO activity in 332 physiological and pathophysiological immune tolerance. It was first used to implicate IDO 333 in protecting allogeneic concepti from maternal immunity and later enabled us to validate 334 the immune escape mechanism associated with *Bin1*-null cells as being IDO mediated. The 335 different stereoisomers appear to distinguish between the IDO activity in tumor cells and in 336 tolerogenic pDCs from within tumor-draining lymph nodes, and this in turn has led us to 337 identify the novel IDO-related isoform IDO2 as the possible target for D-1MT in pDCs 338 while L-1MT may preferentially target IDO expressed in tumor cells. These distinctions 339 may not, however, be quite so clear cut. D-1MT, can, in combination with cyclopho- 340 sphomide, suppress the outgrowth of B16-F10 tumor isografts in wild-type mice and pDCs 341 isolated from the tumor-draining lymph nodes from B16-F10 tumor-bearing mice 342 effectively suppress T cell activation *in vitro*. However, when these experiments were 343 performed using *INDO* knockout mice, the combination of D-1MT with cyclophosphamide 344 no longer suppressed B16-F10 tumor outgrowth and pDCs isolated from the tumor- 345 draining lymph nodes were ineffectual at blocking T cell activation [50]. If IDO2 is the 346 direct target of D-1MT, then IDO is still somehow critically involved. One possibility is that 347 these enzymes may functionally interact in some manner, and indeed, from the IDO crystal 348 structure there does appear to be a surface that might act as a dimerization domain 349 (J. Lalonde, personal communication). Alternatively, the expression of these genes may be 350 co-regulated so that the loss of expression of one impacts on the expression of the other. 351 Elucidating the possible crosstalk between these two enzymes has relevance to the possible 352 use of IDO inhibitors in the clinic, as it may become important to determine whether 353 targeting IDO, IDO2 or both enzymes is the best approach for treating a particular patient. 354 This determination may not be the same for different tumor types, and may particularly 355 depend on whether the tumor itself or the tumor-draining lymph nodes is the more 356 important site for IDO activity. Another concern specific to the development of selective 357 IDO2 inhibitors, such as D-1MT, is the high frequency of apparently inactive *IDO2* alleles 358 in the general population. Because of this, genotype analysis to determine the IDO2 359 functional status should be an important consideration in the evaluation of any clinical 360 studies performed with such compounds. 361

One fundamental question raised by our data is why should D-1MT be a better inhibitor 362 of IDO2 than L-1MT? This is particularly puzzling since tryptophan occurs naturally in the 363 L configuration and there is no known physiological role for the D isomer, although an 364 isomerase for converting D-tryptophan to L-tryptophan does exist in the rat [61]. Does this 365 finding suggest that D rather than L-tryptophan is the preferred substrate for IDO2 or, 366 alternatively, is this possibly indicative that tryptophan is not the primary substrate at all? 367 The latter idea would provide an explanation for the finding that excess tryptophan does not 368 block the induction of LIP expression by IDO2 as it does for IDO, however, what might 369 actually serve as an alternative substrate for IDO2 remains an open question. 370

We have identified novel inhibitors of IDO that also effectively inhibit IDO2. These 371 include MTH-tryptophan [35,52], as well as the phytoalexin brassinin and its synthetic 372 derivative 5-Br-brassinin ([62] and unpublished results). These compounds have worked as 373 well if not better than 1MT in pre-clinical mouse tumor models with no sign of adverse 374

mechanism-based side effects resulting from dual enzyme inhibition. For instance, 5-Br- 375
brassinin, when administered as single agent, can substantially suppress the outgrowth of 376
tumors formed by the B16-F10 melanoma cell line (unpublished results), an outcome that 377
could not be achieved with 1MT except in combination with chemotherapy. This suggests 378
that identifying effective inhibitors that target both IDO isoforms should be possible and 379
that, in the end, such compounds may be the most effective therapeutic agents.   380

References   381

[1] L.M. Coussens, Z. Werb, Inflammation and cancer, Nature 420 (6917) (2002) 860–867.   382
[2] G.P. Dunn, et al., Cancer immunoediting: from immunosurveillance to tumor escape, Nat. Immunol. 3 (11) 383
    (2002) 991–998.   384
[3] W. Zou, Immunosuppressive networks in the tumour environment and their therapeutic relevance, Nat. Rev., 385
    Cancer 5 (4) (2005) 263–274.   386
[4] S.A. Rosenberg, J.C. Yang, N.P. Restifo, Cancer immunotherapy: moving beyond current vaccines, Nat. 387
    Med. 10 (9) (2004) 909–915.   388
[5] T.R. Malek, A.L. Bayer, Tolerance, not immunity, crucially depends on IL-2, Nat. Rev., Immunol. 4 (9) (2004) 389
    665–674.   390
[6] P.A. Antony, N.P. Restifo, CD4+CD25+ T regulatory cells, immunotherapy of cancer, and interleukin-2, 391
    J. Immunother. 28 (2) (2005) 120–128.   392
[7] C.N. Manzotti, et al., Inhibition of human T cell proliferation by CTLA-4 utilizes CD80 and requires CD25+ 393
    regulatory T cells, Eur. J. Immunol. 32 (10) (2002) 2888–2896.   394
[8] P. Attia, et al., Autoimmunity correlates with tumor regression in patients with metastatic melanoma treated 395
    with anti-cytotoxic T-lymphocyte antigen-4, J. Clin. Oncol. 23 (25) (2005) 6043–6053.   396
[9] C. Wrzesinski, N.P. Restifo, Less is more: lymphodepletion followed by hematopoietic stem cell transplant 397
    augments adoptive T-cell-based anti-tumor immunotherapy, Curr. Opin. Immunol. 17 (2) (2005) 195–201. 398
[10] A.J. Muller, P.A. Scherle, Targeting the mechanisms of tumoral immune tolerance with small-molecule 399
    inhibitors, Nat. Rev., Cancer. 6 (8) (2006) 613–625.   400
[11] K. Higuchi, S. Kuno, O. Hayaishi, Enzymatic formation of D-kynurenine, Fed. Proc. 22 (1963) 243 (abstr.). 401
[12] T. Shimizu, et al., Indoleamine 2,3-dioxygenase. Purification and some properties, J. Biol. Chem. 253 (13) 402
    (1978) 4700–4706.   403
[13] E. Boyland, D.C. Williams, The metabolism of tryptophan. 2. The metabolism of tryptophan in patients 404
    suffering from cancer of the bladder, Biochem. J. 64 (3) (1956) 578–582.   405
[14] E. Boyland, D.C. Williams, The estimation of tryptophan metabolites in the urine of patients with cancer of 406
    the bladder, Process Biochem. 60 (1955) (Annual General Meeting:v.).   407
[15] S. Gailani, et al., Studies on tryptophan metabolism in patients with bladder cancer, Cancer Res. 33 (5) (1973) 408
    1071–1077.   409
[16] K. Higuchi, O. Hayaishi, Enzymic formation of D-kynurenine from D-tryptophan, Arch. Biochem. Biophys. 410
    120 (2) (1967) 397–403.   411
[17] Y. Ozaki, M.P. Edelstein, D.S. Duch, Induction of indoleamine 2,3-dioxygenase: a mechanism of the 412
    antitumor activity of interferon gamma, Proc. Natl. Acad. Sci. U. S. A. 85 (4) (1988) 1242–1246. 413
[18] A.L. Mellor, D.H. Munn, Tryptophan catabolism and T-cell tolerance: immunosuppression by starvation, 414
    Immunol. Today 20 (1999) 469–473.   415
[19] D.H. Munn, et al., Inhibition of T cell proliferation by macrophage tryptophan catabolism, J. Exp. Med. 189 416
    (1999) 1363–1372.   417
[20] S.G. Cady, M. Sono, 1-methyl-DL-tryptophan, beta-(3-benzofuranyl)-DL-alanine (the oxygen analog of 418
    tryptophan), and beta-[3-benzo(b)thienyl]-DL-alanine (the sulfur analog of tryptophan) are competitive 419
    inhibitors for indoleamine 2,3-dioxygenase, Arch. Biochem. Biophys. 291 (1991) 326–333. 420
[21] D.H. Munn, et al., Prevention of allogeneic fetal rejection by tryptophan catabolism, Science 281 (1998) 421
    1191–1193.   422
[22] A.L. Mellor, et al., Prevention of T cell-driven complement activation and inflammation by tryptophan 423
    catabolism during pregnancy, Nat. Immunol. 2 (1) (2001) 64–68.   424

[23] A.J. Muller, W.P. Malachowski, G.C. Prendergast, Indoleamine 2,3-dioxygenase in cancer: targeting pathological immune tolerance with small-molecule inhibitors, Expert Opin. Ther. Targets 9 (4) (2005) 831–849.

[24] D. Sakamuro, et al., BIN1 is a novel MYC-interacting protein with features of a tumour suppressor, Nat. Genet. 14 (1) (1996) 69–77.

[25] B.J. Peter, et al., BAR domains as sensors of membrane curvature: the amphiphysin BAR structure, Science 303 (5657) (2004) 495–499.

[26] K. Ge, et al., Losses of the tumor suppressor BIN1 in breast carcinoma are frequent and reflect deficits in programmed cell death capacity, Int. J. Cancer 85 (3) (2000) 376–383.

[27] K. Ge, et al., Loss of heterozygosity and tumor suppressor activity of Bin1 in prostate carcinoma, Int. J. Cancer 86 (2) (2000) 155–561.

[28] K. Ge, et al., Mechanism for elimination of a tumor suppressor: aberrant splicing of a brain-specific exon causes loss of function of Bin1 in melanoma, Proc. Natl. Acad. Sci. U. S. A. 96 (17) (1999) 9689–9694.

[29] T. Tajiri, et al., Expression of a MYCN-interacting isoform of the tumor suppressor BIN1 is reduced in neuroblastomas with unfavorable biological features, Clin. Cancer Res. 9 (9) (2003).

[30] M.Y. Chang, et al., Bin1 ablation increases susceptibility to cancer during aging, particularly lung cancer. Cancer Res. in press.

[31] K. Elliott, et al., Bin1 functionally interacts with Myc and inhibits cell proliferation via multiple mechanisms, Oncogene 18 (24) (1999) 3564.

[32] L. Kadlec, A.M. Pendergast, The amphiphysin-like protein 1 (ALP1) interacts functionally with the cABL tyrosine kinase and may play a role in cytoskeletal regulation, Proc. Natl. Acad. Sci. U. S. A. 94 (23) (1997) 12390–12395.

[33] K. Elliott, et al., The c-Myc-interacting adaptor protein Bin1 activates a caspase-independent cell death program, Oncogene 19 (41) (2000) 4669–4684.

[34] J.B. DuHadaway, et al., Bin1 mediates apoptosis by c-Myc in transformed primary cells, Cancer Res. 61 (7) (2001) 3151–3156.

[35] A.J. Muller, et al., Inhibition of indoleamine 2,3-dioxygenase, an immunoregulatory target of the cancer suppression gene Bin1, potentiates cancer chemotherapy, Nat. Med. 11 (3) (2005) 312–319.

[36] M. van de Vijver, et al., Amplification of the neu (c-erbB-2) oncogene in human mammmary tumors is relatively frequent and is often accompanied by amplification of the linked c-erbA oncogene, Mol. Cell. Biol. 7 (5) (1987) 2019–2023.

[37] D.J. Slamon, et al., Human breast cancer: correlation of relapse and survival with amplification of the HER-2/ neu oncogene, Science 235 (4785) (1987) 177–182.

[38] R.D. Cardiff, S.R. Wellings, The comparative pathology of human and mouse mammary glands, J. Mammary Gland Biol. Neoplasia 4 (1) (1999) 105–122.

[39] R.T. Reilly, et al., HER-2/neu is a tumor rejection target in tolerized HER-2/neu transgenic mice, Cancer Res. 60 (13) (2000) 3569–3576.

[40] A.M. Ercolini, et al., Identification and characterization of the immunodominant rat HER-2/neu MHC class I epitope presented by spontaneous mammary tumors from HER-2/neu-transgenic mice, J. Immunol. 170 (8) (2003) 4273–4280.

[41] W.J. Muller, et al., Single-step induction of mammary adenocarcinoma in transgenic mice bearing the activated c-neu oncogene, Cell 54 (1) (1988) 105–115.

[42] M. Friberg, et al., Indoleamine 2,3-dioxygenase contributes to tumor cell evasion of T cell-mediated rejection, Int. J. Cancer 101 (2) (2002) 151–155.

[43] C. Uyttenhove, et al., Evidence for a tumoral immune resistance mechanism based on tryptophan degradation by indoleamine 2,3-dioxygenase, Nat. Med. 9 (10) (2003) 1269–1274.

[44] D. Yu, et al., Overexpression of c-erbB-2/neu in breast cancer cells confers increased resistance to Taxol via mdr-1-independent mechanisms, Oncogene 13 (6) (1996) 1359–1365.

[45] O. Takikawa, et al., Mechanism of interferon-gamma action. Characterization of indoleamine 2,3-dioxygenase in cultured human cells induced by interferon-gamma and evaluation of the enzyme-mediated tryptophan degradation in its anticellular activity, J. Biol. Chem. 263 (4) (1988) 2041–2048.

[46] A.C. Peterson, et al., Evaluation of functionalized tryptophan derivatives and related compounds as competitive inhibitors of indoleamine 2,3-dioxygenase, Med. Chem. Res. 3 (1994) 531–544.

[47] D.H. Munn, et al., Potential regulatory function of human dendritic cells expressing indoleamine 2,3-dioxygenase, Science 297 (5588) (2002) 1867–1870.

Q1

[48] D.Y. Hou, et al., Inhibition of indoleamine 2,3-dioxygenase in dendritic cells by stereoisomers of 1-methyl- 479
      tryptophan correlates with antitumor responses, Cancer Res. 67 (2) (2007) 792–801.   480
[49] D.H. Munn, A.L. Mellor, Indoleamine 2,3-dioxygenase and tumor-induced tolerance, J. Clin. Invest. 117 (5) 481
      (2007) 1147–1154.   482
[50] D.H. Munn, et al., Expression of indoleamine 2,3-dioxygenase by plasmacytoid dendritic cells in tumor-   483
      draining lymph nodes, J. Clin. Invest. 114 (2) (2004) 280–290.   484
[51] H.J. Ball, et al., Characterization of an indoleamine 2,3-dioxygenase-like protein found in humans and mice, 485
      Gene 396 (1) (2007) 203–213.   486
[52] R. Metz, et al., Novel tryptophan catabolic enzyme IDO2 is the preferred biochemical target of the antitumor 487 **Q2**
      IDO inhibitory compound D-1MT. Cancer Res. in press.   488
[53] D.H. Munn, et al., GCN2 kinase in T cells mediates proliferative arrest and anergy induction in response to 489
      indoleamine 2,3-dioxygenase, Immunity 22 (5) (2005) 633–642.   490
[54] J. Fernandez, et al., Regulation of internal ribosome entry site-mediated translation by eukaryotic initiation factor- 491
      2alpha phosphorylation and translation of a small upstream open reading frame, J. Biol. Chem. 277 (3) (2002) 492
      2050–2058.   493
[55] P. Descombes, U. Schibler, A liver-enriched transcriptional activator protein, LAP, and a transcriptional 494
      inhibitory protein, LIP, are translated from the same mRNA, Cell 67 (3) (1991) 569–579.   495
[56] S. Akira, T. Kishimoto, NF-IL6 and NF-kappa B in cytokine gene regulation, Adv. Immunol. 65 (1997) 1–46. 496
[57] I. Screpanti, et al., Lymphoproliferative disorder and imbalanced T-helper response in C/EBP beta-deficient 497
      mice, EMBO J. 14 (9) (1995) 1932–1941.   498
[58] D.V. Kalvakolanu, S.K. Roy, CCAAT/enhancer binding proteins and interferon signaling pathways, J. Interferon 499
      Cytokine Res. 25 (12) (2005) 757–769.   500
[59] T.K. Littlejohn, et al., Asp274 and His346 are essential for heme binding and catalytic function of human 501
      indoleamine 2,3-dioxygenase, J. Biol. Chem. 278 (32) (2003) 29525–29531.   502
[60] H. Sugimoto, et al., Crystal structure of human indoleamine 2,3-dioxygenase: catalytic mechanism of O2   503
      incorporation by a heme-containing dioxygenase, Proc. Natl. Acad. Sci. U. S. A. 103 (8) (2006) 2611–2616. 504
[61] I. Ohara, et al., Inversion of D-tryptophan to L-tryptophan and excretory patterns in the rat and chick, J. Nutr. 505
      110 (4) (1980) 641–648.   506
[62] P. Gaspari, et al., Structure-activity study of brassinin derivatives as indoleamine 2,3-dioxygenase inhibitors, 507
      J. Med. Chem. 49 (2) (2006) 684–692.   508
                                                                                                                 509

Indoleamine 2,3-Dioxygenase Is the Anticancer Target for a Novel Series of Potent Naphthoquinone-Based Inhibitors

Sanjeev Kumar,[†] William P. Malachowski,*,[†] James B. DuHadaway,[‡] Judith M. LaLonde,*,[†] Patrick J. Carroll,[§] Daniel Jaller,[‡] Richard Metz,[∥] George C. Prendergast,[‡,⊥,#] and Alexander J. Muller*,[‡,#,∇]

Department of Chemistry, Bryn Mawr College, Bryn Mawr, Pennsylvania 19010, Lankenau Institute for Medical Research, Wynnewood, Pennsylvania 19096, Department of Chemistry, X-ray Crystallography Facility, University of Pennsylvania, Philadelphia, Pennsylvania 19104, LIMR Development, Inc., Wynnewood, Pennsylvania 19096, and Departments of Pathology, Anatomy & Cell Biology, Microbiology and Immunology, Jefferson Medical School, Kimmel Cancer Center, Thomas Jefferson University, Philadelphia, Pennsylvania 19104

Indoleamine 2,3-dioxygenase (IDO) is emerging as an important new therapeutic target for the treatment of cancer, chronic viral infections, and other diseases characterized by pathological immune suppression. While small molecule inhibitors of IDO exist, there remains a dearth of high-potency compounds offering *in vivo* efficacy and clinical translational potential. In this study, we address this gap by defining a new class of naphthoquinone-based IDO inhibitors exemplified by the natural product menadione, which is shown in mouse tumor models to have similar antitumor activity to previously characterized IDO inhibitors. Genetic validation that IDO is the critical *in vivo* target is demonstrated using IDO-null mice. Elaboration of menadione to a pyranonaphthoquinone has yielded low nanomolar potency inhibitors, including new compounds which are the most potent reported to date (K_i = 61–70 nM). Synthetic accessibility of this class will facilitate preclinical chemical−genetic studies as well as further optimization of pharmacological parameters for clinical translation.

Introduction

Of the major diseases that plague the developed and developing worlds, many are associated with immunosuppressed states that can impede effective treatment and recovery. Some prominent examples are cancer, where, as a consequence of immunoediting,[1] tumor cells are under strong selective pressure to develop the capacity to undermine an effective immune response, and chronic infections, such as HIV and HCV infections, where immunosuppression contributes to disease persistence. A growing body of evidence implicates the involvement of the enzyme indoleamine 2,3-dioxygenase (IDO)[a] in mediating pathological immunosuppression in such settings, indicating that IDO may be an attractive therapeutic target for pharmacological intervention in cancer as well as other diseases in which effective immunity is impaired.[2,3] In preclinical models of cancer, IDO inhibition has been demonstrated to safely and dramatically improve chemotherapeutic efficacy.[4,5] However, while bioactive small molecule inhibitors of IDO exist, they are low potency and perhaps better suited to proof-of-concept experiments than clinical translation. Thus, one present barrier to drug development is a dearth of potent and bioactive drug-like molecules that offer translational potential.

IDO (EC 1.13.11.42) is a monomeric heme-containing enzyme that catalyzes tryptophan degradation in the initial step of the kynurenine pathway, the *de novo* biosynthetic route for nicotinamide adenine dinucleotide (NAD) production.[6–8] IDO is active with the heme iron in the ferrous (Fe^{2+}) form and inactive in the ferric (Fe^{3+}) form; substrate inhibition of IDO is believed to result from tryptophan binding to the ferric form.[9,10] While the primary catalytic cycle of IDO does not involve redox changes, IDO is prone to auto-oxidation and so a reductant is necessary to reactivate the enzyme. *In vivo*, IDO is thought to rely on a flavin or tetrahydrobiopterin cofactor for which methylene blue and ascorbic acid can be substituted in reactions performed with purified IDO enzyme.[7] Using such an *in vitro* assay, the landmark competitive inhibitor 1-methyltryptophan (1MT, Figure 1) was identified in the early 1990s.[11,12] Widely employed for IDO studies, 1MT is bioactive and selective but is a rather low potency compound (K_i = 34 μM). Other bioactive but also relatively low potency inhibitors have been described, all of which retain the indole ring of tryptophan, including a thiohydantoin derivative of tryptophan and derivatives of the natural product brassinin.[13,14] Metabolic enzymes often evolve an affinity for their natural substrate that closely matches the physiological concentration of the substrate,[15,16] which is ~60 μM for circulating tryptophan.[17–19] Thus, IDO inhibitors with submicromolar potency may be more likely to arise from structures lacking the indole core of tryptophan.

* Address correspondence regarding the chemistry to W.P.M. Tel: 610-526-5016. Fax: 610-526-5086. E-mail: wmalacho@brynmawr.edu. Address correspondence regarding the biology A.J.M. or G.C.P. Tel: 610-645-8034. Fax: 610-645-2095. E-mail: mullera@mlhs.org. Address correspondence regarding the computational chemistry J.M.L. Tel: 610-526-5016. Fax: 610-526-5679. E-mail: jlalonde@brynmawr.edu.

[†] Department of Chemistry, Bryn Mawr College.
[‡] Lankenau Institute for Medical Research.
[§] Department of Chemistry, University of Pennsylvania.
[∥] LIMR Development, Inc.
[⊥] Departments of Pathology, Anatomy & Cell Biology, Thomas Jefferson University.
[#] Kimmel Cancer Center, Thomas Jefferson University.
[∇] Microbiology and Immunology, Thomas Jefferson University.

[a] Abbreviations: ATP, adenosine 5′-triphosphate; GSH, glutathione; IDO, indoleamine 2,3-dioxygenase; LD50, median lethal dose; MMTV, mouse mammary tumor virus; 1-MT, 1-methyltryptophan; MTD, maximum tolerated dose; NAD, nicotinamide adenine dinucleotide; NAD(P)H reduced nicotinamide adenine dinucleotide phosphate; NOQ1, NAD(P)H:quinone oxidoreductase 1; NOQ2, NRH:quinone oxidoreductase 2; pDC, plasmacytoid dendritic cells; 4-PI, 4-phenyl-imidazole; ROS, reactive oxygen species.

Table 1. IDO Inhibition from Commercially Available Quinone Structures

	compd	IC$_{50}$ (μM)	E (mV)		compd	IC$_{50}$ (μM)	E (mV)
1	2,3-dichloro-1,4-naphthoquinone	0.28	−604[22]	**7**	2-hydroxy-1,4-naphthoquinone	∼675	−357[23]
2	2-methoxy-1,4-naphthoquinone	0.72		**8**	benzoquinone	no activity	−401[24]
3	1,4-naphtho-quinone	0.99	−140[25]	**9**	2-methyl-1,4-benzoquinone	no activity	−466[24]
4	5-hydroxy-1,4-naphthoquinone	1.0	−93[26]	**10**	2-phenyl-1,4-benzoquinone	no activity	
5	2-methyl-1,4-naphthoquinone	1.1	−203[27]	**11**	vitamin K1	no activity	−170[28]
6	1,2-napthoquinone	7.1	−89[25]	**12**	chromone	no activity	

IC$_{50}$ (inhibitory concentration 50%) is the concentration of compound that inhibits enzyme activity by half. E is the reduction potential for the one electron reduction of the quinone to the semiquinone.
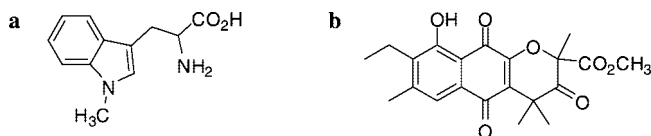
Figure 1. Structure of two small molecule inhibitors of IDO: (a) 1-methyL-tryptophan (1MT), a widely used IDO inhibitor that is bioactive; (b) annulin B, a potent IDO inhibitor isolated from a marine invertebrate, which lacks an indole core structure.
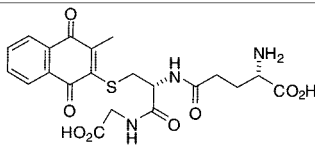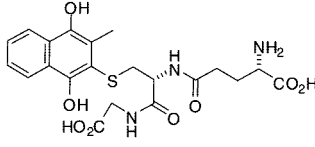
Herein, we describe the discovery of highly potent IDO inhibitors that lack the indole core of IDO's natural substrate. These potent inhibitors are inspired by the natural product annulin B[20,21] (Figure 1) and contain naphthoquinone as the key pharmacophore. In this study, we demonstrate through mouse tumor models that the naphthoquinone natural product, menadione, has antitumor activity mediated through IDO inhibition. Furthermore, we describe the synthesis and characterization of a new structural class of IDO inhibitors based on the naphthoquinone pharmacophore. The most active compounds are pyranonaphthoquinones, and they represent the most potent IDO inhibitors described to date.

Results

Naphthoquinone Is the Pharmacophore of Natural Product Annulin B. Andersen et al. recently described[20,21] several natural products isolated from a marine hydroid with potent activity as IDO inhibitors, the most potent of which was annulin B with a $K_i = 0.12$ μM. Most of the marine natural product inhibitors contained a naphthoquinone core, and by comparing the structure of 1MT with annulin B (Figure 1), we hypothesized that the relevant pharmacophore in annulin B was the naphthoquinone core. In support of the notion that naphthoquinone is an indole mimetic, commercially available compounds containing a quinone structure were screened for IDO inhibitory activity and several demonstrated micromolar levels of inhibitory potency (Table 1). The 1,2- or 1,4-naphthoquinone unit was essential for activity (cf. **1–6** vs **8–10**, **12**), and substitution was permitted on either the benzene (e.g., **4**) or the quinone ring (e.g., **1**, **2**, and **5**) of the naphthoquinone core. Exceptions to this principle were found with the phytylated 1,4-naphthoquinone derivative vitamin K1 and the 2-hydroxy derivative **7**; the latter was particularly noteworthy given the activity of the structurally analogous 1,2-naphthoquinone **6**. All benzoquinone derivatives were inactive, thereby confirming the need for a fused benzene-quinone structure for activity as an IDO inhibitor. Although quinones are well-known oxidants, there was no apparent correlation between the IDO inhibitory potency and the reduction potential of these different quinone-based compounds (Table 1).

IDO Is an Essential Target for the Antitumor Activity of the Naphthoquinone Menadione. Included among the naphthoquinone-based compounds evaluated for IDO inhibitory activity was menadione, also known as vitamin K3 (**5**), which exhibited low micromolar potency (IC$_{50}$ = 1.0 μM) (Table 1).

Table 2. IC$_{50}$ Values for Glutathione-Conjugated Menadione (Quinone and Hydroquinone Forms)

	compound	IC$_{50}$ (μM)
13		0.88
14		0.34

This was a specific feature of this vitamin K precursor molecule, as vitamin K1 (**11**) lacked activity as an IDO inhibitor. Although other naphthoquinones in our initial screen were more potent, menadione is a known anticancer agent[29] and clinical studies have provided evidence of its activity as a radiosensitizer and its ability to cooperate with chemotherapeutic agents, reminiscent of other IDO inhibitors.[4,14] Consequently, we chose to explore the in vivo activity of the naphthoquinones with menadione.

While a variety of hypotheses for the mechanism of action of menadione have been proposed, a definitive understanding has yet to emerge. Most studies have focused on its ability to generate reactive oxygen species (ROS) or to deplete intracellular glutathione through the formation of menadione−glutathione and glutathione−glutathione conjugates,[30] which may have cytotoxic consequences.[31] Interestingly, we found that the glutathione conjugate of menadione (both in quinone **13** and hydroquinone **14** forms) retained IDO inhibitory activity, exhibiting even greater potencies than the parent compound (Table 2). In a cell-based assay, the IC$_{50}$ of menadione for IDO inhibition was determined to be lower than the LD$_{50}$ for cellular cytotoxicity by >4-fold (Figure 2a), indicating that there is a window between IDO inhibitory activity and general cytotoxicity for this compound.

Based on available information in the NCI database about menadione in different mouse models of cancer (http://dtp.nci.nih.gov/dtpstandard/InvivoSummary/index.jsp), we evaluated whether menadione, administered at levels near the maximum tolerated dose (MTD), would cooperate with paclitaxel in the MMTV-*Neu* transgenic mouse model of breast cancer, an assay where the antitumor efficacy of various IDO inhibitors has previously been demonstrated.[14,32] Administration of menadione alone at 25 mg/kg once a day (qd) resulted in some evidence of growth inhibition, while the same dose administered twice a day (bid) was lethal, indicating that no further dose escalation would be possible. However, like other IDO inhibitors, which
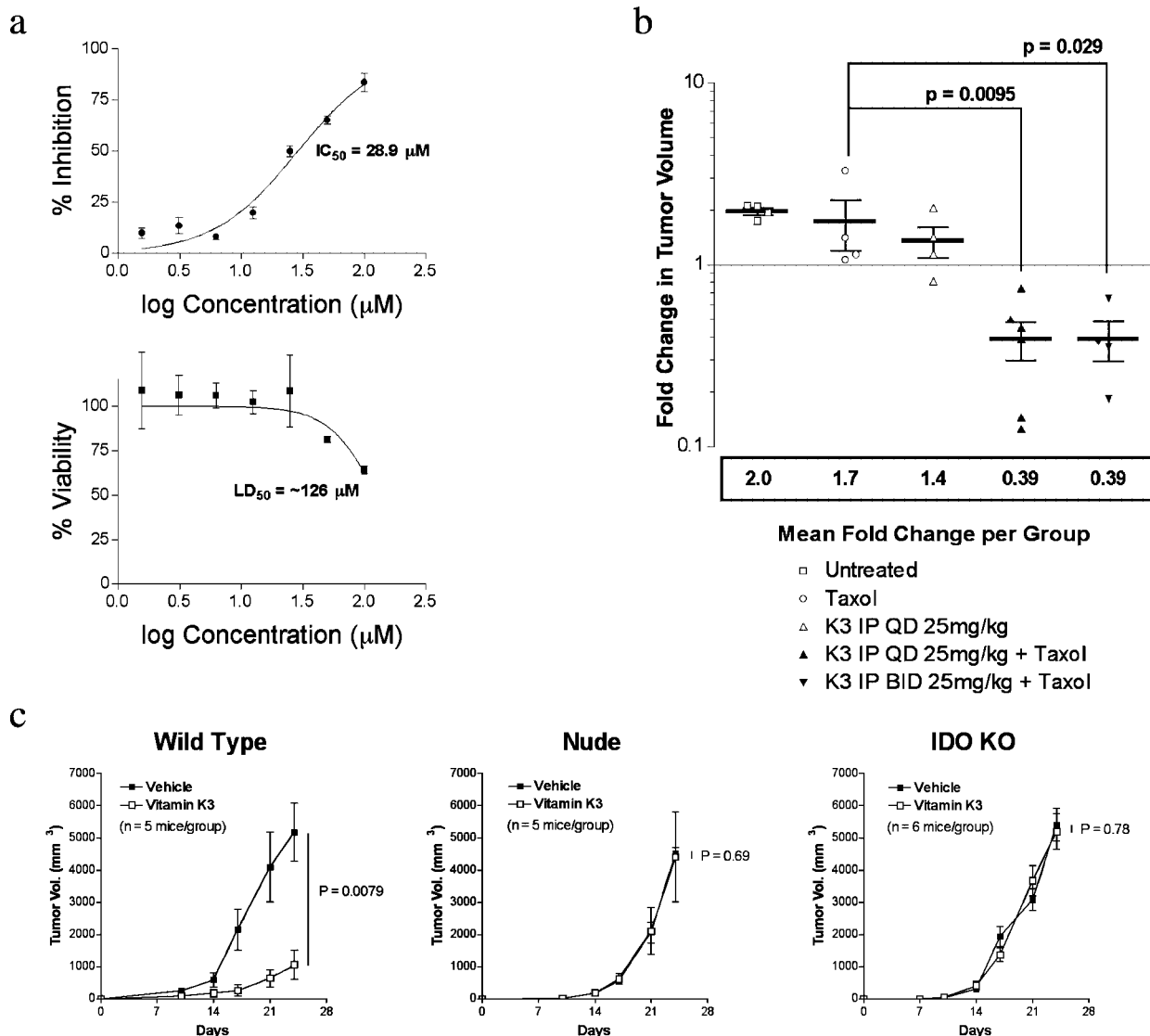
Figure 2. *In vivo* validation of IDO as an essential target of menadione antitumor activity. (a) Cell-based comparison of IDO inhibition and cytotoxicity of menadione. A clonal T-REx-derived cell line, stably transfected with doxycyclin-inducible IDO, was exposed to a range of menadione concentrations. The top graph shows the percent inhibition of IDO activity (adjusted for cell viability) based on comparison of kynurenine levels in the culture supernatant of menadione-exposed cells to that of untreated controls. The bottom graph shows the percent viability of the same cells used for the IDO inhibition assay based on SRB assay results from menadione-exposed cells compared to untreated controls. IC_{50} and LD_{50} values were determined from the sigmoidal dose–response curves. The assays were performed in triplicate and graphed as means $\pm$ SD. (b) Menadione effectively combines with paclitaxel chemotherapy to regress established breast tumors. Parous MMTV-*Neu* mice with 0.5–1.0 cm mammary gland tumors were randomly enrolled for 2-week treatment studies. Tumor volume determinations were made at the beginning and end of the treatment period. Cohorts receiving menadione (K3) were administered compound i.p. either once a day (qd) or twice a day (bid) as indicated at 25 mg/kg for 5 consecutive days during the first week of treatment. Paclitaxel (Taxol) was administered to the indicated cohorts i.v. at 13.3 mg/kg qd 3×/week over the entire course of the 2-week treatment period. Each point represents the fold change in volume for an individual tumor with the mean $\pm$ SEM indicated for each group. The significance of the differences between the paclitaxel alone and the paclitaxel + menadione treatment groups was assessed using a nonparametric two-tailed Mann–Whitney test to determine the indicated *P* values. (c) Menadione suppresses outgrowth of B16-F10 tumors in a T cell and host IDO dependent manner. Menadione treatment, administered i.p. at 25 mg/kg qd 5 days a week until termination of the experiment, was initiated 7 days following s.c. injection of C57BL/6 mice with 1×10^5 B16-F10 melanoma-derived cells. Caliper measurements of tumors were performed biweekly until the control tumors reached a volume of ~5000 mm³. From left to right are the results obtained from C57BL/6 mice, athymic NCr-nu/nu mice, and C57BL/6-strain, IDO knockout mice as indicated above each graph, plotted as mean tumor size $\pm$ SEM at each time point. At the conclusion of each study, the difference in tumor volumes between the treatment and nontreatment groups was assessed using a nonparametric two-tailed Mann–Whitney test to determine the *P* value indicated on each graph.

also display weak antitumor activity on their own,[14] combining menadione at the 25 mg/kg qd dose with paclitaxel produced significant tumor regressions in the model (Figure 2b). Surprisingly, mice receiving the combination of paclitaxel with menadione at 25 mg/kg bid all survived; however, the antitumor response was similar irrespective of whether the compound was administered once or twice daily (Figure 2b).

To validate the requirement of IDO as a target for the antitumor efficacy of menadione, we compared the activity of this compound in a mouse model of cancer where we could genetically assess the consequences of IDO loss. Briefly, tumors formed by the mouse melanoma cell line B16-F10 do not express IDO *in vitro* or *in vivo*[33] Nevertheless, growth of tumor isografts formed by these cells can be suppressed significantly
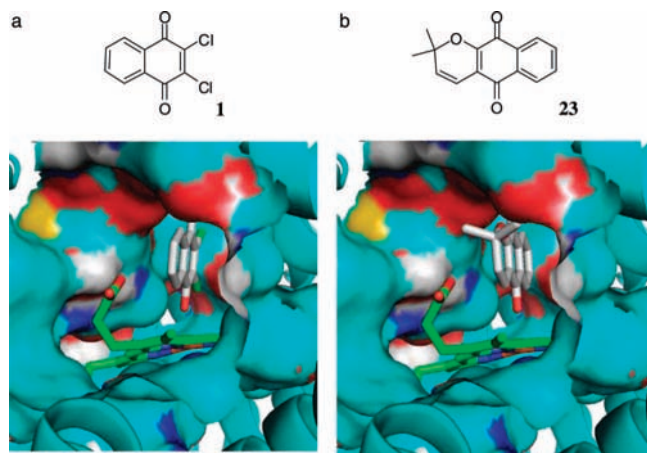
Figure 3. Docking naphthoquinones at the IDO active site by molecular modeling. (a) Proposed binding mode of compound **1** in IDO active site. (b) Proposed binding mode of pyranonaphthoquinone **23** in IDO active site. Graphics generated with PyMOL 098 (http//www.py-mol.org), an open-source molecular graphics system developed supported and maintained by DeLano Scientific LLC (http//www.delano-scientific.com).

by single agent treatment with an IDO inhibitor,[32] due, presumably, to inhibition of IDO expressed in tolerogenic dendritic cells that accumulate in tumor draining lymph nodes of the host animal.[33] In this model, we confirmed that the growth of B16-F10 isograft tumors could be reduced significantly by single agent menadione treatment (Figure 2c). In contrast, we detected no growth inhibition of tumor grafts in either athymic nude mice or syngeneic IDO knockout mice (Figure 2c). These findings indicate that the antitumor activity of menadione requires both IDO inhibition and T cell involvement, thereby validating IDO as a critical therapeutic target for menadione—a prototypical representative of the naphthoquinone class of IDO inhibitors.

Molecular Modeling with Naphthoquinone Leads. We noted that the commercially available naphthoquinone structures with activity as IDO inhibitors generally displayed a noncompetitive mode of inhibition (Table 1). Noncompetitive or uncompetitive modes of inhibition usually suggest a basis in allosteric binding; however, there exists a precedent for IDO inhibitors to bind at the active site and yet display noncompetitive or uncompetititve kinetics. For example, 4-phenylimidizole (4-PI) has been reported to bind preferentially to the heme iron in the inactive ferric form of IDO.[34,35] Also, β-carboline has been reported to compete with oxygen for ferrous heme iron binding.[34] Nonetheless, in a mechanistic study, both 4-PI and β-carboline demonstrated noncompetitive kinetics,[34] while the original report describing β-carboline as an IDO inhibitor reported uncompetitive inhibition.[36] Consequently, noncompetitive inhibition of IDO may not preclude heme iron binding at the active site by the naphthoquinone derivatives. Monodentate heme iron binding by quinones is not common,[37] but several recent studies of photosynthesis and, particularly one involving study of cytochrome b_6f,[38,39] have demonstrated monodentate iron heme binding by quinones.

Utilizing the recently reported crystal structure of IDO,[35] computational docking studies in the absence of molecular oxygen placed several naphthoquinones at the active site with the quinone oxygen coordinated to the heme iron. Furthermore, the docking studies showed that the orientation of a particular naphthoquinone will depend on the substituents on the naphthoquinone core. With relatively small substituents on the C-2 or C-3 position (e.g., **1**), the naphthoquinone entered the active

Scheme 1. General Synthetic Path to Pyranonaphthoquinone Derivatives
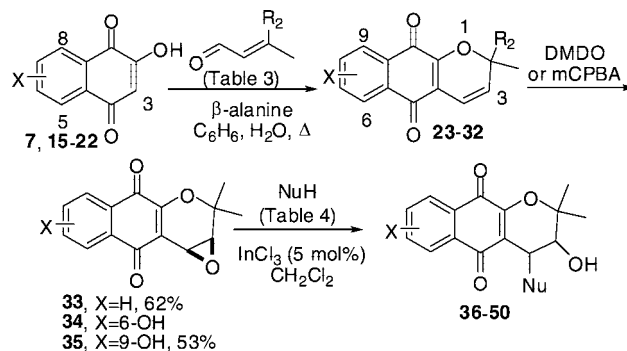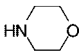

Table 3. 6π Electrocyclization Reactions

naphthoquinone		product			
	X		X	R_2	yield(%)
7	H	**23**	H	CH_3	77
7	H	**24**	H	CO_2CH_3	22
15	5-OH	**25**	6-OH	CH_3	69
16	5-OCH$_3$	**26**	6-OCH$_3$	CH_3	76
17	6-OH	**27**	7-OH	CH_3	71
18	6-OCH$_3$	**28**	7-OCH$_3$	CH_3	71
19	7-OH	**29**	8-OH	CH_3	75
20	7-OCH$_3$	**30**	8-OCH$_3$	CH_3	72
21	8-OH	**31**	9-OH	CH_3	56
22	8-OCH$_3$	**32**	9-OCH$_3$	CH_3	52

site with the benzene ring projecting toward the entrance of the active site (Figure 3a). In contrast, tricyclic pyranonaphthoquinones, such as **23**, which include the pyran ring of annulin B, entered with the benzene ring projecting into the posterior of the active site (Figure 3b). Similarly, docking of annulin B confirmed that the substituted benzene ring is nestled in the back of the IDO active site, with the pyran ring located at the opening of the active site (data not shown). These docking studies provided an initial working model to direct synthetic modifications to the naphthoquinone core to improve potency.

Synthesis of Novel Pyranonaphthoquinone Inhibitors of IDO. Initial efforts were directed at mimicking the structure of annulin B, by installing and elaborating the pyran ring through chemical syntheses. Naphthoquinones **7** and **15–22** were easily converted to pyranonaphthoquinones **23–32** via a one-pot 6π electrocyclization reaction in modest to good yield (Scheme 1 and Table 3).[40–42] The naphthoquinones with substituents in the benzene ring were synthesized according to literature procedures. Epoxidation of **23** proceeded with dimethyldioxirane to afford **33**, while epoxidation of **25** and **31** was accomplished with m-CPBA to provide **34** and **35**, respectively. Further derivatization of the pyran ring was accomplished by nucleophilic substitution of the epoxides (Scheme 1 and Table 4). The cis and trans diastereomers (**36–50**) were separable by column chromatography. Assignment of the cis and trans diastereomers was based on an X-ray crystal structure of **36** (Supporting Information) and an analysis of NMR coupling constants. Hydrogenation, bromohydrin formation, and dihydroxylation[41] were also employed to selectively modify the pyran alkene (Scheme 2).

Evaluation of Pyran Ring Derivatives. The docked binding mode of annulin B, with its pyran ring located at the opening of the active site, suggested focusing synthesis on the pyran ring as a means of embellishing the naphthoquinone core and restoring or enhancing the level of IDO inhibition displayed

Table 4. Epoxide Opening Reactions

epoxide	NuH	cis (yield, %)	trans (yield, %)
33 (X=H)	PhCH$_2$NH$_2$	**36** (53)	**37** (37)
33	CH$_2$=CHCH$_2$NH$_2$	**38** (58)	**39** (29)
33	CH$_3$(CH$_2$)$_3$NH$_2$	**40** (58)	**41** (16)
33	HN◯O (morpholine)	**42** (57)	**43** (14)
33	CH$_3$OH	**44** (54)	**45** (28)
33	PhCH$_2$OH	**46** (48)	—
33	PhCH$_2$SH	**47** (45)	**48** (27)
34 (6-OH)	PhCH$_2$NH$_2$[a]	**49** (34)	—
35 (9-OH)	PhCH$_2$NH$_2$[a]	**50** (57)	—

[a] Reaction in 2-propanol without indium(III) chloride, InCl$_3$.

Table 5. IC$_{50}$ Values of Pyran Ring Derivatives of Naphthoquinone IDO Inhibitors

compd	IC$_{50}$ (μM)	compd	IC$_{50}$ (μM)	compd	IC$_{50}$ (μM)
23[a]	0.214	**40**	0.130	**46**	1.09
24	0.247	**41**	0.082	**47**	3.45
33	4.95	**42**	1.10	**48**	2.12
36	0.055	**43**	0.361	**51**	4.34
37	0.252	**44**	0.976	**52**	0.512
38	0.186	**45**	3.96	**53**[b]	1.50
39	0.183				

[a] Natural product commonly referred to as dehydro-α-lapachone. [b] Natural product commonly referred to as α-lapachone.

Scheme 2
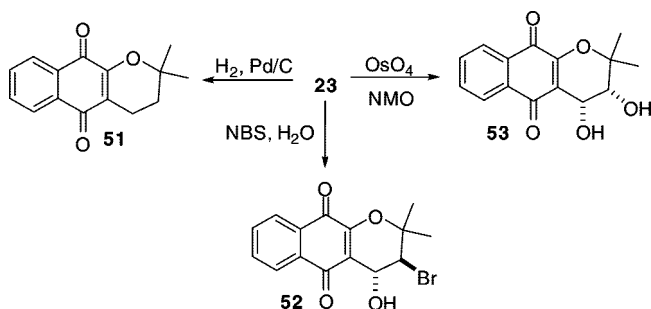
with the more complex marine natural product. To begin, we synthesized and tested the simplified pyranonaphthoquinone **23** (Table 5), where the tricyclic structure was found to restore essentially all the activity of annulin B. Notably, antitumor activity has been associated with compound **23**, which is also known as dehydro-α-lapachone.[43,44] Incorporation of the ester from annulin B onto the pyran ring (**24**) had little effect on the potency of the pyranonaphthoquinone nucleus. However, reduction of the pyran ring (**51**) resulted in a dramatic loss in activity. Similarly, oxidation of the alkene to an epoxide (**33**) also dramatically reduced the activity of this tricyclic inhibitor. Based on the docking model of **23** (Figure 3b) and the hypothesized exposure of the pyran ring to solvent, we expected elaboration of the pyran ring to be permissible and therefore analyzed a selection of compounds with functionalized pyran rings. We found the most potent of these pyran ring derivatives to be 1,2-amino-alcohol derivatives (i.e., **36** and **41**). The absence of consistent differences between the cis and trans diastereomers

Table 6. IC$_{50}$ Values of Benzene Ring Derivatives of Naphthoquinone IDO Inhibitors

compd	IC$_{50}$ (μM)	compd	IC$_{50}$ (μM)
25	0.190	**29**	2.05
26	2.13	**30**	0.933
27	5.52	**31**[a]	0.121
28	3.02	**32**	2.92

[a] Natural product commonly referred to as α-caryopterone.

supports the notion that the region of the IDO enzyme occupied by these groups is not constrained, such as found at the opening of the active site.

Evaluation of Benzene Ring Derivatives. The study of the benzene ring of annulin B focused on the position and the nature of the oxygen substituent which was viewed as the most important functionality for intermolecular interactions in the active site. A distinct preference was observed with the C-6- and C-9 hydroxy-substituted pyranonaphthoquinones **25** and **31**, demonstrating between 5- and 45-fold greater potency than the other oxygen-substituted annulin B derivatives (Table 6). Nevertheless, the activity of **25** and **31** is roughly equal to that of the unsubstituted parent compound **23**. Consequently, the C-6 or C-9 hydroxyl substitution is permissible but does not appear to lead to any favorable interaction with IDO. Conversely, larger substitution in C-6 or C-9 or substituents in C-7 or C-8 clearly have a detrimental effect, probably due to steric interactions.

After an exploration of the optimal elements in the pyran ring (Table 5) and the benzene ring (Table 6), we synthesized two inhibitors (**49** and **50**) that combined the best elements of both ring substitutions. These compounds were also highly potent with IC$_{50}$'s of 0.058 and 0.059, respectively, thereby demonstrating that substitution is permitted in both rings. Although the substitution pattern of annulin B suggested this was possible, it was not to the extent demonstrated with the benzyl amine in **49** and **50**.

Further Evaluation of Most Active Inhibitors. Three of the most potent pyranonaphthoquinone derivatives, based on IC$_{50}$ values, were further analyzed to determine their inhibition constants and mode of inhibition. The inhibition constants for **36**, **41**, and **50** were determined to be 70, 61, and 66 nM, respectively. All three are more potent than annulin B (K_i = 120 nM[20,21]) and thus represent the highest potency IDO inhibitors reported to date. Each of these compounds is also roughly 500-fold more potent than the most commonly employed IDO inhibitor 1MT. Interestingly, all three compounds exhibited reversible uncompetitive kinetics of inhibition (Supporting Information). Preincubation of three pyranonaphthoquinones (**31**, **36**, and **41**) with IDO failed to demonstrate any irreversible inhibition.

Due to the surprising activity of the hydroquinone derivative **14**, we attempted to generate and evaluate a hydroquinone derivative of one of the potent pyranonaphthoquinone derivatives. However, the rapid aerobic oxidation of each compound tested precluded analysis of the inhibitory activity of the hydroquinone form. Evaluation of the effect of the isolated enzyme assay reduction system (ascorbic acid/methylene blue) on these pyranonaphthoquinones did reveal evidence of hydroquinone formation (data not shown). Consequently, it is likely that both forms are present under the normal assay conditions, and it is possible that both are relevant to IDO inhibition as was witnessed with **13** and **14**.

Analysis of compounds **31**, **36**, and **41** in the same cell-based assay used to analyze menadione showed an attenuation of their activity versus the isolated enzyme assay (Table 7). However, unlike menadione which demonstrated clear cellular cytotoxicity

Table 7. IC$_{50}$ Values of Pyranonaphthoquinones Tested in Cell-Based Assay

compd	IC$_{50}$ (μM)
31	69
36	6.8
41	87

(Figure 2a), compounds **31**, **36**, and **41** demonstrated minimal impact on cell viability at 100 μM after 24 h. Future studies will endeavor to improve the cell-based activity of the pyranonaphthoquinones.

Discussion

Focusing on the naphthoquinone core of the complex natural product annulin B, we have identified commercially available compounds with naphthoquinone core structures that display potent IDO inhibitory activity. Notably, some of these compounds were up to ~100-fold more potent than the commonly used IDO inhibitor 1MT. Reinforcing the definition of this series as a potentially important class of IDO inhibitors, the majority of high potency hits identified in a recently conducted screen of the NCI compound collection included either a naphthoquinone core or mimetic (unpublished results). We have established the applicability of IDO inhibition by compounds in this structural class to cancer treatment through *in vivo* evaluation of the representative bioactive compound menadione and followed with the development of novel pyranonapthoquinone-based IDO inhibitors exhibiting submicromolar potencies produced from commercially available materials in a short number of synthetic steps.

Although the antitumor properties of menadione have long been recognized, this is the first report to demonstrate that IDO inhibition is an important mechanism of action. Previous studies of menadione antitumor activity have focused on oxidative stress as the primary mechanism of action. Intracellular redox cycling of menadione is catalyzed by bioreductive enzymes such as NAD(P)H:quinone oxidoreductase 1 (NOQ1), NRH:quinone oxidoreductase 2 (NOQ2), and cytochrome P450 reductase. Additional studies have also implicated nitric oxide synthases,[45] which are potentially interesting insofar as NO is known to directly antagonize IDO activity.[46] Depletion of glutathione (GSH) through direct conjugate formation and active export has also been proposed as a mechanism for menadione-mediated cytotoxicity.[47] More recently, menadione has been suggested to act by disrupting signaling pathways as an alternative to biochemical cytotoxic mechanisms.[29] In particular, treatment with menadione has been correlated with changes in the expression of molecules involved in controlling cell cycle progression.[48] All of these proposed mechanisms of action are based on the assumption that the antitumor activity of menadione is mediated through direct cytotoxicity to the tumor target. However, we have demonstrated here that the dramatic suppression of B16-F10 tumor growth that was elicited by menadione treatment in wild type mice was completely abolished in T cell-deficient nude mice. These data argue against direct cytoxicity as the operative mechanism of action, instead implying that a T cell dependent, immune-mediated mechanism is crucial to the antitumor activity of menadione. In the B16-F10 tumor model, IDO is expressed not in the melanoma-derived tumor cells but rather in highly toleragenic, plasmacytoid dendritic cells (pDCs) within the tumor-draining lymph nodes.[33] Since the antitumor activity of menadione was also abolished in tumor-bearing, IDO nullizygous mice, where no IDO was present in the system, it is also evident that menadione must

inhibit IDO in order to manifest antitumor activity, providing genetic validation of the concept that IDO is an essential target of menadione.

Ingested phylloquinone (vitamin K1 produced by plants) is substantially converted to circulating menadione in humans.[49] As a vitamin K precursor, circulating menadione may be a significant source of menaquinone biosynthesis (vitamin K2 produced by bacteria and animals) in extra-hepatic tissues through uptake and prenylation. It remains to be determined whether levels of menadione achieved through dietary intake or supplementation of vitamin K are sufficient to have a meaningful effect on IDO activity. In a mouse lung tumor isograft model in which menaquinone supports metastasis through its role in the coagulation system (e.g., by impacting Factor X activation[50]), the pro-metastatic effect of menaquinone can be combated with compounds that target the regenerative vitamin K cycle such as warfarin, which inhibits the enzyme vitamin K epoxide reductase. Interestingly, warfarin has also been shown to block both the *in vitro* and *in vivo* conversion of menadione to menaquinone.[51,52] Taken together, this suggests that by inhibiting the conversion of endogenous menadione to menaquinone, anticoagulants could potentially leverage IDO inhibition by menadione while concomitantly interfering with the ability of menaquinone to support metastasis. Given the importance of both immune escape and metastasis in the pathophysiology of advanced cancers, further study in this area seems warranted.

One concern regarding the proposed mechanism of action of menadione was how the metabolism of this compound might affect its ability to inhibit IDO in cells. Menadione is sufficiently hydrophilic to be soluble in aqueous solution, but it also is sufficiently hydrophobic to diffuse across the plasma membrane.[53] Once menadione has entered a cell, it is rapidly conjugated to glutathione through nucleophilic addition to form **13** (quinone form) and **14** (hydroquinone form), which are no longer cell permeable and in fact are actively transported out of the cell.[30,54] Nevertheless, we found that the menadione−glutathione conjugated compounds **13** and **14** were no less potent inhibitors of IDO than menadione itself despite the large size of the conjugated glutathione moiety. Since **13/14** are actively transported out of the cell, counteracting this (e.g., by inhibiting the ATP-dependent pump responsible for removing glutathione-conjugated menadione) might increase intracellular retention, thereby lowering the effective antitumor dose and perhaps also mitigating glutathione depletion (a side effect implicated in endothelial barrier damage[31]). Although the synthetic inhibitors reported in this study can also undergo redox cycling similar to menadione, they are chemically incapable of conjugation with glutathione since they are tetra-substituted quinones.[55] Consequently, glutathione processing is irrelevant to the cellular chemistry of the pyranonaphthoquinone-based IDO inhibitors.

In this study, we have identified the pyranonaphthoquinone moiety as the IDO inhibitory pharmacophore in the complex natural product annulin B, but the mechanism by which this structure achieves inhibition remains somewhat unclear. The quinone core is clearly important for IDO inhibition and the quinone oxygen may be the iron-binding group seen in previous inhibitor designs, most notably β-carboline, 4-phenylimidazole, and dithiocarbamates. Quinones are one of nature's privileged structures, performing essential roles as biological oxidants, e.g. vitamin K, vitamin E, ubiquinone, and plastoquinone. The unique nature of IDO as an oxidoreductase that is inactive in the ferric state and its sensitivity to inhibition by H$_2$O$_2$,[56,57] combined with the oxidation potential of the quinone structure,

suggests that redox chemistry might be involved in the mechanism of inhibition. However, the absence of any correlation between inhibitor potency and the oxidation potential of the quinones (Table 1) tends to argue against such a mechanism as the primary basis for inhibition.

Indeed, the structure–activity relationships that we discovered in the preliminary screen (Table 1) and subsequent structural modifications (Tables 2–6) support a more complex interaction between IDO and the quinone-based inhibitors. Particularly intriguing in this regard is the potent IDO inhibitory activity exhibited by the menadione–glutathione conjugates **13** and **14** despite the fact that the hydroquinone could in theory replace ascorbic acid as a reductant, thereby activating IDO. There is strong evidence for phenols, such as in hydroquinone, to be monodentate ligands for iron,[58–64] in line with speculation that iron binding by this moiety is important for IDO inhibition. One possible interpretation of this model is that the quinone **13** may be acting as a prodrug for the hydroquinone **14** since, presumably, under the assay conditions some of the quinone is reduced by ascorbic acid/methylene blue to the hydroquinone. This hypothesis is consistent with the observation that **14** is a more potent IDO inhibitor than **13**.

Future experiments will endeavor to understand the role of the quinone structure as well as redox chemistry in the inhibition of IDO. Based on the structure–activity relationships in the pyranonaphthoquinones, structural complementarity between the inhibitor and IDO clearly has an important role in inhibition as well. Moreover, computational docking predicted binding at the active site and rationalized many of the successful structural modifications. The uncompetitive mode of inhibition displayed by the most potent inhibitors (**34**, **39**, and **50**) would normally point to allosteric binding and regulation; however, other IDO inhibitors with a similar mode of inhibition have been shown to actually bind at the active site. Detailed kinetic analysis may shed further light on the precise molecular mechanism of IDO inhibition by this class of compounds. In addition, studies will also focus on enhancing the cell-based potency of this intriguing and highly potent class of IDO inhibitors.

Experimental Section

General Procedures. All reactants and reagents were commercially available and were used without further purification unless otherwise indicated. Anhydrous CH_2Cl_2, benzene, and 2-propanol were obtained by distillation from calcium hydride under nitrogen. Anhydrous MeOH was obtained by distillation from Mg metal under nitrogen. All reactions were carried out under an inert atmosphere of argon or nitrogen unless otherwise indicated. Concentrated refers to the removal of solvent with a rotary evaporator at normal water aspirator pressure followed by further evacuation with a two-stage mechanical pump. Thin-layer chromatography was performed using silica gel 60 Å precoated glass or aluminum-backed plates (0.25 mm thickness) with fluorescent indicator, which were cut. Developed TLC plates were visualized with UV light (254 nm), iodine, or $KMnO_4$. Flash column chromatography was conducted with the indicated solvent system using normal-phase silica gel 60 Å, 230–400 mesh. Yields refer to chromatographically and spectroscopically pure (>95%) compounds, except as otherwise indicated. All new compounds were determined to be >95% pure by NMR, HPLC, and/or GC as indicted. Melting points were determined using an open capillary and are uncorrected. ^{1}H and ^{13}C NMR spectra were recorded at 300 and 75 MHz, respectively. Chemical shifts are reported in δ values (ppm) relative to an internal reference (0.05% v/v) of tetramethylsilane (TMS) for ^{1}H NMR and the solvent peak in ^{13}C NMR, except where noted. Peak splitting patterns in the ^{1}H NMR are reported as follows: s, singlet; d, doublet; t, triplet; q, quartet; m, multiplet; br, broad. ^{13}C experiments with the attached proton

test (APT) sequence have multiplicities reported as δ_u (up) for methyl and methine and δ_d (down) for methylene and quaternary carbons. Normal-phase HPLC (NP-HPLC) analysis was performed with UV detection at 254 nm and a 5 μm silica gel column (250–4.6 mm) eluted with 90:10 or 85:15 n-hexane/IPA at 0.5 or 1 mL/min. Reversed-phase HPLC (RP-HPLC) analysis was performed with UV detection at 254 nm and a 5 μm Eclipse XDB-C_8 column (250–4.6 mm) eluted with 50:50 solvent A/solvent B; solvent A, 40% acetonitrile in water; solvent B, 0.1 M ammonium acetate adjusted to pH 5.3 with glacial acetic acid. IR data were obtained with an FT-IR spectrometer. MS data were recorded with atmospheric pressure chemical ionization (APCI) or atmospheric pressure electrospray ionization (APESI) mode.

(S)-2-Amino-5-((R)-1-(carboxymethylamino)-3-(3-methyl-1, 4-dioxo-1,4-dihydronaphthalen-2-ylthio)-1-oxopropan-2-ylamino)-5-oxopentanoic Acid (13). Prepared according to the literature procedure[65] with a minor modification. To a solution of 2-methyl-1,4-naphthoquinone (200 mg, 1.16 mmol) in dimethyl sulfoxide (6 mL) and 95% ethanol (6 mL) at 0 °C was added L-glutathione (178 mg, 0.581 mmol) as a solution in water (2 mL). After the reaction mixture was stirred for 1 h, the reaction was diluted with ethyl acetate (50 mL) and filtered. The precipitate (220 mg) was boiled with water (30 mL) and filtered; the filtrate was diluted with ethanol (15 mL) and left undisturbed overnight. The precipitated product was isolated as a yellow solid (83 mg) in 30% yield, mp = 195–197 °C dec. The product has poor solubility in many solvents, which made it difficult to obtain NMR information: TLC R_f = 0.40 (30% H_2O/MeOH with 0.1% CF_3CO_2H); ^{1}H NMR (CDCl$_3$ + TFA) δ 10.99 (s, 1H), 8.49–8.07 (m, 2H), 7.86–7.78 (m, 4H), 4.84 (dd, 1H, J = 5.55, 2.75 Hz), 4.35 (m, 1H), 4.19 (d, 2H, J = 1.02 Hz), 3.46 (dd, 1H, J = 8.55, 5.58 Hz), 3.34 (dd, 1H, J = 7.68, 6.3 Hz), 2.83–2.87 (m, 2H), 2.45–2.36 (m, 2H), 2.40 (s, 3H); ^{13}C NMR (DMSO-d_6) δ_u 134.4, 134.2, 126.9, 126.5, 53.6, 15.6 (2C); δ_d 182.3, 180.8, 172.5, 171.4, 171.0, 170.6, 148.3, 145.3, 132.8, 131.8, 41.5, 35.6, 31.8, 26.9; IR (KBr) 3353, 1682, 1642, 1511 cm^{-1}; APESI-MS m/z 500 (M$^+$ + Na, 55), 478 (M$^+$ + 1, 100); RP-HPLC t_R = 6.14 min (50:50; solvent A/solvent B, 0.5 mL/min).

(S)-2-Amino-5-((R)-1-(carboxymethylamino)-3-(1,4-dihydroxy-3-methylnaphthalen-2-ylthio)-1-oxopropan-2-ylamino)-5-oxopentanoic Acid (14). Prepared according to the literature procedure[65] with a minor modification. To a solution of 2-methyl-1,4-naphthoquinone (100 mg, 0.581 mmol) under nitrogen in 95% ethanol (10 mL) at 0 °C was added L-glutathione (178 mg, 0.581mmol) as a solution in water (2 mL). After being stirred overnight at rt, the precipitated product was filtered and washed with water. The crude product (210 mg) was boiled with water (2 – 20 mL) and filtered while hot to afford the product as a violet solid in 57% yield: mp = 216–217 °C dec; TLC R_f = 0.40 (30% H_2O/MeOH with 0.1% CF_3CO_2H); ^{1}H NMR (DMSO-d_6) δ 8.51 (d, 1H, J = 7.35 Hz), 8.38 (s, 1H), 7.98–7.94 (m, 2H), 7.35–7.24 (m, 2H), 4.12 (m, 1H), 3.51 (d, 2H, J = 4.5 Hz), 3.32–3.25 (m, 1H), 2.90–2.74 (m, 2H), 2.33 (s, 3H), 2.22–2.07 (m, 2H), 1.82 (m, 2H); ^{13}C NMR (DMSO-d_6) δ_u 126.3, 124.7, 122.7, 121.9, 53.2, 52.8, 14.9; δ_d 172.2, 171.0, 170.8, 170.7, 148.8, 142.5, 127.1, 123.0, 122.1, 113.1, 41.2, 37.5, 31.5, 26.7; IR (KBr) 3410, 3350, 1687, 1629, 1512 cm^{-1}; APESI-MS m/z 502 (M$^+$ + Na, 15), 480 (M$^+$ + 1, 100); RP-HPLC t_R = 6.06 min (50:50; solvent A/solvent B, 0.5 mL/min).

8-Methoxy-2-(phenylamino)-1,4-naphthaquinone. Prepared from 5-methoxy-1,4-naphthoquinone[66] according to the literature procedure[67] in 77% yield: mp = 150–151 °C (lit mp 152 °C); TLC R_f = 0.45 (10% MeOH/CHCl$_3$); ^{1}H NMR (CDCl$_3$) δ 7.78 (dd, 1H, J = 6.58, 1.11 Hz), 7.71–7.66 (m, 2H), 7.43–7.38 (m, 2H), 7.27–7.17 (m, 3H), 6.35 (s, 1H), 4.03 (s, 3H); ^{13}C NMR (CDCl$_3$) δ_u 136.3, 129.8, 125.7, 122.9, 119.2, 116.4, 102.0, 56.6; δ_d 183.7, 180.4, 160.4, 145.9, 137.9, 135.7, 118.3; IR (KBr) 3302, 3275, 1670, 1616 cm^{-1}.

2-Hydroxy-8-methoxy-1,4-naphthoquinone (22[68]). A mixture of 8-methoxy-2-(phenylamino)-1,4-naphthaquinone (0.500 g, 1.79 mmol) was heated to reflux for 5 h in concd HCl (15 mL). The reaction mixture was allowed to cool to rt, diluted with water (20

mL), and extracted with CHCl$_3$. The organic extract was dried (Na$_2$SO$_4$) and concentrated to afford a brownish solid: 325 mg in 89% yield; mp = 202–207 °C dec (lit.[68] mp = 211–214 °C dec; TLC R_f = 0.18 (10% MeOH/CHCl$_3$); ^{1}H NMR (CDCl$_3$) δ 7.80–7.71 (m, 3H), 7.28 (d, 1H, J = 1.23 Hz), 6.29 (s, 1H), 4.04 (s, 3H); ^{13}C NMR (CDCl$_3$) δ$_u$ 137.0, 119.7, 117.1, 108.7, 56.7; δ$_d$ 184.9, 180.3, 160.6, 157.0, 135.5; IR (KBr) 3206, 1662 cm^{-1}.

2,8-Dihydroxy-1,4-naphthoquinone (21). Prepared from **22** according to the literature procedure[67] in 73% yield: mp = 214–216 °C dec (lit.[67] mp = 210–215 °C dec; TLC R_f = 0.33(20% MeOH/ CHCl$_3$); ^{1}H NMR (CDCl$_3$ + CD$_3$OD) δ 7.67–7.57 (m, 2H), 7.21 (dd, 1H, J = 6.33, 1.62 Hz), 6.23 (s, 1H); ^{13}C NMR (CDCl$_3$ + CD$_3$OD) δ$_u$ 137.2, 123.3, 118.7, 111.7; δ$_d$ 185.9, 185.1, 161.3, 159.2, 132.4, 113.8.

General Procedure for the Synthesis of Pyranonaphtho-quinones by the 6π Electrocyclization Reaction. A solution of the appropriate 1,4-naphthoquinone (1.00 mmol) and α,β-unsaturated aldehyde (1.25 mmol), β-alanine (0.15 mmol), and acetic acid (6.0 mmol) in benzene (15 mL) was heated to reflux for 18 h. The reaction mixture was then concentrated *in vacuo*. Flash chromatography afforded the desired products.

2,2-Dimethyl-2H-benzo[g]chromene-5,10-dione (23). Pyranonaphthoquinone **23** was synthesized from 2-hydroxy-1,4-naphthoquinone **7** and 3-methylcrotonaldehyde according to the general procedure to yield 68%: mp = 142–143 °C (lit. mp = 145–146 °C). The product matched previously reported analytical data in the literature.[41]

Methyl 2-Methyl-5,10-dioxo-5,10-dihydro-2H-benzo[g]chromene-2-carboxylate (24). Pyranonaphthoquinone **24** was synthesized from 2-hydroxy-1,4-naphthoquinone **7** and fumaraldehydic acid methyl ester[69,70] according to the general procedure to afford **24** as a yellow solid in 22% yield: mp = 131–132 °C; TLC R_f = 0.43 (20% EtOAc/ hexanes); ^{1}H NMR (CDCl$_3$) δ 8.14–8.08 (m, 2H), 7.76–7.70 (m, 2H), 6.79 (d, 1H, J = 9.84 Hz), 5.88 (d, 1H, J = 9.84 Hz), 3.77 (s, 3H), 1.84 (s, 3H); ^{13}C NMR (CDCl$_3$) δ$_u$ 134.3, 133.7, 126.6, 126.5, 126.2, 118.0, 53.3, 25.5; δ$_d$ 181.8, 178.9, 170.8, 152.6, 131.6, 131.5, 117.9, 81.1; IR (KBr) 1749, 1671, 1651 cm^{-1}; APCI-MS m/z 284 (M$^+$, 100); NP-HPLC t_R = 7.1 min (85:15; n-hexane/IPA, 0.5 mL/ min).

6-Hydroxy-2,2-dimethyl-2H-benzo[g]chromene-5,10-dione (25). Pyranonaphthoquinone **25** was synthesized from 2,5-dihydroxy-1,4-naphthoquinone **15**[71] and 3-methylcrotonaldehyde according to the general procedure to afford **25** as an orange-red solid in 69% yield: mp = 159–160 °C (lit.[72] mp = 156–158 °C); TLC R_f = 0.65 (20% EtOAc/hexanes); ^{1}H NMR (CDCl$_3$) δ 12.2 (s, 1H), 7.61 (dd, 1H, J = 6.18, 1.26 Hz), 7.53 (t, 1H, J = 8.22 Hz), 7.22 (dd, 1H, J = 7.08, 1.26 Hz), 6.60 (d, 1H, J = 10.02 Hz), 5.73 (d, 1H, J = 10.05 Hz), 1.56 (s, 6H); ^{13}C NMR (CDCl$_3$)δ$_u$ 135.5, 130.9, 125.1, 119.3, 114.7, 28.6; δ$_d$ 187.6, 179.3, 161.3, 153.2, 131.6, 117.7, 113.8, 81.1; IR (KBr) 3452, 1671, 1620 cm^{-1}; APCI-MS m/z 258 (M$^+$ + 2, 15), 257 (M$^+$ + 1, 100); NP-HPLC t_R = 7.4 min (85:15; n-hexane/IPA, 0.5 mL/min).

6-Methoxy-2,2-dimethyl-2H-benzo[g]chromene-5,10-dione (26). Pyranonaphthoquinone **26** was synthesized from 2-hydroxy-5-methoxy-1,4-naphthoquinone **16**[71] and 3-methylcrotonaldehyde according to the general procedure to afford **26** as a yellow solid in 76% yield: mp = 126–127 °C; TLC R_f = 0.45 (40% EtOAc/ hexanes); ^{1}H NMR (CDCl$_3$)δ 7.78 (dd, 1H, J = 6.57, 1.08 Hz), 7.61 (t, 1H, J = 8.40 Hz), 7.30 (d, 1H, J = 0.90 Hz), 6.67 (d, 1H, J = 9.96 Hz), 5.72 (d, 1H, J = 9.99 Hz), 4.0 (s, 3H), 1.53 (s, 6H); ^{13}C NMR (CDCl$_3$) δ$_u$ 134.3, 131.4, 119.2, 118.6, 116.0, 56.7, 28.4; δ$_d$ 181.6, 180.2, 159.7, 150.8, 133.9, 119.5, 119.4, 79.9; IR (KBr) 1716, 1670, 1644 cm^{-1}; APCI-MS m/z 271 (M$^+$ + 1, 25), 270 (M$^+$, 100); NP-HPLC t_R = 11.8 min (85:15; n-hexane/IPA, 0.5 mL/min).

7-Hydroxy-2,2-dimethyl-2H-benzo[g]chromene-5,10-dione (27). Pyranonaphthoquinone **27** was synthesized from 2,6-dihydroxy-1,4-naphthoquinone **17**[73] and 3-methylcrotonaldehyde according to the general procedure to afford **27** as an orange-red solid in 71% yield: mp = 195 °C dec; TLC R_f = 0.50 (5% MeOH/CHCl$_3$); ^{1}H NMR (CDCl$_3$ + CD$_3$OD) δ 7.96 (dd, 1H, J = 6.09, 2.40 Hz), 7.38 (d, 1H, J = 1.83 Hz), 7.05 (dd, 1H, J = 6.27, 2.19 Hz), 6.59 (dd, 1H, J = 7.89, 2.1 Hz), 5.67 (d, 1H, J = 9.99 Hz), 1.54 (s, 3H); ^{13}C NMR (CDCl$_3$ + CD$_3$OD) δ$_u$ 130.3, 129.5, 120.2, 115.4, 112.7, 28.4; δ$_d$ 182.6, 179.1, 163.2, 153.3, 134.0, 124.0, 117.5, 80.8. IR (KBr) 3343, 3246, 1738, 1660, 1630 cm^{-1}; APCI-MS m/z 256 (M$^+$, 15), 255 (M$^+$ − 1, 100); NP-HPLC t_R = 8.4 min (85:15; n-hexane/ IPA, 0.5 mL/min).

7-Methoxy-2,2-dimethyl-2H-benzo[g]chromene-5,10-dione (28). Pyranonaphthoquinone **28** was synthesized from 2-hydroxy-6-methoxy-1,4-naphthoquinone **18**[73] and 3-methylcrotonaldehyde according to the general procedure to afford **28** as a yellow solid in 71% yield: TLC R_f = 0.43 (20% EtOAc/hexanes); ^{1}H NMR (CDCl$_3$) δ 8.02 (d, 1H, J = 8.61 Hz), 7.53 (s, 1H), 7.12 (dd, 1H, J = 6.06, 2.25 Hz), 6.63 (d, 1H, J = 9.96 Hz), 5.67 (d, 1H, J = 9.99 Hz), 3.93 (s, 3H), 1.54 (s, 6H); ^{13}C NMR (CDCl$_3$) δ$_u$ 130.4, 129.0, 119.4, 115.7, 110.4, 56.1, 28.6; δ$_d$ 181.9, 179.1, 164.6, 153.1, 134.1, 125.2, 117.7, 80.7; IR (KBr) 1663, 1646 cm^{-1}; APCI-MS m/z 272 (M$^+$ + 2, 20), 271 (M$^+$ + 1, 100); NP-HPLC t_R = 8.4 min (90:10; n-hexane/IPA, 0.5 mL/min).

8-Hydroxy-2,2-dimethyl-2H-benzo[g]chromene-5,10-dione (29). Pyranonaphthoquinone **29** was synthesized from 2,7-dihydroxy-1,4-naphthoquinone **19**[73] and 3-methylcrotonaldehyde according to the general procedure to afford a 75% yield of **29**, an orange-red solid: mp = 206–210 °C dec; TLC R_f = 0.50 (5% MeOH/CHCl$_3$); ^{1}H NMR (CDCl$_3$) δ 7.94 (d, 1H, J = 8.46 Hz), 7.42 (d, 1H, J = 2.4 Hz), 7.10 (dd, 1H, J = 6.03, 2.43 Hz), 6.62 (d, 1H, J = 9.96 Hz), 5.74 (d, 1H, J = 9.99 Hz), 1.54 (s, 6H); ^{13}C NMR (CDCl$_3$ + CD$_3$OD) δ$_u$ 131.2, 129.1, 120.9, 115.7, 112.6, 28.3; δ$_d$ 181.7, 180.7, 162.3, 152.2, 133.5, 123.9, 118.0, 80.3; IR (KBr) 3354, 1673, 1638, 1570 cm^{-1}; APCI-MS m/z 256 (M$^+$, 20), 255 (M$^+$ − 1, 100); NP-HPLC t_R = 8.6 min (85:15; n-hexane/IPA, 0.5 mL/min).

8-Methoxy-2,2-dimethyl-2H-benzo[g]chromene-5,10-dione (30). Pyranonaphthoquinone **30** was synthesized from 2-hydroxy-7-methoxy-1,4-naphthoquinone **20**[73] and 3-methylcrotonaldehyde according to the general procedure to afford **30** as a yellow solid in 72% yield. mp=130 °C. TLC R_f = 0.43 (20% EtOAc/Hexanes); ^{1}H NMR (CDCl$_3$) δ 8.02 (d, 1H, J = 8.58 Hz), 7.53 (d, 1H, J = 2.31 Hz), 7.15 (dd, 1H, J = 6.09, 2.49 Hz), 6.64 (d, 1H, J = 9.96 Hz), 5.70 (d, 1H, J = 9.96 Hz), 3.93 (s, 3H), 1.54 (s, 6H); ^{13}C NMR (CDCl$_3$) δ$_u$ 131.1, 128.8, 120.2, 115.9, 110.2, 56.1, 28.5; δ$_d$181.5, 180.1, 163.9, 152.4, 133.7, 125.1, 118.0, 80.4. IR (KBr) 1673, 1641, 1595, 1578 cm^{-1}; APCI-MS m/z 271 (M$^+$ + 1, 20), 270 (M$^+$, 100); NP-HPLC t_R = 8.0 min (85:15; n-hexane/IPA, 0.5 mL/min).

9-Hydroxy-2,2-dimethyl-2H-benzo[g]chromene-5,10-dione (31). Pyranonaphthoquinone **31** was synthesized from 2,8-dihydroxy-1,4-naphthoquinone **21** and 3-methylcrotonaldehyde according to the general procedure to afford **31** as an orange solid in 56% yield: mp = 155–157 °C (lit.[72] mp = 160–165 °C; lit.[74] mp = 143.5–145.5 °C dec); TLC R_f = 0.57 (25% EtOAc/hexanes); ^{1}H NMR (CDCl$_3$) δ 11.86 (s, 1H), 7.62–7.54 (m, 2H), 7.19 (dd, 1H, J = 5.70, 1.95 Hz), 6.61 (d, 1H, J = 10.02 Hz), 5.72 (d, 1H, J = 10.02 Hz), 1.55 (s, 6H); ^{13}C NMR (CDCl$_3$)δ$_u$ 136.9, 131.5, 124.1, 119.2, 115.6, 28.6; δ$_d$ 184.9, 181.2, 161.7, 152.3, 131.7, 118.7, 114.7, 80.9; IR (KBr) 3418, 1641, 1624, 1577 cm^{-1}; APCI-MS m/z 257 (M$^+$ + 1, 15), 226 (M$^+$, 100); NP-HPLC t_R = 7.5 min (85:15; n-hexane/IPA, 0.5 mL/min).

9-Methoxy-2,2-dimethyl-2H-benzo[g]chromene-5,10-dione (32). Pyranonaphthoquinone **32** was synthesized from 2-hydroxy-8-methoxy-1,4-naphthoquinone **22** and 3-methylcrotonaldehyde according to the general procedure to afford **32** as a yellow solid in 52% yield: mp 135–136 °C (lit.[75] mp = 139.5–141.5 °C; lit.[76] mp = 132–134 °C); TLC R_f = 0.40 (40% EtOAc/hexanes); ^{1}H NMR (CDCl$_3$) δ 7.75 (dd, 1H, J = 6.81, 0.78 Hz), 7.63 (t, 1H, J = 8.19 Hz), 7.23 (d, 1H, J = 8.43 Hz), 6.60 (d, 1H, J = 9.93 Hz), 5.65 (d, 1H, J = 9.93), 3.98 (s, 3H), 1.52 (s, 6H); ^{13}C NMR (CDCl$_3$) δ$_u$ 135.2, 130.2, 119.2, 117.7, 115.5, 56.7, 28.5; δ$_d$181.8, 178.8, 160.0, 153.5, 134.2, 119.6, 116.2, 80.6. IR (KBr): 1734, 1671, 1644, 1583 cm^{-1}; APCI-MS m/z 272 (M$^+$ + 2, 15), 271 (M$^+$ + 1, 100); NP-HPLC t_R = 12.3 min (85:15; n-hexane/IPA, 0.5 mL/min).

2,2-Dimethyl-3,4-epoxy-2*H*-naphtho[2,3-*b*]pyran-5,10-dione (33). The compound was synthesized via the reported procedure[41] to afford a 62% yield: mp = 138–139 °C (lit.[41] mp 139–140 °C). The spectroscopic data matched the reported information in the literature.

5-Hydroxy-2,2-dimethyl-1a*H*-benzo[*g*]oxireno[2,3-*c*]chromene-4,9(2*H*,9b*H*)-dione (35). Alkene **31** (150 mg, 0.585 mmol) was dissolved in CH_2Cl_2, cooled to 0 °C, and treated with mCPBA (152 mg, 0.878 mmol).[77] The reaction was stirred overnight at 0 °C. The solvent was removed *in vacuo*, and the crude product was chromatographed on silica gel to afford 84 mg of the epoxide **35** (53% yield), a yellow solid. Unreacted **31** was also recovered (48 mg). Characterization data for **35**: mp = 145–150 °C; yellow solid; TLC R_f = 0.33 (20% EtOAc/hexanes); ^{1}H NMR (CDCl$_3$) δ 11.74 (s, 1H), 7.70−7.61 (m, 2H), 7.27–7.22 (m, 1H), 4.33 (d, 1H, *J* = 4.41 Hz), 3.55 (d, 1H, *J* = 4.44 Hz), 1.71 (s, 3H), 1.46 (s, 3H); ^{13}C NMR (CDCl$_3$) δ_u 137.3, 124.3, 119.3, 61.6, 43.8, 25.3, 23.5; δ_d 184.1, 182.4, 162.1, 153.7, 131.9, 118.1, 114.5, 78.5; IR (KBr) 3421, 1644, 1612 cm^{-1}; APCI-MS *m/z* 305 (M$^+$ + MeOH, 100), 273 (M$^+$ + 1, 18).

General Procedure for the Epoxide-Opening Reaction. To a solution of epoxide **33** (256 mg, 1.0 mmol) in CH_2Cl_2 (10 mL) at 0 °C was added InCl$_3$ (0.05 mmol) followed by the addition of the appropriate nucleophile (4 equiv), and the reaction mixture was allowed to warm to rt and stirred for 1–3 h. The solvent was evaporated, and the crude product was chromatographed on silica to give the desired products. The relative stereochemical conformation was assigned based on the coupling constant of the methine protons in ^{1}H NMR and confirmed in the case of **34** by an X-ray crystal structure.

(3*S*,4*S* and 3*R*,4*R*)-4-(Benzylamino)-3-hydroxy-2,2-dimethyl-3,4-dihydro-2*H*-benzo[*g*]chromene-5,10-dione (36). Compound **36** was synthesized using the general procedure with benzylamine. Chromatographic separation afforded pure cis diastereomer **36** as a yellow solid in 53% yield: mp = 155 °C; TLC R_f = 0.30 (25% EtOAc/hexanes); ^{1}H NMR (CDCl$_3$) δ 8.07–8.01 (m, 2H), 7.72–7.63 (m, 2H), 7.45 −7.25 (m, 5H), 4.66 (br s, 1H), 3.99–3.88 (m, 3H), 3.72 (d, 1H, *J* = 4.47 Hz), 3.32 (br s, 1H), 1.67 (s, 3H), 1.25 (s, 3H); ^{13}C NMR (CDCl$_3$) δ_u 134.4, 133.5, 128.8, 128.5, 127.7, 126.6, 126.3, 66.9, 51.6, 24.8, 22.5; δ_d 185.7, 179.4, 155.0, 139.1, 132.4, 131.0, 117.3, 80.7, 51.9; IR (KBr) 3342, 1681, 1643, 1612, 1578 cm^{-1}; APCI-MS *m/z* 365 (M$^+$ + 2, 25), 364 (M$^+$ + 1, 100); NP-HPLC t_R = 7.6 min (85:15; *n*-hexane/IPA, 0.5 mL/min).

(3*R*,4*S* and 3*S*,4*R*)-4-(Benzylamino)-3-hydroxy-2,2-dimethyl-3,4-dihydro-2*H*-benzo[*g*]chromene-5,10-dione (37). Compound **37** was synthesized using the general procedure with benzylamine. Chromatographic separation afforded pure trans diastereomer **37** as a yellow solid in 37% yield: mp = 88–89 °C; TLC R_f = 0.50 (5% MeOH/CHCl$_3$); ^{1}H NMR (CDCl$_3$) δ 8.12–8.08 (m, 2H), 7.77–7.67 (m, 2H), 7.33–7.19 (m, 5H), 3.90 (d, 1H, *J* = 8.58 Hz), 3.79 (d, 1H, *J* = 8.55 Hz), 3.68 (d, 1H, *J* = 12.39 Hz), 3.53 (d, 1H, *J* = 12.36 Hz), 2.97 (br s, 1H), 1.65 (s, 3H), 1.31 (s, 3H); ^{13}C NMR (CDCl$_3$) δ_u 134.4, 133.5, 128.7, 128.4, 127.4, 126.7, 126.3, 70.0, 55.3, 26.1, 19.3; δ_d 184.9, 179.6, 155.5, 140.0, 132.4, 131.3, 119.5, 82.2, 48.3; IR (KBr) 3343, 1723, 1683, 1640, 1607, 1577 cm^{-1}; APCI-MS *m/z* 365 (M$^+$ + 2, 25), 364 (M$^+$ + 1, 100); NP-HPLC t_R = 8.0 min (85:15; *n*-hexane/IPA, 0.5 mL/min).

(3*S*,4*S* and 3*R*,4*R*)-4-(Allylamino)-3-hydroxy-2,2-dimethyl-3,4-dihydro-2*H*-benzo[*g*]chromene-5,10-dione (38). Compound **38** was synthesized using the general procedure with allylamine. Chromatographic separation afforded pure cis diastereomer **38** as a yellow solid in 58% yield: mp = 127–128 °;. TLC R_f = 0.60 (5% MeOH/CHCl$_3$); ^{1}H NMR (CDCl$_3$) δ 8.10–8.04 (m, 2H), 7.76–7.66 (m, 2H), 6.06–5.93 (m, 1H), 5.31 (dd, 1H *J* = 15.66, 1.51 Hz), 5.20 (dd, 1H, *J* = 8.97, 1.26 Hz), 3.94 (d, 1H, *J* = 4.53 Hz), 3.67 (d, 1H, *J* = 4.53 Hz), 3.43–3.40 (m, 2H), 1.67 (s, 3H), 1.28 (s, 3H); ^{13}C NMR (CDCl$_3$) δ_u 135.9, 134.3, 133.4, 126.6, 126.3, 66.8, 51.3, 24.8, 22.5; δ_d 185.6, 179.3, 155.1, 132.5, 131.0, 117.4, 117.2, 80.7, 50.1; IR (KBr) 3355, 1681, 1641, 1609 cm^{-1}; APCI-MS *m/z* 315 (M$^+$ + 2, 20), 314 (M$^+$ + 1, 100); NP-HPLC t_R = 10.0 min (85:15; *n*-hexane/IPA, 0.5 mL/min).

(3*R*,4*S* and 3*S*,4*R*)-4-(Allylamino)-3-hydroxy-2,2-dimethyl-3,4-dihydro-2*H*-benzo[*g*]chromene-5,10-dione (39). Compound **39** was synthesized using the general procedure with allylamine. Chromatographic separation afforded pure trans diastereomer **39** as a yellow solid in 29% yield: mp = 131–132 °C; TLC R_f = 0.60 (10% MeOH/CHCl$_3$); ^{1}H NMR (CDCl$_3$) δ 8.12–8.06 (m, 2H), 7.77–7.67 (m, 2H), 5.94–5.81 (m, 1H), 5.18 (dd, 1H *J* = 15.6, 1.53 Hz), 5.13 (dd, 1H, *J* = 8.91, 1.32 Hz), 3.88 (d, 1H, *J* = 8.64 Hz), 3.76 (d, 1H, *J* = 8.64 Hz), 3.20 (dd, 1H, *J* = 7.98, 5.70 Hz), 3.01 (dd, 1H, *J* = 7.59, 6.03 Hz), 1.65 (s, 3H), 1.32 (s, 3H); ^{13}C NMR (CDCl$_3$) δ_u 136.3, 134.5, 133.6, 126.7, 126.3, 70.1, 54.9, 26.2, 19.2; δ_d 184.9, 179.5, 155.5, 132.3, 131.2, 119.2, 116.7, 82.3, 46.6; IR (KBr) 3319, 3149, 1678, 1634, 1621 cm^{-1}; APCI-MS *m/z* 315 (M$^+$ + 2, 20), 314 (M$^+$ + 1, 100); NP-HPLC t_R = 10.5 min (85:15; *n*-hexane/IPA, 0.5 mL/min).

(3*S*,4*S*)-4-(Butylamino)-3-hydroxy-2,2-dimethyl-3,4-dihydro-2*H*-benzo[*g*]chromene-5,10-dione (40). Compound **40** was synthesized using the general procedure with allylamine. Chromatographic separation afforded pure cis diastereomer **40** as a yellow solid in 58% yield: mp = 120–121 °C; TLC R_f = 0.60 (5% MeOH/CHCl$_3$); ^{1}H NMR (CDCl$_3$) δ 8.11–8.05 (m, 2H), 7.76–7.66 (m, 2H), 3.85 (d, 1H, *J* = 4.50 Hz), 3.70 (d, 1H, *J* = 4.50 Hz), 2.86–2.68 (m, 2H), 1.68 (s, 3H), 1.62–1.38 (m, 4H), 1.29 (s, 3H), 0.96 (t, 3H, *J* = 7.11 Hz); ^{13}C NMR (CDCl$_3$) δ_u 134.4, 133.5, 126.6, 126.3, 67.0, 52.5, 24.9, 22.4, 14.2; δ_d 185.8, 179.5, 155.0, 132.5, 131.2, 117.3, 80.8, 47.6, 32.4, 20.6; IR (KBr) 3335, 3281, 1680, 1629, 1602, 1575 cm^{-1}; APCI-MS *m/z* 331 (M$^+$ + 2, 25), 330 (M$^+$ + 1, 100); NP-HPLC t_R = 10.07 min (85:15; *n*-hexane/IPA, 0.5 mL/min).

(3*R*,4*S* and 3*S*,4*R*)-4-(Butylamino)-3-hydroxy-2,2-dimethyl-3,4-dihydro-2*H*-benzo[*g*]chromene-5,10-dione (41). Compound **41** was synthesized using the general procedure with allylamine. Chromatographic separation afforded pure trans diastereomer **41** as a yellow solid in 16% yield: mp = 103–104 °C; TLC R_f = 0.60 (10% MeOH/CHCl$_3$); ^{1}H NMR (CDCl$_3$) δ 8.11–8.05 (m, 2H), 7.75–7.66 (m, 2H), 3.81 (d, 1H, *J* = 9.00 Hz), 3.72 (d, 1H, *J* = 8.97 Hz), 2.52–2.44 (m, 1H), 2.31–2.23 (m, 1H), 1.65 (s, 3H), 1.43–1.30 (m, 4H), 1.30 (s, 3H), 0.86 (t, 3H, *J* = 7.20 Hz); ^{13}C NMR (CDCl$_3$) δ_u 134.4, 133.5, 126.7, 126.3, 69.9, 55.1, 26.3, 18.9, 14.1; δ_d 184.9, 179.6, 155.5, 132.4, 131.4, 119.6, 82.2, 43.2, 32.9, 20.5; IR (KBr) 3210, 1681, 1637, 1612 cm^{-1}; APCI-MS *m/z* 331 (M$^+$ + 2, 20), 330 (M$^+$ + 1, 100); NP-HPLC t_R = 9.8 min (85:15; *n*-hexane/IPA, 0.5 mL/min).

(3*S*,4*S* and 3*R*,4*R*)-3-Hydroxy-2,2-dimethyl-4-morpholino-3,4-dihydro-2*H*-benzo[*g*]chromene-5,10-dione (42). Compound **42** was synthesized using the general procedure with morpholine. Chromatographic separation afforded pure cis diastereomer **42** as a yellow solid in 57% yield: mp = 103–104 °C; TLC R_f = 0.44 (5% MeOH/CHCl$_3$); ^{1}H NMR (CDCl$_3$) δ 8.09 (d, 2H, *J* = 7.59 Hz), 7.77–7.69 (m, 2H), 3.67 (t, 4H, *J* = 4.47 Hz), 3.57 (s, 2H), 3.06 (m, 2H), 2.94 (s, 1H), 2.65–2.58 (m, 2H), 1.64 (s, 3H), 1.34 (s, 3H); ^{13}C NMR (CDCl$_3$) δ_u 134.5, 133.4, 126.6, 71.7, 62.1, 26.4, 19.6; δ_d 184.9, 179.6, 155.9, 132.5, 131.1, 119.8, 81.9, 68.3, 50.7; IR (KBr) 3500, 2938, 2854, 2819, 1666, 1645, 1611, 1581 cm^{-1}; APCI-MS *m/z* 345 (M$^+$ + 2, 20), 344 (M$^+$ + 1, 100); NP-HPLC t_R = 13.3 min (85:15; *n*-hexane/IPA, 0.5 mL/min).

(3*R*,4*S* and 3*S*,4*R*)-3-Hydroxy-2,2-dimethyl-4-morpholino-3,4-dihydro-2*H*-benzo[*g*]chromene-5,10-dione (43). Compound **43** was synthesized using the general procedure with morpholine. Chromatographic separation afforded pure trans diastereomer **43** as a yellow solid in 14% yield: mp = 157–158 °C; TLC R_f = 0.70 (5% MeOH/CHCl$_3$); ^{1}H NMR (CDCl$_3$) δ 8.13–8.09 (m, 2H), 7.79–7.68 (m, 2H), 4.17 (s, 1H), 3.95 (d, 1H, *J* = 6.15 Hz), 3.73–3.64 (m, 5H), 2.99 (m, 2H), 2.73–2.66 (m, 2H), 1.51 (s, 3H), 1.44 (s, 3H); ^{13}C NMR (CDCl$_3$) δ_u 134.5, 133.6, 126.8, 126.6, 70.6, 56.6, 26.4, 22.2; δ_d 185.1, 179.3, 155.9, 132.1, 131.2, 118.3, 81.5, 67.9, 52.8; IR (KBr) 3487, 2990, 2852, 1679, 1638, 1578 cm^{-1}; APCI-MS *m/z* 345 (M$^+$ + 2, 25), 344 (M$^+$ + 1, 100); NP-HPLC t_R = 13.1 min (85:15; *n*-hexane/IPA, 0.5 mL/min).

(3S,4S and 3R,4R)-3-Hydroxy-4-methoxy-2,2-dimethyl-3,4-dihydro-2H-benzo[g]chromene-5,10-dione (44). Compound **44** was synthesized using the general procedure with methanol as previously described in the literature.[41] Chromatographic separation afforded pure cis diastereomer **44** in 54% yield: ^{1}H NMR (CDCl$_3$) δ 8.10–8.07 (m, 2H), 7.73–7.67 (m, 2H), 4.35 (d, 1H, J = 3.0 Hz), 3.91 (br s, 1H), 3.64 (s, 3H), 1.88 (br s, 1H), 1.55 (s, 3H), 1.50 (s, 3H). The analytical data matched the literature report.[41]

(3R,4S and 3S,4R)-3-Hydroxy-4-methoxy-2,2-dimethyl-3,4-dihydro-2H-benzo[g]chromene-5,10-dione (45). Compound **45** was synthesized using the general procedure with methanol as previously described in the literature.[41] Chromatographic separation afforded pure trans diastereomer **45** in 28% yield: ^{1}H NMR (CDCl$_3$) δ 8.21–8.05 (m,2H), 7.79–7.73 (m, 2H), 7.01 (d, 1H, J = 2.49 Hz), 4.29 (d, 1H, J = 4.89 Hz), 3.17 (s, 3H), 2.02 (d, 1H, J = 5.61 Hz), 1.49 (s, 3H), 1.44 (s, 3H). The analytical data matched the literature report.[41]

(3S,4S and 3R,4R)-4-(Benzyloxy)-3-hydroxy-2,2-dimethyl-3,4-dihydro-2H-benzo[g]chromene-5,10-dione (46). Compound **46** was synthesized using the general procedure with benzyl alcohol. Chromatographic separation afforded pure trans diastereomer **46** as a yellow solid in 48% yield: mp = 149–150 °C; TLC R_f = 0.30 (20% EtOAc/hexanes); ^{1}H NMR (CDCl$_3$) δ 8.05 (t, 2H, J = 7.50 Hz), 7.72–7.62 (m, 2H), 7.38–7.26 (m, 5H), 4.97 (d, 1H, J = 11.28 Hz), 4.84 (d, 1H, J = 11.30 Hz), 4.60 (d, 1H, J = 2.88 Hz), 3.85 (d, 1H, J = 2.94 Hz), 2.18 (s, 1H), 1.55 (s, 3H), 1.52 (s, 3H); ^{13}C NMR (CDCl$_3$) δ$_u$ 134.5, 133.3, 128.6, 128.1, 128.0, 126.6, 126.4, 72.4, 71.5, 24.0, 23.7; δ$_d$ 184.4, 180.1, 154.0, 138.6, 132.5, 131.2, 118.4, 81.4, 74.0; IR (KBr) 3481, 1635, 1591 cm^{-1}; APCI-MS m/z 366 (M$^+$ + 2, 10), 365 (M$^+$ + 1, 35), 257 (100); NP-HPLC t_R = 8.3 min (85:15; n-hexane/IPA, 0.5 mL/min).

(3R,4S and 3S,4R)-4-(Benzylthio)-3-hydroxy-2,2-dimethyl-3,4-dihydro-2H-benzo[g]chromene-5,10-dione (47). Compound **47** was synthesized using the general procedure with benzyl mercaptan. Chromatographic separation afforded pure cis diastereomer **47** as a yellow solid in 45% yield: mp = 151 °C; TLC R_f = 0.30 (25% EtOAc/hexanes); ^{1}H NMR (CDCl$_3$) δ 8.06–8.01 (m, 2H), 7.72–7.61 (m, 2H), 7.41–7.15 (m, 5H), 4.30 (d, 1H, J = 13.08 Hz), 4.05 (d, 1H, J = 13.08 Hz), 3.65–3.58 (m, 2H), 2.32 (d, 1H, J = 3.96 Hz), 1.49 (s, 3H), 1.29 (s, 3H); ^{13}C NMR (CDCl$_3$) δ$_u$ 134.3, 133.3, 129.4, 128.9, 127.6, 126.5, 126.4, 74.5, 42.4, 25.5, 20.8; δ$_d$ 183.9, 179.5, 153.2, 138.6, 132.6, 131.1, 121.4, 81.1, 38.8; IR (KBr) 3453, 1673, 1645, 1603, 1574 cm^{-1}; APCI-MS m/z 382 (M$^+$ + 2, 25), 381 (M$^+$ + 1, 100); NP-HPLC t_R = 7.5 min (85:15; n-hexane/IPA, 0.5 mL/min).

(3S,4S and 3R,4R)-4-(Benzylthio)-3-hydroxy-2,2-dimethyl-3,4-dihydro-2H-benzo[g]chromene-5,10-dione (48). Compound **48** was synthesized using the general procedure with benzyl mercaptan. Chromatographic separation afforded pure trans diastereomer **48** as a yellow solid in 27% yield: mp = 127–128 °C; TLC R_f = 0.46 (20% EtOAc/hexanes); ^{1}H NMR (CDCl$_3$) δ 8.15–8.07 (m, 2H), 7.77–7.66 (m, 2H), 7.45–7.26 (m, 5H), 4.26 (d, 1H, J = 12.69 Hz), 4.14 (d, 1H, J = 12.69 Hz), 4.09 (d, 1H, J = 6.15 Hz), 3.74 (dd, 1H, J = 6.15, 3.39 Hz), 2.88 (d, 1H, J = 9.57 Hz), 1.50 (s, 3H), 1.24 (s, 3H); ^{13}C NMR (CDCl$_3$) δ$_u$ 134.4, 133.5, 129.5, 129.1, 127.9, 126.7, 126.5, 69.6, 42.6, 26.5, 20.3; δ$_d$ 183.8, 179.6, 152.9, 138.1, 132.5, 131.2, 121.8, 81.7, 40.2; IR (KBr) 3421, 1681, 1645, 1609, 1574 cm^{-1}; APCI-MS m/z 382 (M$^+$ + 2, 25), 381 (M$^+$ + 1, 100); NP-HPLC t_R = 8.0 min (85:15; n-hexane/IPA, 0.5 mL/min).

(3S,4S)-4-(Benzylamino)-3,6-dihydroxy-2,2-dimethyl-3,4-dihydro-2H-benzo[g]chromene-5,10-dione (49). Alkene **25** (50 mg, 0.195 mmol) was dissolved in CH$_2$Cl$_2$ (3 mL), cooled to 0 °C, and treated with mCPBA (50.0 mg, 0.290 mmol).[77] The reaction was stirred overnight at 0 °C. The solvent was removed *in vacuo*, and the crude solid epoxide product **34** was treated with benzylamine (0.975 mmol) in 2-propanol (3 mL). After the reaction was stirred for 30 min, the solvent was removed *in vacuo*, and the crude was purified by preparative TLC to afford 25 mg of product **49** in 34% yield: TLC R_f = 0.30 (25% EtOAc/hexanes); ^{1}H NMR (CDCl$_3$) δ 12.27 (s, 1H), 7.64–7.22 (m, 8H), 4.01–3.90 (m, 3H), 3.72 (d, 1H,

J = 4.21 Hz), 1.67 (s, 3H), 1.26 (s, 3H); ^{13}C NMR (CDCl$_3$) δ$_u$ 135.6, 128.9, 128.5, 127.8, 125.5, 119.6, 66.9, 51.4, 24.8, 22.6; δ$_d$ 191.5, 161.4, 155.9, 139.0, 131.1, 116.9, 81.2, 52.0; APCI-MS m/z 381(M$^+$ + 2, 20), 380 (M$^+$ + 1, 100); NP-HPLC t_R = 4.0 min (85:15; n-hexane/IPA, 1 mL/min).

(3S,4S)-4-(Benzylamino)-3,9-dihydroxy-2,2-dimethyl-3,4-dihydro-2H-benzo[g]chromene-5,10-dione (50). To a solution of epoxide **35** (50 mg, 0.184 mmol) in 2-propanol (5 mL) at rt was added benzylamine (0.734 mmol), and the reaction mixture was stirred for 30 min. The solvent was removed *in vacuo*, and the crude was chromatographed on silica gel to afford the desired cis isomer **50** as a yellow solid (40 mg, 58% yield): mp = 140–141 °C; TLC R_f = 0.30 (20% EtOAc/hexanes); ^{1}H NMR (CDCl$_3$) δ 11.70 (s, 1H), 7.59–7.18 (m, 8H), 3.99–3.88 (m, 3H), 3.71 (d, 1H, J = 4.26 Hz), 1.67 (s, 3H), 1.26 (s, 3H); ^{13}C NMR (CDCl$_3$) δ$_u$ 137.1, 128.9, 128.6, 127.8, 124.0, 119.2, 66.9, 51.7, 24.9, 22.6; δ$_d$ 184.8, 184.2, 161.9, 154.8, 139.0, 132.5, 118.1, 114.2, 81.0, 51.9; IR (KBr) 3340, 1636, 1603 cm^{-1}; APCI-MS m/z 381(M$^+$ + 2, 25), 380 (M$^+$ + 1, 100); NP-HPLC t_R = 7.8 min (85:15; n-hexane/IPA, 0.5 mL/min).

2,2-Dimethyl-3,4-dihydro-2H-benzo[g]chromene-5,10-dione (51). Prepared according to the literature procedure[41] to afford 92% yield of **51**: mp = 114–115 °C (lit.[41] mp = 113–114 °C); ^{1}H NMR (CDCl$_3$) δ 8.10–8.05 (m, 2H), 7.73–7.63 (m, 2H), 2.62 (t, 2H, J = 6.66 Hz), 1.83 (t, 2H, J = 6.60 Hz), 1.44 (s, 6H). The product matched previously reported analytical data in the literature.[41]

(3R,4S and 3S,4R)-3-Bromo-4-hydroxy-2,2-dimethyl-3,4-dihydro-2H-benzo[g]chromene-5,10-dione (52). Prepared according to the literature procedure[41] to afford 26% yield of **52**: mp = 174–175 °C (lit.[41] mp = 176 °C); ^{1}H NMR (CDCl$_3$) δ 8.14–8.09 (m, 2H), 7.79–7.72 (m, 2H), 5.09 (dd, 1H, J = 5.31, 1.62 Hz), 4.16 (d, 1H, J = 6.93 Hz), 4.04 (d, 1H, J = 1.5 Hz), 1.73 (s, 3H), 1.58 (s, 3H). The product matched previously reported analytical data in the literature.[41]

(3S,4S and 3R,4R)-3,4-Dihydroxy-2,2-dimethyl-3,4-dihydro-2H-benzo[g]chromene-5,10-dione (53). Prepared according to the literature procedure[41] to afford 53% yield of **53**: mp = 168–169 °C; TLC R_f = 0.20 (25% EtOAc/hexanes); ^{1}H NMR (CDCl$_3$) δ 8.12–8.06 (m, 2H), 7.77–7.68 (m, 2H), 5.01 (d, 1H, J = 4.47 Hz), 4.80 (s, 1H), 3.84 (d, 1H, J = 4.44 Hz), 3.12 (s, 1H), 1.63 (s, 3H), 1.37 (s, 3H); ^{13}C NMR (CDCl$_3$) δ$_u$ 134.5, 133.9, 126.9, 126.2, 70.1, 63.0, 23.9, 23.6; δ$_d$ 187.2, 179.4, 154.1, 132.2, 131.3, 117.2, 82.0; NP-HPLC t_R = 9.9 min (85:15; n-hexane/IPA, 1 mL/min).

Biochemical Assays. Recombinant human IDO was expressed and purified as described.[78] The IC$_{50}$ inhibition assays were performed in a 96-well microtiter plate as described by Littlejohn et al.[78] with some modification. Briefly, the reaction mixture contained 50 mM potassium phosphate buffer (pH 6.5), 40 mM ascorbic acid, 400 μg/mL catalase, 20 μM methylene blue, and ~27 nM purified recombinant IDO per reaction. The reaction mixture was added to the substrate, L-tryptophan (L-Trp), and the inhibitor. The inhibitors were serially diluted in 3-fold increments ranging from 100 μM to 1.69 nM, and the L-Trp was tested at 100 μM (K_m = 80 μM). The reaction was carried out at 37 °C for 60 min and stopped by the addition of 30% (w/v) trichloroacetic acid. The plate was incubated at 65 °C for 15 min to convert *N*-formylkynurenine to kynurenine and was then centrifuged at 1250g for 10 min. Lastly, 100 μL of supernatant from each well was transferred to a new 96-well plate and mixed at equal volume with 2% (w/v) *p*-dimethylaminobenzaldehyde in acetic acid. The yellow color generated from the reaction with kynurenine was measured at 490 nm using a Synergy HT microtiter plate reader (Bio-Tek, Winooski, VT). The data were analyzed using Graph Pad Prism 4 software (Graph Pad Software Inc., San Diego, CA). For the K_i determinations of **36**, **41**, and **50**, tryptophan concentrations were varied from 25 to 200 μM (K_m= 42 μM), and inhibitor concentrations were varied between 3-fold above and below the calculated IC$_{50}$. Otherwise, reaction conditions were exactly as described above. Data were analyzed with the Enzyme Kinetics module in SigmaPlot version 10.

Cell-Based IDO Inhibition and Cytotoxicity Assays. T-REx cells containing an inducible human *INDO* cDNA[79] were seeded in a 96-well plate at a density of 20000 cells per well in 100 μL of DMEM + 10% FBS. IDO expression was induced for 72 h by the addition of 100 μL of media containing 20 ng/mL doxycycline. The media was then discarded, the wells rinsed once, and serial dilutions of menadione in 200 μL of phenol red-free DMEM + 10% FBS was added in triplicate and incubated for 18 h. The reaction was stopped by the addition of 40 μL of 50% (w/v) TCA to each well, and the cells were fixed by incubating for 1 h at 4 °C.

To Assess IDO Activity. Following the TCA fixation step, the supernatants were transferred to a round-bottomed 96-well plate and incubated at 65 °C for 15 min. The plates were then centrifuged at 1250*g* for 10 min, and 100 μL of clarified supernatant was transferred to a new flat-bottomed 96-well plate and mixed at equal volume with 2% (w/v) *p*-dimethylaminobenzaldehyde in acetic acid. The yellow reaction was measured at 490 nm using a Synergy HT microtiter plate reader (Bio-Tek, Winooski,VT).

To Assess Cell Viability. The TCA-fixed cells remaining in the 96-well plate following transfer of the media were processed essentially as described.[80] Fixed cells were washed four times in tap water, blotted, air-dried, and treated for 15 min at room temperature with 100 μL of 0.4% (w/v) sulfarhodamine B (SRB) (Sigma-Aldrich, St. Louis, MO) prepared in 1% acetic acid. Wells were then rinsed four times in 1% acetic acid, air-dried, and developed by adding 200 μL of 10 mM unbuffered Tris-HCl and incubating for 15 min at room temperature with gentle shaking. Staining intensity, proportional to cell number, was determined by reading the absorbance at 570 nm on a plate reader. Data were collected and analyzed using Excel software (Microsoft).

Tumor Formation and Drug Response. FVB-strain MMTV-*Neu* transgenic mice were obtained from the Jackson Laboratory. C57BL/6 and athymic NCr-*nu/nu* (nude mice) were obtained from NCI-Frederick. IDO knockout mice have previously been described.[81] Studies involving mice were approved by the institutional animal use committee of the Lankenau Institute for Medical Research. For autochthonous mammary gland tumor treatment studies, parous, FVB-strain MMTV-*Neu* mice expressing the wild type form of the rat *HER2/Neu* proto-oncogene were used as described.[14] B16-F10 melanoma-derived cell line isograft tumor challenge experiments were carried out as described.[4] Menadione administered to mice as a single agent at the nonlethal dose of 25 mg/kg q.d. did not result in any appreciable change in body weight over the treatment period. The combination of menadione + paclitaxel administered to MMTV-Neu mammary gland tumor-bearing mice did result in average weight loss of ~8%, however, a comparable degree of weight loss was observed in the taxol-alone treatment cohort and there was no indication that this was further exacerbated by menadione treatment. Graphing and statistical analysis of the data was performed using Prism 4 software (GraphPad Software Inc., San Diego, CA).

Computational Methods. Small Molecule Preparation. Molecules were constructed in MOE (MOE Molecular Operating Environment Chemical Computing Group, version 2005.06 Montreal Canada http//www.chemcomp.com/) and ionized using MOE's WashMDB function, and hydrogens were added. The small molecule conformation was minimized to a gradient of 0.01 in the MMFF94x force field[82,83] using a distance-dependent dielectric constant of 1.

Protein Preparation. Using the IDO crystal structure (PDB code 2D0T), hydrogen atoms were added, and tautomeric states and orientations of Asn, Gln, His residues were determined with Molprobity (http://molprobity.biochem.duke.edu/).[84,85] Hydrogens were added to crystallographic waters using MOE (MOE Molecular Operating Environment Chemical Computing Group, version 2005.06 Montreal Canada http//www.chemcomp.com/). The Amber99[86] force field in MOE was used, and iron was parametrized in the Fe^{3+} state. Dioxygen was not added to the iron. All hydrogens were minimized to an rms gradient of 0.01 holding the remaining heavy atoms fixed. A stepwise minimization followed for all atoms

using a quadratic force constant (100) to tether the atoms to their starting geometries; for each subsequent minimization, the force constant was reduced by a half-until zero.

Docking Calculations. The 2-[*N*-cyclohexylamino]ethanesulfonic acid and 4-phenyl-1-imidazole ligands were removed from the active site prior to docking. Preliminary docking calculations performed with annulin B were carried out using MolDock.[87] Gold (version 3.1)[88,89] and AutoDock (version 3.05)[90] were used with default parameters and reproduced the crystallographic position of 4-phenyl-1-imidazole binding to the heme. Docking of the napthquinone series of compounds using AutoDock and Gold produced a top scoring binding pose with a ketone oxygen within coordination distance to the heme iron.

Supporting Information Available: Copies of ^{1}H and ^{13}C NMR spectra and liquid chromatograms for compounds **13**, **14**, **24**−**32**, **36**−**43**, **46**−**50**, and **53**. Copies of ^{1}H and ^{13}C NMR spectra for **35**. Copies of ^{1}H NMR spectra for previously synthesized compounds **45**, **51**, and **52**. X-ray crystal structure of **36** and Hanes−Woolf plots for **36**, **41**, and **50**. This material is available free of charge via the Internet at http://pubs.acs.org.

References

(1) Dunn, G. P.; Bruce, A. T.; Ikeda, H.; Old, L. J.; Schreiber, R. D. Cancer immunoediting: from immunosurveillance to tumor escape. *Nat. Immunol.* **2002**, *3*, 991–8.

(2) Mellor, A. L.; Munn, D. H. IDO expression by dendritic cells: tolerance and tryptophan catabolism. *Nat. Rev. Immunol* **2004**, *4*, 762–74.

(3) Muller, A. J.; Scherle, P. A. Targeting the mechanisms of tumoral immune tolerance with small-molecule inhibitors. *Nat. Rev. Cancer* **2006**, *6*, 613–625.

(4) Hou, D. Y.; Muller, A. J.; Sharma, M. D.; DuHadaway, J.; Banerjee, T.; Johnson, M.; Mellor, A. L.; Prendergast, G. C.; Munn, D. H. Inhibition of indoleamine 2,3-dioxygenase in dendritic cells by stereoisomers of 1-methyl-tryptophan correlates with antitumor responses. *Cancer Res.* **2007**, *67*, 792–801.

(5) Muller, A. J.; Malachowski, W. P.; Prendergast, G. C. Indoleamine 2,3-dioxygenase in cancer: targeting pathological immune tolerance with small-molecule inhibitors. *Expert Opin. Ther. Targets* **2005**, *9*, 831–49.

(6) Sono, M.; Roach, M. P.; Coulter, E. D.; Dawson, J. H. Heme-Containing Oxygenases. *Chem. Rev.* **1996**, *96*, 2841–2888.

(7) Botting, N. P. Chemistry and Neurochemistry of the Kynurenine Pathway of Tryptophan Metabolism. *Chem. Soc. Rev.* **1995**, *24*, 401–12.

(8) Sono, M.; Hayaishi, O. The Reaction Mechanism of Indoleamine 2,3-Dioxygenase. *Biochem. Rev.* **1980**, *50*, 173–81.

(9) Sono, M.; Taniguchi, T.; Watanabe, Y.; Hayaishi, O. Indoleamine 2,3-dioxygenase. Equilibrium studies of the tryptophan binding to the ferric, ferrous, and CO-bound enzymes. *J. Biol. Chem.* **1980**, *255*, 1339–45.

(10) Kobayashi, K.; Hayashi, K.; Sono, M. Effects of tryptophan and pH on the kinetics of superoxide radical binding to indoleamine 2,3-dioxygenase studied by pulse radiolysis. *J. Biol. Chem.* **1989**, *264*, 15280–3.

(11) Cady, S. G.; Sono, M. 1-Methyl-DL-tryptophan, beta-(3-benzofuranyl)-DL-alanine (the oxygen analog of tryptophan), and beta-[3-benzo.(b)thienyl]-DL-alanine (the sulfur analog of tryptophan) are competi-

tive inhibitors for indoleamine 2,3-dioxygenase. *Arch. Biochem. Biophys.* **1991**, *291*, 326–33.

(12) Peterson, A. C.; Migawa, M. T.; Martin, M. J.; Hamaker, L. K.; Czerwinski, K. M.; Zhang, W.; Arend, R. A.; Fisette, P. L.; Ozaki, Y.; Will, J. A.; Brown, R. R.; Cook, J. M. Evaluation of functionalized tryptophan derivatives and related compounds as competitive inhibitors of indoleamine 2,3-dioxygenase. *Med. Chem. Res.* **1994**, *3*, 531–544.

(13) Gaspari, P.; Banerjee, T.; Malachowski, W. P.; Muller, A. J.; Prendergast, G. C.; DuHadaway, J.; Bennett, S.; Donovan, A. M. Structure-activity study of brassinin derivatives as indoleamine 2,3-dioxygenase inhibitors. *J. Med. Chem.* **2006**, *49*, 684–92.

(14) Muller, A. J.; DuHadaway, J. B.; Donover, P. S.; Sutanto-Ward, E.; Prendergast, G. C. Inhibition of indoleamine 2,3-dioxygenase, an immunoregulatory target of the cancer suppression gene Bin1, potentiates cancer chemotherapy. *Nat. Med.* **2005**, *11*, 312–9.

(15) Benner, S. A. Enzyme Kinetics and Molecular Evolution. *Chem. Rev.* **1989**, *89*, 789–806.

(16) Fersht, A. R. Catalysis, binding and enzyme-substrate complementarity. *Proc. R. Soc. London B Biol. Sci.* **1974**, *187*, 397–407.

(17) Amirkhani, A.; Heldin, E.; Markides, K. E.; Bergquist, J. Quantitation of tryptophan, kynurenine and kynurenic acid in human plasma by capillary liquid chromatography-electrospray ionization tandem mass spectrometry. *J Chromatogr. B Anal. Technol. Biomed. Life Sci.* **2002**, *780*, 381–7.

(18) Huengsberg, M.; Winer, J. B.; Gompels, M.; Round, R.; Ross, J.; Shahmanesh, M. Serum kynurenine-to-tryptophan ratio increases with progressive disease in HIV-infected patients. *Clin. Chem.* **1998**, *44*, 858–62.

(19) Laich, A.; Neurauter, G.; Widner, B.; Fuchs, D. More rapid method for simultaneous measurement of tryptophan and kynurenine by HPLC. *Clin. Chem.* **2002**, *48*, 579–81.

(20) Pereira, A.; Vottero, E.; Roberge, M.; Mauk, A. G.; Andersen, R. J. Indoleamine 2,3-dioxygenase inhibitors from the Northeastern Pacific Marine Hydroid Garveia annulata. *J. Nat. Prod.* **2006**, *69*, 1496–9.

(21) Brastianos, H. C.; Vottero, E.; Patrick, B. O.; Van Soest, R.; Matainaho, T.; Mauk, A. G.; Andersen, R. J. Exiguamine A, an indoleamine-2,3-dioxygenase (IDO) inhibitor isolated from the marine sponge Neopetrosia exigua. *J. Am. Chem. Soc.* **2006**, *128*, 16046–7.

(22) Shaikh, I. A.; Johnson, F.; Grollman, A. P. Streptonigrin. 1. Structure-activity relationships among simple bicyclic analogues. Rate dependence of DNA degradation on quinone reduction potential. *J. Med. Chem.* **1986**, *29*, 1329–40.

(23) Conant, J. B.; Fieser, L. F. Reduction Potentials of Quinones. II. The Potentials of Certain Derivatives of Benzoquinone, Naphthoquinone and Anthraquinone. *J. Am. Chem. Soc.* **1924**, *46*, 1858–1881.

(24) Prince, R. C.; Dutton, P. L.; Bruce, J. M. Electrochemistry of ubiquinones, Menaquinones and plastoquinones in aprotic solvents. *Fed. Eur. Biochem. Soc. Lett.* **1983**, *160*, 273–276.

(25) Butler, J.; Hoey, B. M. The apparent inhibition of superoxide dismutase activity by quinones. *J. Free Radic. Biol. Med.* **1986**, *2*, 77–81.

(26) Mukherjee, T. One-electron reduction of juglone (5-hydroxy-1,4-naphthoquinone): a pulse radiolysis study. *Radiat. Phys. Chem.* **1987**, *29*, 455–462.

(27) Wilson, I.; Wardman, P.; Lin, T. S.; Sartorelli, A. C. One-electron reduction of 2- and 6-methyl-1,4-naphthoquinone bioreductive alkylating agents. *J. Med. Chem.* **1986**, *29*, 1381–4.

(28) Ilan, Y. A.; Czapski, G.; Meisel, D. The one-electron transfer redox potentials of free radicals. I. The oxygen/superoxide system. *Biochim. Biophys. Acta* **1976**, *430*, 209–24.

(29) Lamson, D. W.; Plaza, S. M. The anticancer effects of vitamin K. *Altern. Med. Rev.* **2003**, *8*, 303–18.

(30) Ross, D.; Thor, H.; Orrenius, S.; Moldeus, P. Interaction of menadione (2-methyl-1,4-naphthoquinone) with glutathione. *Chem. Biol. Interact.* **1985**, *55*, 177–84.

(31) McAmis, W. C.; Schaeffer, R. C., Jr.; Baynes, J. W.; Wolf, M. B. Menadione causes endothelial barrier failure by a direct effect on intracellular thiols, independent of reactive oxidant production. *Biochim. Biophys. Acta* **2003**, *1641*, 43–53.

(32) Banerjee, T.; DuHadaway, J. B.; Gaspari, P.; Sutanto-Ward, E.; Munn, D. H.; Mellor, A. L.; Malachowski, W. P.; Prendergast, G. C.; Muller, A. J. A key in vivo antitumor mechanism of action of natural product-based brassinins is inhibition of indoleamine 2,3-dioxygenase. *Oncogene* advance online publication 2007 (DOI 10.1038/sj.onc.1210939).

(33) Munn, D. H.; Sharma, M. D.; Hou, D.; Baban, B.; Lee, J. R.; Antonia, S. J.; Messina, J. L.; Chandler, P.; Koni, P. A.; Mellor, A. L. Expression of indoleamine 2,3-dioxygenase by plasmacytoid dendritic cells in tumor-draining lymph nodes. *J. Clin. Invest.* **2004**, *114*, 280–90.

(34) Sono, M.; Cady, S. G. Enzyme kinetic and spectroscopic studies of inhibitor and effector interactions with indoleamine 2,3-dioxygenase. 1. Norharman and 4-phenylimidazole binding to the enzyme as inhibitors and heme ligands. *Biochemistry* **1989**, *28*, 5392–5399.

(35) Sugimoto, H.; Oda, S.; Otsuki, T.; Hino, T.; Yoshida, T.; Shiro, Y. Crystal structure of human indoleamine 2,3-dioxygenase: catalytic mechanism of O2 incorporation by a heme-containing dioxygenase. *Proc. Natl. Acad. Sci. U.S.A.* **2006**, *103*, 2611–6.

(36) Eguchi, N.; Watanabe, Y.; Kawanishi, K.; Hashimoto, Y.; Hayaishi, O. Inhibition of Indoleamine 2,3-Dioxygenase and Tryptophan 2,3-Dioxygenase by beta-Carboline and Indole Derivatives. *Arch. Biochem. Biophys.* **1984**, *232*, 602–609.

(37) Castro, C. E.; Hathaway, G. M.; Havlin, R. Oxidation and Reduction of Iron Porphyrins and Hemoproteins by Quinone and Hydroquinones. *J. Am. Chem. Soc.* **1977**, *99*, 8032–8039.

(38) Yamashita, E.; Zhang, H.; Cramer, W. A. Structure of the Cytochrome b(6)f Complex: Quinone Analogue Inhibitors as Ligands of Heme c. (n). *J. Mol. Biol.* **2007**, *370*, 39–52.

(39) Baymann, F.; Giusti, F.; Picot, D.; Nitschke, W. The ci/bH moiety in the b6f complex studied by EPR: a pair of strongly interacting hemes. *Proc. Natl. Acad. Sci. U.S.A.* **2007**, *104*, 519–24.

(40) Lee, Y. R.; Lee, W. K. Efficient Synthesis of Biologically Interesting Dehydro-alpha-Lapachone and alpha-Lapachone. *Synth. Commun.* **2004**, *34*, 4537–4543.

(41) Lee, Y. R.; Choi, J. H.; Trinh, D. T. L.; Kim, N. W. A Concise Route for the Synthesis of Pyranonaphthoquinone Derivatives. *Synthesis* **2005**, 3026–3034.

(42) Kopanski, L.; Karbach, D.; Selbitschka, G.; Steglich, W. Vesparion, ein Naphtho[2,3-b]pyrandion-Derivativ aus dem Schleimpilz Metatrichia vesparium (Myxomycetes). *Liebigs Ann. Chem.* **1987**, 793–796.

(43) Itoigawa, M.; Ito, C.; Tan, H. T. W.; Okuda, M.; Tokuda, H.; Nishino, H.; Furukawa, H. Cancer chemopreventive activity of naphthoquinones and their analogs from Avicennia plants. *Cancer Lett.* **2001**, *174*, 135–139.

(44) Planchon, S. M.; Wuerzberger-Davis, S. M.; Pink, J. J.; Robertson, K. A.; Bornmann, W. G.; Boothman, D. A. Bcl-2 protects against beta-lapachone-mediated caspase 3 activation and apoptosis in human myeloid leukemia (HL-60) cells. *Oncol. Rep.* **1999**, *6*, 485–492.

(45) Garner, A. P.; Paine, M. J.; Rodriguez-Crespo, I.; Chinje, E. C.; Ortiz De Montellano, P.; Stratford, I. J.; Tew, D. G.; Wolf, C. R. Nitric oxide synthases catalyze the activation of redox cycling and bioreductive anticancer agents. *Cancer Res.* **1999**, *59*, 1929–34.

(46) Samelson-Jones, B. J.; Yeh, S. R. Interactions between nitric oxide and indoleamine 2,3-dioxygenase. *Biochemistry* **2006**, *45*, 8527–38.

(47) Chang, M.; Shi, M.; Forman, H. J. Exogenous glutathione protects endothelial cells from menadione toxicity. *Am. J. Physiol.* **1992**, *262*, L637–43.

(48) Kuriyama, S.; Hitomi, M.; Yoshiji, H.; Nonomura, T.; Tsujimoto, T.; Mitoro, A.; Akahane, T.; Ogawa, M.; Nakai, S.; Deguchi, A.; Masaki, T.; Uchida, N. Vitamins K2, K3 and K5 exert in vivo antitumor effects on hepatocellular carcinoma by regulating the expression of G1 phase-related cell cycle molecules. *Int. J. Oncol.* **2005**, *27*, 505–11.

(49) Thijssen, H. H.; Vervoort, L. M.; Schurgers, L. J.; Shearer, M. J. Menadione is a metabolite of oral vitamin K. *Br. J. Nutr.* **2006**, *95*, 260–6.

(50) Fasco, M. J.; Eagan, G. E.; Wilson, A. C.; Gierthy, J. F.; Lincoln, D. L. Loss of metastatic and primary tumor factor X activator capabilities by Lewis lung carcinoma cells cultured in vitamin K-dependent protein deficient serum. *Cancer Res.* **1988**, *48*, 6504–9.

(51) Dialameh, G. H. Stereobiochemical aspects of warfarin isomers for inhibition of enzymatic alkylation of menaquinone-0 to menaquinone-4 in chick liver. *Int. J. Vitam. Nutr. Res.* **1978**, *48*, 131–5.

(52) Taggart, W. V.; Matschiner, J. T. Metabolism of menadione-6,7–3H in the rat. *Biochemistry* **1969**, *8*, 1141–6.

(53) Watanabe, N.; Dickinson, D. A.; Liu, R. M.; Forman, H. J. Quinones and glutathione metabolism. *Methods Enzymol.* **2004**, *378*, 319–40.

(54) Mauzeroll, J.; Bard, A. J.; Owhadian, O.; Monks, T. J. Menadione metabolism to thiodione in hepatoblastoma by scanning electrochemical microscopy. *Proc. Natl. Acad. Sci. U.S.A.* **2004**, *101*, 17582–7.

(55) Mundy, R. Activation and Detoxification of Naphthoquinones by NAD(P)H: Quinone Oxidoreductase. In *Quinones and Quinone Enzymes*; Sies, H., Packer, L., Eds.; Elsevier Academic Press: San Diego, CA, 2004; Vol. 382, pp 364–380..

(56) Ohnishi, T.; Hirata, F.; Hayaish, O. Indoleamine 2,3-dioxygenase. Potassium superoxide as substrate. *J. Biol. Chem.* **1977**, *252*, 4643–7.

(57) Poljak, A.; Grant, R.; Austin, C. J.; Jamie, J. F.; Willows, R. D.; Takikawa, O.; Littlejohn, T. K.; Truscott, R. J.; Walker, M. J.; Sachdev, P.; Smythe, G. A. Inhibition of indoleamine 2,3-dioxygenase activity by H2O2. *Arch. Biochem. Biophys.* **2006**, *450*, 9–19.

(58) Lanznaster, M.; Neves, A.; Bortoluzzi, A. J.; Assumpcao, A. M.; Vencato, I.; Machado, S. P.; Drechsel, S. M. Electronic effects of electron-donating and -withdrawing groups in model complexes for iron-tyrosine-containing metalloenzymes. *Inorg. Chem.* **2006**, *45*, 1005–11.

(59) Kanamori, D.; Yamada, Y.; Onoda, A.; Okamura, T.-a.; Adachi, S.; Yamamoto, H.; Ueyama, N. Structures and properties of octaethylporphinato. (phenolate)iron(III) complexes with NH--O hydrogen bonds: modulation of Fe-O bond character by the hydrogen bond. *Inorg. Chim. Acta* **2005**, *358*, 331–338.

(60) Darensbourg, D. J.; Ortiz, C. G.; Billodeaux, D. R. Synthesis and structural characterization of iron(III) salen complexes possessing appended anionic oxygen donor ligands. *Inorg. Chim. Acta* **2004**, *357*, 2143–2149.

(61) Nee, M. W.; Lindsay Smith, J. R. Axial ligand exchange of iron(III) tetramesitylporphyrin phenolate complexes. *J. Chem. Soc., Dalton Trans.: Inorg. Chem.* **1999**, 3373–3377.

(62) Uno, T.; Hatano, K.; Nishimura, Y.; Arata, Y. Spectrophotometric and resonance Raman studies on the formation of phenolate and thiolate complexes of (octaethylporphinato)iron(III). *Inorg. Chem.* **1990**, *29*, 2803–2807.

(63) Roe, A. L.; Schneider, D. J.; Mayer, R. J.; Pyrz, J. W.; Widom, J.; Que, L. X-ray absorption spectroscopy of iron-tyrosinate proteins. *J. Am. Chem. Soc.* **1984**, *106*, 1676–1681.

(64) Milburn, R. M. Iron(III)-Phenol Complexes. III. Enthalpies and Entropies of Iron(III)-Phenolate Associations. *J. Am. Chem. Soc.* **1967**, *89*, 54–58.

(65) Nickerson, W. J.; Falcone, G.; Strauss, G. Studies on Quinone-Thioethers. I. Mechanism of Formation and Properties of Thiodione. *Biochemistry* **1963**, *2*, 537–543.

(66) Tietze, L. F.; Güntner, C.; Gericke, K. M.; Schuberth, I.; Bunkoczi, G. A Diels-Alder Reaction for the Total Synthesis of the Novel Antibiotic Antitumor Agent Mensacarcin. *Eur. J. Org. Chem.* **2005**, 2459–2467.

(67) MacLeod, J. W.; Thomson, R. H. Studies in the Juglone Series. IV. The Addition of Aniline and Toluene-p-thiol to 5-Substituted 1,4-Naphthoquinones. *J. Org. Chem.* **1960**, *25*, 36–42.

(68) Ameer, F.; Giles, R. G. F.; Green, I. R.; Pearce, R. Synthesis of Methoxy-2-hydroxy-1,4-naphthoquinones and Reaction of One Isomer with Aldehydes Under Basic Conditions. *Synth. Commun.* **2004**, *34*, 1247–1258.

(69) Wolff, M.; Seemann, M.; Grosdemange-Billiard, C.; Tritsch, D.; Campos, N.; Rodriguez-Concepcion, M.; Boronat, A.; Rohmer, M. Isoprenoid biosynthesis via the methylerythritol phosphate pathway. (E)-4-Hydroxy-3-methylbut-2-enyl diphosphate: chemical synthesis and formation from methylerythritol cyclodiphosphate by a cell-free system from Escherichia coli. *Tetrahedron Lett.* **2002**, *43*, 2555–2559.

(70) Ishida, A.; Mukaiyama, T. Total Synthesis of (±)Variotin and Its Analogs. *Bull. Chem. Soc. Jpn.* **1978**, *51*, 2077–2081.

(71) Lothar, K.; Doris, K.; Gerhard, S.; Wolfgang, S. Fungal pigments. 53. Vesparione, a naphtho[2,3-b]pyrandione derivative from the slime mold Metatrichia vesparium (Myxomycetes). *Liebigs Ann. Chem.* **1987**, 793–796.

(72) De Oliveira, A. B.; Ferreira, D. T.; Raslan, D. S. Synthesis of the naturally occurring naphtho[2,3-b]pyran-5,10-quinones a-caryopterone, dihydro-alpha-caryopterone and their isomers, 6-hydroxydehydro-alpha-lapachone and 6-hydroxy-alpha-lapachone. *Tetrahedron Lett.* **1988**, *29*, 155–8.

(73) Malerich, J. P.; Maimone, T. J.; Elliott, G. I.; Trauner, D. Biomimetic Synthesis of Antimalarial Naphthoquinones. *J. Am. Chem. Soc.* **2005**, *127*, 6276–6283.

(74) Matsumoto, T.; Mayer, C.; Eugster, C. H. α-Caryopteron, a new Pyrano-juglone from *Caryopteris clandonensis*. *Helv. Chim. Acta* **1969**, *52*, 808–812.

(75) Tapia, R.; Valderrama, J. A.; Quintanar, C. Synthesis of Naphtho[2,3-b]pyranoquinones and it's Aza-analogues from a Useful Benzopyranoquinone Intermediate. *Heterocycles* **1994**, *38*, 1797–1804.

(76) Giles, R. G. F.; Roos, G. H. P. Syntheses of the naturally occurring naphtho[2,3-b]pyran-5,10-quinones α-caryopterone, dihydro-α-caryopterone, and O-methyldihydro-α-caryopterone. *J. Chem. Soc., Perkin Trans. 1* **1976**, 1632–1635.

(77) Burns, C. J.; Gill, M.; Saubern, S. Pigments of fungi. XXI. Synthesis of (±)-6-demethoxyaustrocortirubin. *Aust. J. Chem.* **1991**, *44*, 1427–1445.

(78) Littlejohn, T. K.; Takikawa, O.; Skylas, D.; Jamie, J. F.; Walker, M. J.; Truscott, R. J. Expression and purification of recombinant human indoleamine 2, 3-dioxygenase. *Protein Expr. Purif.* **2000**, *19*, 22–9.

(79) Metz, R.; Duhadaway, J. B.; Kamasani, U.; Laury-Kleintop, L.; Muller, A. J.; Prendergast, G. C. Novel tryptophan catabolic enzyme IDO2 is the preferred biochemical target of the antitumor indoleamine 2,3-dioxygenase inhibitory compound D-1-methyl-tryptophan. *Cancer Res.* **2007**, *67*, 7082–7.

(80) Skehan, P.; Storeng, R.; Scudiero, D.; Monks, A.; McMahon, J.; Vistica, D.; Warren, J. T.; Bokesch, H.; Kenney, S.; Boyd, M. R. New colorimetric cytotoxicity assay for anticancer-drug screening. *J. Natl. Cancer Inst.* **1990**, *82*, 1107–12.

(81) Baban, B.; Chandler, P.; McCool, D.; Marshall, B.; Munn, D. H.; Mellor, A. L. Indoleamine 2,3-dioxygenase expression is restricted to fetal trophoblast giant cells during murine gestation and is maternal genome specific. *J. Reprod. Immunol.* **2004**, *61*, 67–77.

(82) Halgren, T. A. MMFF VI. MMFF94s option for energy minimization studies. *J. Comput. Chem.* **1999**, *20*, 720–729.

(83) Halgren, T. A. MMFF MMFF VII. Characterization of MMFF94, MMFF94s, and other widely available force fields for conformational energies and for intermolecular-interaction energies and geometries. *J. Comput. Chem.* **1999**, *20*, 740–774.

(84) Word, J. M.; Lovell, S. C.; Richardson, J. S.; Richardson, D. C. Asparagine and glutamine: Using hydrogen atom contacts in the choice of side-chain amide orientation. *J. Mol. Biol.* **1999**, *285*, 1735–1747.

(85) Lovell, S. C.; Davis, I. W.; Arendall, W. B., III; de Bakker, P. I. W.; Word, J. M.; Prisant, M. G.; Richardson, J. S.; Richardson, D. C. Structure Validation by Cα Geometry: φ,Ψ and Cβ Deviation. *Proteins: Struct. Funct. Genet.* **2003**, *50*, 437–450.

(86) Ponder, J. W.; Case, D. A. Force Fields for Protein Simulations. *Adv. Protein Chem.* **2003**, *66*, 27–85.

(87) Thomsen, R.; Christensen, M. H. MolDock: A New Technique for High-Accuracy Molecular Docking. *J. Med. Chem.* **2006**, *49*, 3315–3321.

(88) Jones, G.; Willet, P.; Glen, R. C.; Leach, A. R.; Taylor, R. Development And Validation Of A Genetic Algorithm For Flexible Docking. *J. Mol. Biol.* **1997**, *267*, 727–748.

(89) Verdonk, M. L.; Cole, J. C.; Hartshorn, M. J.; W, M. C.; R.D., T. Improved Protein-Ligand Docking Using GOLD. *Proteins* **2003**, *52*, 609–623.

(90) Morris, G. M.; Goodsell, D. S.; Halliday, R. S.; Huey, R.; Hart, W. E.; Belew, R. K.; Olson, A. J. Automated Docking Using a Lamarckian Genetic Algorithm and and Empirical Binding Free Energy Function. *J. Comput. Chem.* **1998**, *19*, 1639–1662.

Bin3 Deletion Causes Cataracts and Increased Susceptibility to Lymphoma during Aging

Arivudainambi Ramalingam,[1] James B. Duhadaway,[1] Erika Sutanto-Ward,[1] Yan Wang,[2]
Joseph Dinchuk,[3] Minzhou Huang,[1] Preston S. Donover,[1] Janette Boulden,[1]
Lois M. McNally,[4,5] Alejandro P. Soler,[1,6] Alexander J. Muller,[1,7]
Melinda K. Duncan,[2] and George C. Prendergast[1,7]

[1]Lankenau Institute for Medical Research, Wynnewood, Pennsylvania; [2]Department of Biological Sciences, University of Delaware, Newark, Delaware; [3]DuPont Pharmaceuticals Company, Wilmington, Delaware; [4]New York Eye and Ear Infirmary, New York, New York; Departments of [5]Ophthalmology and [6]Pathology, SUNY Downstate Medical Center, Brooklyn, New York; and [7]Department of Pathology, Anatomy and Cell Biology and Kimmel Cancer Center, Thomas Jefferson University, Philadelphia, Pennsylvania

Abstract

Bin3 encodes an evolutionarily conserved and ubiquitously expressed member of the BAR superfamily of curved membrane and GTPase-binding proteins, which includes the BAR, PCH/F-BAR, and I-BAR adapter proteins implicated in signal transduction and vesicular trafficking. In humans, Bin3 maps to chromosome 8p21.3, a region widely implicated in cancer suppression that is often deleted in non–Hodgkin's lymphomas and various epithelial tumors. Yeast studies have suggested roles for this gene in filamentous actin (F-actin) organization and cell division but its physiologic functions in mammals have not been investigated. Here we report that homozygous inactivation of Bin3 in the mouse causes cataracts and an increased susceptibility to lymphomas during aging. The cataract phenotype was marked by multiple morphologic defects in lens fibers, including the development of vacuoles in cortical fibers and a near total loss of F-actin in lens fiber cells but not epithelial cells. Through 1 year of age, no other phenotypes were apparent; however, by 18 months of age, Bin3$^{-/-}$ mice exhibited a significantly increased incidence of lymphoma. Bin3 loss did not affect normal cell proliferation, F-actin organization, or susceptibility to oncogenic transformation. In contrast, it increased the proliferation and invasive motility of cells transformed by SV40 large T antigen plus activated ras. Our findings establish functions for Bin3 in lens development and cancer suppression during aging. Further, they define Bin3 as a candidate for an unidentified tumor suppressor that exists at the human chromosome 8p21.3 locus. [Cancer Res 2008;68(6):1683–90]

Introduction

BAR adapter proteins, named for a shared sequence motif initially defined in the Bin1, amphiphysin, and yeast RVS proteins (1), function in diverse cellular processes, including membrane dynamics, actin organization, polarity, stress response, antiprolif-eration, immunity, and tumor suppression (2). The signature domain of this class of proteins, the BAR domain, interacts with and facilitates tubulation of curved membranes and also binds to small GTPases and other cell regulatory proteins in the cytosol and nucleus (3). Recently, crystallographic studies have revealed a BAR superfamily that includes not only BAR adapters but also members of the PCH (F-BAR) and I-BAR adapter families (4). Within the original BAR family subgroup, Bin3 is, along with Bin1/amphiphysin II, one of only two members that are both ubiquitously expressed in mammalian cells and conserved throughout evolution to yeast (5). Studies of the budding and fission yeast homologues, termed Rvs161 and hob3+, have highlighted essential functions in filamentous actin (F-actin) organization and cell division (5–8). Extending these observations, a recent study revealed that in fission yeast Hob3p can recruit the Rho family small GTPase Cdc42 to support its role in polarized cell division (9). However, the physiologic functions of Bin3 in mammals have yet to be investigated in any depth.

One stimulus to investigation of the Bin3 gene is its interesting location at human chromosome 8p21.3 within a region that has been implicated widely in cancer suppression (10). Indeed, losses of chromosome 8p represent one of the most common events in epithelial tumors and B lymphomas and such events have been associated strongly with progression in advanced metastatic disease. In particular, recent fine-mapping studies have highlighted a ∼1 Mb region at 8p21.3, including Bin3, as the site of a tumor suppressor gene(s) involved in the development of non–Hodgkin's lymphoma, head and neck cancer, and prostate adenocarcinoma (11–13). However, among the genes within the region implicated, a clear suppressor has yet to been identified. In support of the notion that Bin3 may be germane, another prototypical BAR family member, Bin1/amphiphysin II, has been shown to function in cancer suppression (1, 14–21). To evaluate the physiologic functions of Bin3, we studied the consequences of its genetic deletion in the mouse.

Materials and Methods

Generation and genotyping of Bin3 nullizygous mice. The proximal promoter and exon 1 of the murine Bin3 gene was replaced with a PGK-neo cassette using standard methods for homologous recombination in the mouse. Briefly, a genomic targeting plasmid with the structure noted in Fig. 1A was introduced by electroporation into AB2.1 murine embryonic stem cells. Clones with the desired homologous recombination event were microinjected into C57BL/6J blastocysts and resulting male chimeric animals were bred with C57BL/6 females to obtain offspring with germ-line transmission of the knockout (KO) allele (as identified by Southern blot
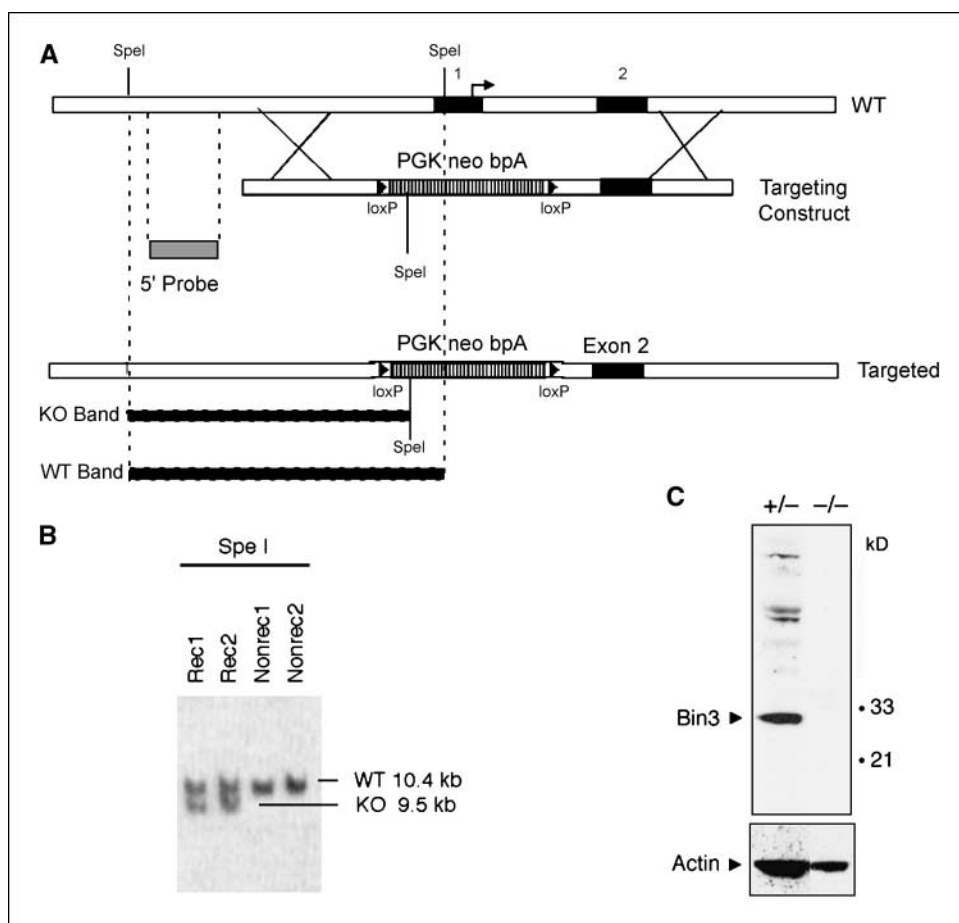
Figure 1. Bin3 deletion in the mouse. *A,* targeting strategy. *B,* evidence of germ-line transmission of the targeted allele. Mouse tail DNAs were prepared and analyzed by Southern blotting as related by the scheme in *A. C,* Western blot analysis of primary MEFs. Blots were probed with a mouse monoclonal antibody raised to a GST-Bin3 fusion protein. Actin was visualized as a loading control to normalize the blot.

analysis). Mice were interbred and maintained on a mixed C57BL/6J-129/SvJ genetic background. PCR was used to genotype mice as follows: Mouse tissue samples were dissociated 1 h at 95°C in lysis buffer (25 mmol/L NaOH plus 0.2 mmol/L EDTA) and then neutralized with equal volume of 40 mmol/L Tris-HCl. DNA-containing supernatant was used for PCR in a volume of 20 μL in a PTC-200 Peltier Thermal Cycler (MJ Research). The primers used were 5'-GTTAGGCCTCAGCTCTCCCTGAAGATTC-3' or 5'-GCTTGGCTGGACG-TAAACTCCTCTTCAG-3' and 5'-CTGGGCCTTGACTCCTCATCTATCA-GAAG-3' with expected sizes of 423 or 264 bp for wild-type (WT) or nullizygous alleles, respectively. Following a 3-min denaturation at 96°C, 35 cycles of PCR were performed at 96°C for 30 s, 61°C for 30 s, and 72°C for 1.5 min with the addition of a 5-min elongation step at 72°C. All experiments using mice were approved by the Lankenau Institute for Medical Research and University of Delaware Animal Care and Use Committees and they conformed to the Association for Research in Vision and Ophthalmology Statement on the Use of Animals in Ophthalmic and Vision Research.

Cell culture. Mouse embryonic fibroblasts (MEF) were generated and cultured as described previously (20, 22). COS cells were cultured and transfected in DMEM supplemented with 10% fetal bovine serum (FBS) and antibiotics. To compare cell proliferation, cells were seeded in triplicate into 100-mm dishes that were uncoated or coated with the nonadherent agent polyHEMA (23), and at the indicated times afterward, cells were counted after trypsinization to determine cell outgrowth. For cell motility as measured by Transwell migration assay, cells were monitored as described (24) in a modified Boyden chamber (8-μm pore size, two-well Costar Transwell, Corning Life Sciences) according to the manufacturer's instructions. Briefly, 10^5 serum-deprived cells were seeded in triplicate in the top wells in medium containing 0.1% FBS, and 48 h later, cells that had migrated into the bottom well containing medium supplemented with 10% FBS were trypsinized and counted.

Antibody preparation and Western blot analysis. Recombinant full-length human Bin3 was expressed in bacteria with a COOH-terminal glutathione *S*-transferase (GST) fusion tag and used to create an anti-Bin3 monoclonal antibody using methods that have been described (25). The resulting hybridoma (3A4) is an IgG2b with a κ light chain and reacts with the highly similar (94% sequence identity) mouse Bin3 on Western blots. MEFs were isolated from WT and Bin3-null mice by standard methods, and cell extracts for Western blot analysis were prepared by harvesting cells, which were washed thrice in PBS, before lysis in 1× radioimmunoprecipitation assay buffer (1× PBS containing 1% NP40, 0.5% sodium deoxycholate, 0.1% SDS, and 10 μg/mL phenylmethylsulfonyl fluoride), including 10 μL/mL Protease Inhibitor Set III and Phosphatase Inhibitor Set II (Calbiochem). Protein was quantitated by Bradford assay and 50 μg protein per sample was analyzed by SDS-PAGE. Gels were processed by standard Western blotting methods using a horseradish peroxidase (HRP)-conjugated goat anti-mouse secondary antibody (1:2,000 dilution; Cell Signaling). For actin, a primary anti-actin goat polyclonal antibody was used (1:500 dilution; Santa Cruz Biotechnology) and HRP-conjugated rabbit anti-goat secondary antibody (1:5,000 dilution; Southern Biotechnology Associates). Antibody detection was carried out using a commercial chemiluminescence kit (Pierce).

Gross and histologic tissue analysis. Slit lamp photographs were taken of anesthetized mice by standard methods. Dark field microscopic analysis of the lens phenotype was performed by dissecting lenses from eyes and placing them in Medium 199 with Earle's salts and L-glutamine (Mediatech), which is isotonic to the lens (26). Lenses were photographed with a dissecting microscope (Stemi SV11 Apo, Carl Zeiss) fitted with a digital camera. The resulting photographs were processed by removing the color information and reducing the brightness in Adobe Photoshop. For histologic analysis, whole eyes were fixed in 4% neutral buffered formalin for

18 h, transferred to 70% ethanol, and stored until paraffin embedding. Sections (6 μm) were prepared, stained with H&E, and photographed on an upright microscope by standard methods.

Phalloidin staining. Lenses were dissected from the eye, fixed for 2 h in 4% neutral buffered formalin, washed thrice for 15 min each in PBS with 0.1% Triton X-100, and stained in PBS with 0.25% Triton X-100, a 1:2,000 dilution of DRAQ5 (Biostatus Ltd.), and 1:200 Alexa Fluor 488–labeled phalloidin (Molecular Probes) overnight at 4°C. Lenses were subjected to three 15-min room temperature washes in 0.1% Triton X-100 in PBS before storage in PBS at 4°C. Whole stained lenses were placed epithelial side down in an uncoated 35-mm #1 glass-bottom culture dish (MatTek Corp.) filled with PBS and imaged in the *XY* plane with a LSM 510 VIS confocal microscope fitted with a 20× objective lens, a 30-mW argon krypton laser, and a 5-mW helium-neon laser (Carl Zeiss).

Bin3 immunofluorescence microscopy. Bin3 localization was analyzed in COS cells transiently transfected with a hemagglutinin (HA)-tagged Bin3 expression construct. Staining methods were essentially as described above and detailed elsewhere (27, 28). MitoTracker (Molecular Probes) and the DNA dye 4′,6-diamidino-2-phenylindole (DAPI) were used as counterstains to identify mitochondria and nuclei, respectively, in COS cells.

Carcinogenesis. For irradiation, 6- to 8-wk-old mice were exposed to a single sublethal dose of 4 or 7 Gy γ-rays from a [137]Cs γ-irradiator and then monitored to an end point of 12 mo when all animals were euthanized. For chemical carcinogenesis, 6- to 8-wk-old mice were subjected to classic protocols of lung, skin, and breast carcinogenesis. For lung carcinogenesis, mice were given as described (29) a single i.p. dose of diethylnitrosamine (DEN) at 20 or 50 mg/kg body weight. Lung tumors induced in this manner occur with a mean latency of 24 wk in A/J mice (29). Mice treated with DEN were monitored up to an end point of 12 mo, after which all animals were euthanized and examined at necropsy for evidence of tumor formation. For skin carcinogenesis, mice were shaved and the dorsal epidermis was treated essentially as described (30, 31) with a single dose of 400 nmol 7,12-dimethylbenz(a)anthracene (DMBA) followed by a twice-weekly application of 17 nmol phorbol ester 12-*O*-tetradecanoylphorbol-13-acetate (TPA). Mice treated with DMBA + TPA were monitored to a 20-wk end point for skin tumors. For mammary carcinogenesis, mice implanted with a subdermal medroxyprogesterone pellet were treated with a single i.p. dose of DMBA and tumor formation was monitored as described (20). All suspected lesions at necropsy were weighed and processed by standard histologic analysis.

Results

**Bin3 is nonessential for embryonic development or fertility.** The murine *Bin3* gene encompasses ∼38 kb and 8 exons on chromosome 14D1-2, encoding a polypeptide composed of a single BAR domain. We used standard methods to replace the proximal promoter and exon 1 of this gene with a PGK-neo cassette (Fig. 1*A*) by homologous recombination in embryonic stem cells, generating chimeric animals by blastocyst microinjection. Germ-line transmission of the targeted allele was observed in heterozygous animals by Southern blot analysis of genomic DNA from two separate founder mice generated by the same embryonic stem cell population (Fig. 1*B*), one of which was further characterized. The loss of Bin3 protein in null mice was confirmed by Western blot analysis of primary MEFs isolated from heterozygous or homozygous null embryos using a monoclonal antibody raised against a recombinant GST-Bin3 fusion protein. This antibody detected a ∼31 kDa protein in MEFs$^{+/-}$ but not MEFs$^{-/-}$ that was consistent with the size of the Bin3 polypeptide predicted from its primary structure (Fig. 1*C*). Somewhat unexpectedly, given the robust defect in cytokinesis produced in fission yeast cells by mutation of the *Bin3* homologue *hob3+* (5, 9), we found that viable homozygous null mice were readily obtained at Mendelian ratios without any apparent defects in survival or fertility (data not shown). This

finding immediately argued that in mammals *Bin3* has a nonessential role in cell division, highlighting some functional differences with fission yeast *hob3+* despite the homology of these genes (5).

Bin3-null mice develop cataracts soon after birth, which are characterized by severe defects in cytoskeletal F-actin organization. Within a few weeks to a few months of birth, *Bin3*$^{-/-}$ mice developed obvious gross lenticular opacities in one or both eyes, whereas mice heterozygous or WT for the deletion did not develop cataracts (Fig. 2*A–H*). This phenotype was highly penetrant, appearing in all nullizygous animals examined by 6 months of age. Histopathologic examination of lenses from 1-week-old *Bin3*$^{-/-}$ mice (Fig. 2*G*) did not reveal any obvious defects; however,
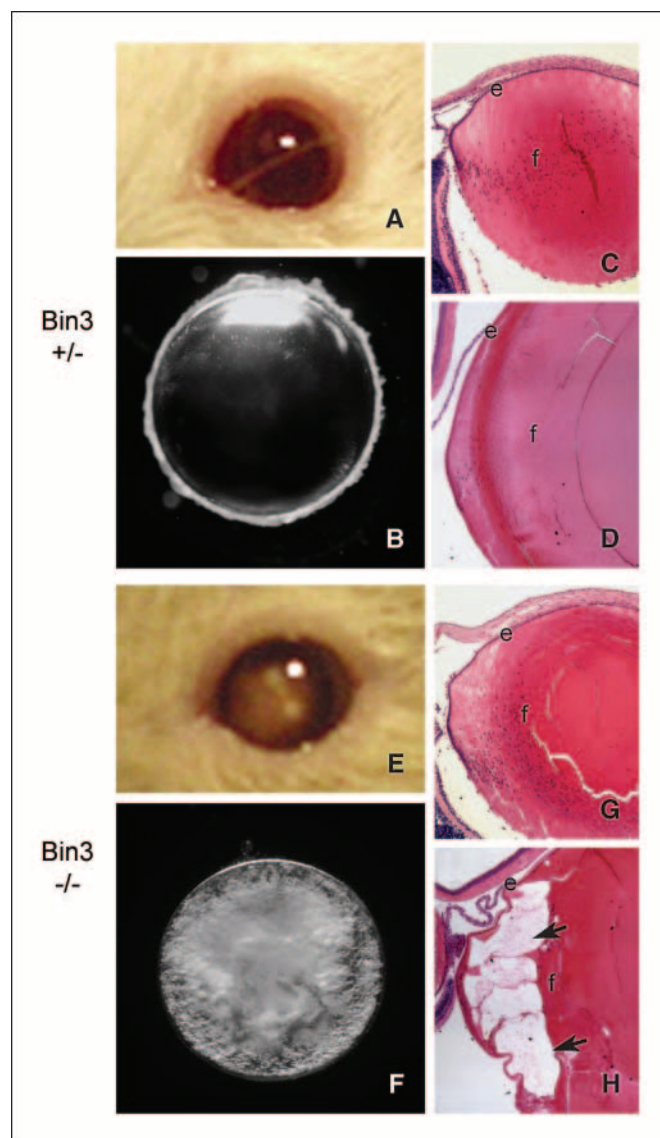
Figure 2. Cataract formation in Bin3 nullizygous mice. Phenotype, gross pathology, and histology of lenses from heterozygous and nullizygous mice are shown. *A* and *E,* phenotype. *B* and *F,* gross pathology. Lenses dissected from euthanized animals were processed and photographed with a dissecting microscope fitted with a digital camera. *C, D, G,* and *H,* histology. Eyes from euthanized animals were fixed, processed for staining with H&E, and photographed at two magnifications. Note the overall disorganization of lens fibers and vacuolar degeneration around the nucleus in the tissue from the nullizygous animal. *e,* epithelial cells; *f,* fiber cells.
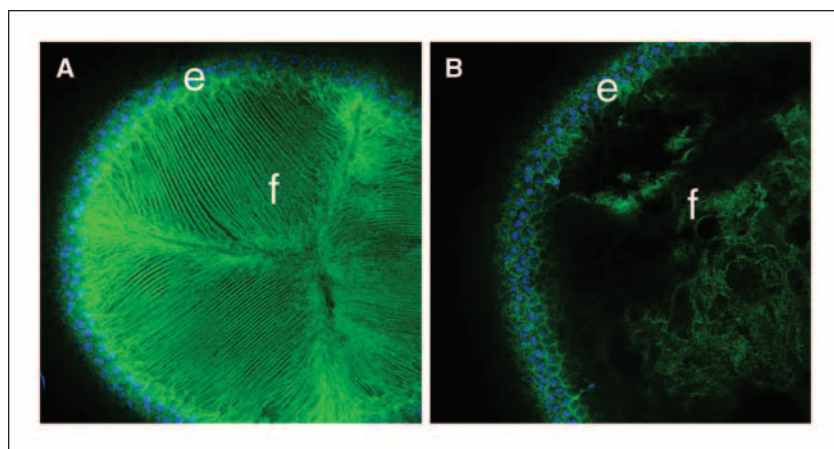
Figure 3. F-actin organization is disrupted in lenses from *Bin3*$^{-/-}$ mice. Lenses from 8-wk-old mice were processed for whole mount staining with fluorescein-conjugated phalloidin (*green*) and the DNA stain DRAQ5 (*blue*) and then imaged on a confocal microscope. *A*, lens from a *Bin3*$^{+/-}$ mouse. *B*, lens from a *Bin3*$^{-/-}$ mouse. Note the lack of apparent F-actin loss or disorganization in lens epithelial cells compared with the lens fiber cells. *e*, epithelial cells; *f*, fiber cells.

by 8 weeks of age, the lens cortex of nullizygous animals had developed numerous large vacuoles (Fig. 2*H*), although the lens epithelium was apparently unaffected. There was no change in the size of the eye in *Bin3*$^{-/-}$ mice and the retina, cornea, and other tissues of the eye did not show obvious pathologic features. In contrast, no lens defects were observed in the lens sections obtained from *Bin3* heterozygous or WT littermates.

Genetic studies of yeast homologues of *Bin3* suggest that this gene functions in F-actin organization (5, 32). Therefore, we analyzed the F-actin organization of lenses from 8-week-old heterozygous and nullizygous mice. In lens fiber cells, F-actin is normally found directly underlying the lateral cell membranes (Fig. 3*A*). In *Bin3*$^{-/-}$ lenses, we observed a striking loss of F-actin from the lens fiber cells and the little actin structure that remained was highly disorganized (Fig. 3*B*). In contrast, F-actin organization in the lens epithelial cells of nullizygous mice seemed to be relatively unaffected. Furthermore, we did not observe any alteration in the actin cytoskeleton of *Bin3*$^{-/-}$ MEFs (data not shown). Taken together, these observations indicated that *Bin3* ablation caused a specific disruption of F-actin structure in lens fiber cells.

Although efforts to visualize endogenous Bin3 by indirect immunofluorescence staining methods were unsuccessful in embryonic or adult murine eye, as well as in other tissue types and MEFs (data not shown), in COS kidney cells where a HA-tagged human Bin3 was expressed transiently, we observed a cytosolic vesicular localization expected for BAR adapter proteins (Fig. 4). Similar results were obtained on expression of WT Bin3 where protein was visualized with Bin3 monoclonal antibody (data not shown). We concluded that Bin3 supported actin organization and likely functioned at cytosolic vesicular membranes in cells. Based on a recent report that fission yeast Hob3p can recruit Cdc42 to support its role in cell division, we compared Cdc42 expression and localization in lenses and embryonic fibroblasts derived from *Bin3*$^{-/-}$ animals. However, we did not detect any differences in Cdc42 expression or localization in either cell type (data not shown). These findings were not unexpected based on the profound contrast between the phenotypes produced by deletions of *Bin3* or *Cdc42*, which in the latter case causes early embryonic lethality in the mouse associated with gross defects in structural organization and primary ectoderm (33). This strong difference in phenotype clearly pointed to greater degeneracy in the function of *Bin3* in mammals compared with fission yeast.

Bin3 suppresses lymphoma during aging and restricts the efficiency of lung carcinogenesis. Other than juvenile cataracts, no other apparent phenotypes were noted in Bin3$^{-/-}$ mice through 1 year of age. In contrast, beyond 1 year of age *Bin3*$^{-/-}$ mice displayed a significantly elevated incidence of lymphoma, with 36% of *Bin3*$^{-/-}$ mice exhibiting lymphomas by 18 months of age compared with none of the age-matched heterozygous or WT control animals (Table 1; Fig. 5*A*). Lymphomas were observed to arise in the lung, liver, intestine, spleen, and lymph nodes. Among
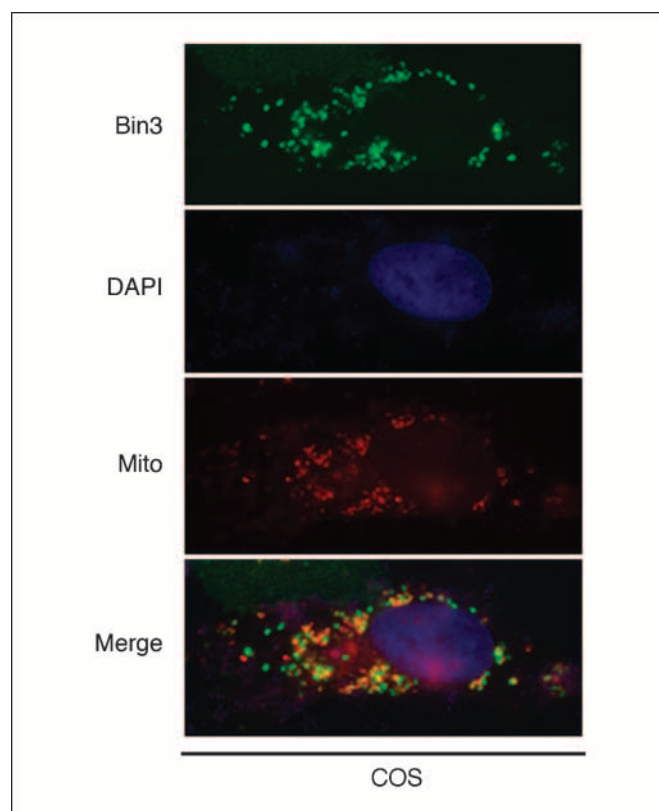
Figure 4. Vesicular membranous localization of Bin3 protein. COS cells were processed for indirect immunofluorescence with monoclonal antibody 12CA5 to HA epitope 48 h after transfection with an expression vector for HA epitope-tagged Bin3. No staining was observed in vector-only–transfected cells. DAPI was used to visualize nuclei and MitoTracker dye was used to visualize mitochondria (*Mito*).

Table 1. Increased incidence of lymphoma formation in *Bin3*⁻/⁻ mice during aging

Pathology	Bin3⁺/⁺ (n = 10)	Bin3⁺/⁻ (n = 23)	Bin3⁻/⁻ (n = 33)
Lymphoma	0/10 (0%)	0/23 (0%)	13/33 (39%)*
Lung			
Congestion, chronic inflammation	0/10 (0%)	0/23 (0%)	3/33 (9%)
Liver			
Congestion, chronic inflammation	0/10 (0%)	1/23 (4%)	2/33 (6%)
Spleen			
Myelodysplastic syndrome	0/10 (0%)	1/23 (4%)	2/33 (6%)
Congestion, extramedullary hemopoiesis	1/10 (10%)	1/23 (4%)	2/33 (6%)

NOTE: Mice were euthanized at 18 mo of age and examined at necropsy for pathologic evidence of tumor formation. All suspected lesions were confirmed by histologic analysis.

*P = 0.0196 (+/+ versus −/−) or 0.0003 (+/− versus −/−) using a two-tailed Fisher's exact test.

these types of tumors, two were identified specifically as mucosa-associated lymphoid tissue lymphoma and two as follicular lymphoma (data not shown). *Bin3*⁻/⁻ mice also exhibited modest increases in congestion and inflammation in the lung or liver and also in myelodysplastic syndrome and congestion with extramedullary hemopoiesis in spleen (∼15% and ∼12% of nullizygous animals, respectively; Table 1; Fig. 5*B*). Taken together, these observations suggested that *Bin3* acted to suppress lymphoma formation during aging.

We reasoned that a negative modifier effect of *Bin3* on cancer might also manifest in animals exposed to a carcinogen. To examine this idea, we compared the responses of *Bin3*⁻/⁻ mice to γ-irradiation, exposure to a chemical carcinogen, or activation of the c-*myc* oncogene in a transgenic cross. In these experiments, heterozygous animals were used as controls based on evidence of haplosufficiency of Bin3 for lymphoma suppression and the desire to control for the neomycin cassette present at the homozygous KO locus. These experiments suggested a specific trend for cooperation of *Bin3* loss with a facilitation of lung tumor formation. For irradiation, mice of 6 to 8 weeks of age were subjected to a single whole-body dose of 4 to 7 Gy γ-radiation from a ¹³⁷Cs source and monitored to a 12-month end point. Although the penetrance of tumor formation on this protocol was limited, the null group exhibited greater sensitivity to lung adenocarcinoma, splenic extramedullary hemopoiesis, and splenomegaly relative to the heterozygous control group (Supplementary Table S1; Supplementary Fig. S1*A* and *B*). Similarly, in mice exposed to a single dose of DEN, a *ras*-activating mutagen that induces lung and liver tumors with limited penetrance (34), null mice also exhibited a greater sensitivity to the formation of lung adenocarcinoma (Supplementary Table S2; Supplementary Fig. S1*C*). Although liver tumors did not arise in these animals, 30% of the *Bin3*⁻/⁻ mice displayed hepatic congestion and 20% displayed hepatocyte atypia (Supplementary Table S2). Neither of these premalignant lesions occurred in the control group. Finally, we also compared the effects of *Bin3* loss in two models of mammary tumorigenesis involving initiation by chemical carcinogen DMBA or overexpression of the c-*myc* oncogene. Briefly, mice were subjected to a standard protocol of carcinogen treatment or interbred with MMTV-c-*myc* mice (35) before nullizygous and heterozygous virgin or parous females were compared for tumor incidence, kinetics, and histology. In both models, *Bin3* loss did not affect mammary tumorigenesis (data not shown), implying that *Bin3* suppressed tumor formation only in specific tissues, only in cooperation with certain oncogenic lesions, or both. In summary, we concluded that *Bin3* restricted the efficiency of lung carcinogenesis and suppressed the development of spontaneous lymphomas during aging.

Bin3 restricts the proliferation and motility of oncogenically transformed cells. Despite evidence that the yeast homologues of *Bin3* function in F-actin organization, endocytosis, and cytokinesis (5, 7, 9, 36), an examination of normal embryonic fibroblasts and liver monocytes derived from *Bin3*⁻/⁻ animals revealed no gross

Figure 5. Lymphoma and splenic histopathology in aging *Bin3*⁻/⁻ mice. Representative lesions scored in nullizygous animals were processed for sectioning and staining with H&E using standard histologic methods. *A*, lymphoma in liver in an 18-mo-old animal. *B*, splenic congestion with extramedullary hemopoiesis in an 18-mo-old animal.
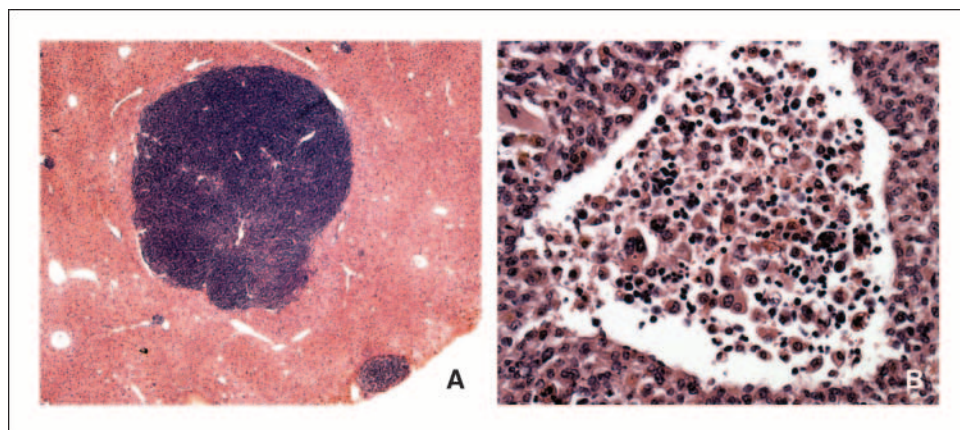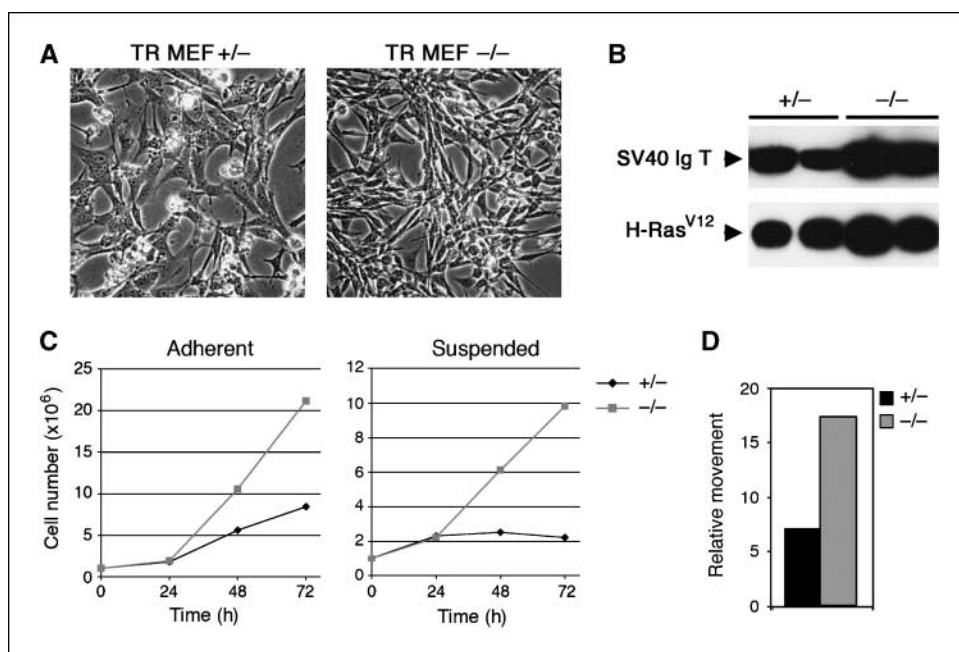
Figure 6. Bin3 loss increases the growth and invasive motility of oncogenically transformed primary cells. *A,* morphology. Cells were photographed in tissue culture at ×200 magnification. *B,* transgene expression. Expression of SV40 large T antigen and mutant H-Ras in transformed cell populations was confirmed by Western blot analysis using antibodies to the oncoproteins. *C,* cell proliferation. Cells (10^6) were seeded into 100-mm dishes and cell number was counted using a hemocytometer after trypsinization at the times indicated. Proliferation was compared on plastic dishes and dishes coated with polyHEMA, a nonadherent substrate. *D,* invasive motility. Cells (10^5) were plated in duplicate into modified Boyden chamber plates (8-μm pore size) and the relative number of cells that penetrated to the bottom of the well 48 h later was determined. The mean of the data is shown.

defects in F-actin organization, endocytotic or phagocytotic activity, or cell division (data not shown). These observations were consistent with the lack of any general acute effects of *Bin3* ablation in the mouse other than cataract formation. In contrast, yet consistent with evidence of roles for *Bin3* yeast homologues *Rvs161* and *hob3+* in stress signaling (7, 36), we found that *Bin3* deletion accentuated the neoplastic phenotype of embryonic fibroblasts (MEFs) that were oncogenically transformed by expression of SV40 large T antigen plus mutant H-ras^{V12}. Specifically, *Bin3*$^{-/-}$-transformed MEFs displayed increased proliferation on adherent or nonadherent substrata and relatively greater invasive motility through Matrigel in transwell cell migration assays (Fig. 6). There was no significant effect of *Bin3* deletion on MEF immortalization (3T3 passage schedule) or on susceptibility to oncogenic transformation, further extending the notion that *Bin3* does not control a fundamental feature of cell division in mammalian cells (data not shown). However, in support of the concept that it negatively modifies cell proliferation under conditions of transformation-related stress, we noted a greater sensitivity of T + Ras–transformed cells to cell death caused by the antiproliferative agents mitomycin C, which inhibits DNA synthesis and nuclear division, or benomyl, which blocks mitosis (data not shown). Taken together, these results corroborated the concept of *Bin3* as a suppressor gene that restricts the proliferation and motility of oncogenically transformed cells.

Discussion

The results of this study define essential functions for *Bin3* in postnatal lens development and lymphoma suppression during aging. Advanced age is the major risk factor for many diseases, yet most preclinical models use young animals that do not fully recapitulate the participation of inflammation, immune senescence, or other factors that are affected significantly by aging. Insights into the cause and treatment of age-associated diseases might benefit from studies of pathways that modify disease susceptibility during aging. However, few such pathways have been defined.

Cataracts are the leading cause of blindness in the world. Although most cataracts are diagnosed in the elderly, congenital cataracts also occur in infants and children at a rate of ∼3 in 10,000 births, accounting for ∼10% of vision loss in children worldwide. Congenital cataracts have been found as components of multisystem syndromes, in association with other defects in ocular development, or as isolated anomalies. Many of the genes responsible for human and mouse autosomal dominant cataracts have been discovered in recent years (37) due to the completion of a saturation mutagenesis screen of the mouse genome for loci responsible for dominant cataract (38). However, the etiology of the vast majority of human congenital cataracts remains unknown (39) and may well represent autosomal recessive traits. Mouse models have been used to define genes involved in congenital eye abnormalities, and in recent years, they have advanced understanding of lens morphogenesis, physiology, and the pathogenesis and pathophysiology of cataract (39, 40). One notable aspect of the human chromosomal localization of *Bin3* at 8p21.3 is its synteny with the midsection of murine chromosome 14, where a highly penetrant cataract locus, termed rupture of lens cataract (Rlc), has been mapped. Rlc causes lens opacity starting at 1 to 2 months of age with vacuole formation and lens nucleus rupture in advanced cases (41–44). Like *Bin3* loss, the effects of *Rlc* seem to be confined to the lens without effects on development, viability, or fertility. Given their relative proximity and similarities in cataractogenesis, the relationship between *Rlc* and *Bin3* may deserve further attention.

In cancer, chromosome 8p is among the most commonly altered regions of the genome, with a large body of literature implying the presence of at least three tumor suppressor genes. Although the identity of these genes has yet to be identified conclusively, inactivation of one or more is strongly implicated in the genesis of a variety of epithelial and hematologic malignancies. In particular, there is extensive evidence pointing to a suppressor locus 8p21.3 that is germane to the development of non–Hodgkin's lymphoma (11), prostate cancer (12, 45–48), head, neck, oral, and laryngeal cancers (13, 49), and lung cancers (50). Indeed, recent fine-mapping

studies of the 8p21.3 region have highlighted a ~1 Mb region containing ~10 genes, including the *Bin3* gene, as a focal point of relevance to non–Hodgkin's lymphoma and prostate adenocarcinoma (11–13). The appearance of lymphomas in *Bin3*$^{-/-}$ mice is clearly consistent with the possible relevance of *Bin3* as a tumor suppressor in this setting. Although we did not see prostate tumors spontaneously arise in *Bin3*$^{-/-}$ mice, this connection needs to be explored more directly because, based on our observations, one would not expect *Bin3* ablation to be sufficient on its own to drive epithelial tumorigenesis in the absence of a cooperating oncogenic stimulus. Although the 8p21-22 region in humans also has been implicated in breast cancer suppression, our results argued against a role for *Bin3* in this setting, suggesting either it is irrelevant or that conditions required for relevance were not operative in the models examined. Nevertheless, our findings as a whole clearly support further evaluation of *Bin3* as a candidate for the tumor suppressor gene inferred to reside at human chromosome 8p21.3.

Our findings provide a biological foundation for further investigation into how *Bin3* functions. During lens fiber cell differentiation, these cells develop elaborated lateral membranes that form high surface area interdigitations with their neighbors to allow for extensive cell communication in this avascular tissue (51). Because these interdigitations also are tightly associated with the actin cytoskeleton (52), this association supports a Bin3 connection in actin cytoskeletal dynamics and membrane structure. However, if this is the case, it remains unclear why the lens phenotype should develop so late, only after eye lid opening. As noted above, yeast homologues of *Bin3* have been implicated in F-actin organization, vesicle trafficking, and cell polarity (5–8, 36). Lens fiber cells normally have most of their F-actin distributed directly under cell membrane in lens fiber (53), whereas *Bin3*$^{-/-}$ lens fiber cells lose much of their F-actin cytoskeleton and what is remaining does not seem to localize along the lateral cell membranes. This phenotype suggests that Bin3 may be essential to maintain the actin cytoskeleton of lens fibers. In support of this notion, *Bin3* is able to complement defects in F-actin localization in fission yeast caused by mutation of its homologue *hob3+*. Alternatively, Bin3 may be important for actin dynamics in the lens by supporting short-term disassembly of actin stress fibers in lens epithelial cells, which seems to be sufficient to induce differentiation in lens fiber cells (54).

A small set of interactions for yeast homologues of Bin3 has been described, but the relevance of two of the best characterized of these interactions remains uncertain in mammals as yet. Studies of the budding yeast homologue Rvs161p indicate a critical reliance on its physical interaction with Rvs167p, the Bin1/amphiphysin orthologue in yeast, yet we have been unable, to date, to obtain any evidence of similar physical interactions between either the fission yeast orthologues Hob1p and Hob3p or the mammalian orthologues Bin1 and Bin3.[8] A second important interaction has been reported between Hob3p and Cdc42p (9), a Rho family small GTPase that contributes to polarized cell division and cytokinesis in fission yeast (55). However, we observed no changes in Cdc42 expression or localization in cells lacking *Bin3*, including in lens cells where *Bin3* loss caused a profound disruption in F-actin organization. The notion that the Bin3 and Cdc42 proteins may not interact constitutively in mammalian cells, as their fission yeast counterparts do, is not entirely unexpected given (*a*) the profound difference in the effects of deleting *Cdc42* and *Bin3* in the mouse, only the former of which yields an early embryonic lethal phenotype associated with gross structural abnormalities, and (*b*) the much greater degeneracy in Rho small GTPases and their regulators in mammals compared with yeast. Given evidence that *Bin3* and its yeast homologues may share roles in stress signaling (5), possibly germane to cancer suppression, along with the involvement of Cdc42 in motility and perhaps cytokinesis (55), it is interesting that oncogenically transformed primary cells lacking *Bin3* displayed an increased sensitivity to the antimitotic agent benomyl as well as an increased motility in transwell migration assays. Thus, interactions of *Bin3* with *Bin1* or *Cdc42* may be contingent on a cellular stress state, including oncogenic stress, the context of which may help define their possible roles in cell proliferation and motility.

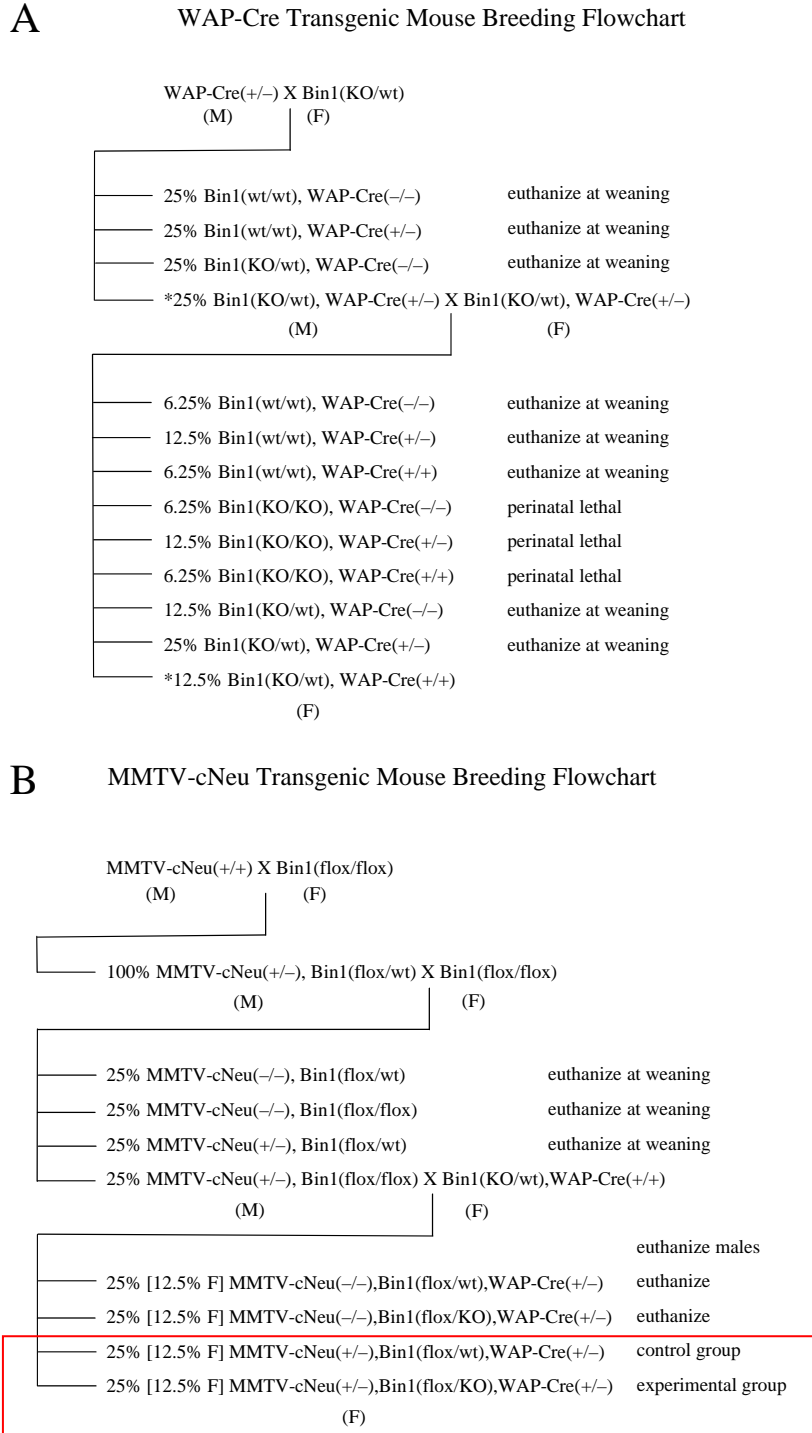[8] E. Routhier et al., unpublished observations.

References

1. Sakamuro D, Elliott K, Wechsler-Reya R, Prendergast GC. BIN1 is a novel MYC-interacting protein with features of a tumor suppressor. Nat Genet 1996;14: 69–77.
2. Ren G, Vajjhala P, Lee JS, Winsor B, Munn AL. The BAR domain proteins: molding membranes in fission, fusion, and phagy. Microbiol Mol Biol Rev 2006;70:37–120.
3. Peter BJ, Kent HM, Mills IG, et al. BAR domains as sensors of membrane curvature: the amphiphysin BAR structure. Science 2003;303:495–9.
4. Chitu V, Stanley ER. Pombe Cdc15 homology (PCH) proteins: coordinators of membrane-cytoskeletal interactions. Trends Cell Biol 2007;17:145–56.
5. Routhier EL, Burn TC, Abbaszade I, Summers M, Albright CF, Prendergast GC. Human Bin3 complements the F-actin localization defects caused by loss of Hob3p,

the fission yeast homolog of Rvs161p. J Biol Chem 2001; 276:2167–21677.
6. Brizzio V, Gammie AE, Rose MD. Rvs161p interacts with Fus2p to promote cell fusion in *Saccharomyces cerevisiae*. J Cell Biol 1998;141:567–84.
7. Balguerie A, Bagnat M, Bonneu M, Aigle M, Breton AM. Rvs161p and sphingolipids are required for actin repolarization following salt stress. Eukaryot Cell 2002;1: 1021–31.
8. Germann M, Swain E, Bergman L, Nickels JT, Jr. Characterizing the sphingolipid signaling pathway that remediates defects associated with loss of the yeast amphiphysin-like orthologs, Rvs161p and Rvs167p. J Biol Chem 2005;280:4270–8.
9. Coll PM, Rincon SA, Izquierdo RA, Perez P. Hob3p, the fission yeast ortholog of human Bin3, localizes Cdc42p to the division site and regulates cytokinesis. EMBO J 2007;26:1865–77.

10. Birnbaum D, Adelaide J, Popovici C, Charafe-Jauffret E, Mozziconacci MJ, Chaffanet M. Chromosome arm 8p and cancer: a fragile hypothesis. Lancet Oncol 2003;4:639–42.
11. Rubio-Moscardo F, Blesa D, Mestre C, et al. Characterization of 8p21.3 chromosomal deletions in B-cell lymphoma: TRAIL-R1 and TRAIL-R2 as candidate dosage-dependent tumor suppressor genes. Blood 2005; 106:3214–22.
12. Chang BL, Liu W, Sun J, et al. Integration of somatic deletion analysis of prostate cancers and germline linkage analysis of prostate cancer families reveals two small consensus regions for prostate cancer genes at 8p. Cancer Res 2007;67:4098–103.
13. Ye H, Pungpravat N, Huang BL, et al. Genomic assessments of the frequent loss of heterozygosity region on 8p21.3 approximately p22 in head and neck squamous cell carcinoma. Cancer Genet Cytogenet 2007;176:100–6.

14. Elliott K, Sakamuro D, Basu A, et al. Bin1 functionally interacts with Myc in cells and inhibits cell proliferation by multiple mechanisms. Oncogene 1999;18:3564–73.

15. Elliott K, Ge K, Du W, Prendergast GC. The c-Myc-interacting adapter protein Bin1 activates a caspase-independent cell death program. Oncogene 2000;19:4669–84.

16. Ge K, DuHadaway J, Du W, Herlyn M, Rodeck U, Prendergast GC. Mechanism for elimination of a tumor suppressor: aberrant splicing of a brain-specific exon causes loss of function of Bin1 in melanoma. Proc Natl Acad Sci U S A 1999;96:9689–94.

17. Ge K, DuHadaway J, Sakamuro D, Wechsler-Reya R, Reynolds C, Prendergast GC. Losses of the tumor suppressor Bin1 in breast carcinoma are frequent and reflect deficits in a programmed cell death capacity. Int J Cancer 2000;85:376–83.

18. Ge K, Minhas F, DuHadaway J, et al. Loss of heterozygosity and tumor suppressor activity of Bin1 in prostate carcinoma. Int J Cancer 2000;86:155–61.

19. Chang M, Boulden J, Katz JB, et al. Bin1 ablation increases susceptibility to cancer during aging, particularly lung cancer. Cancer Res 2007;67:7605–12.

20. Chang M, Boulden J, Sutanto-Ward E, et al. Bin1 ablation in mammary gland delays tissue remodeling and drives cancer progression. Cancer Res 2007;67:100–7.

21. Muller AJ, DuHadaway JB, Donover PS, Sutanto-Ward E, Prendergast GC. Targeted deletion of the suppressor gene Bin1/Amphiphysin2 enhances the malignant character of transformed cells. Cancer Biol Ther 2004;3:1236–42.

22. Liu A-X, Rane N, Liu J-P, Prendergast GC. RhoB is dispensable for mouse development, but it modifies susceptibility to tumor formation as well as cell adhesion and growth factor signaling in transformed cells. Mol Cell Biol 2001;21:6906–12.

23. Lebowitz PF, Sakamuro D, Prendergast GC. Farnesyltransferase inhibitors induce apoptosis in Ras-transformed cells denied substratum attachment. Cancer Res 1997;57:708–13.

24. Korah RM, Sysounthone V, Golowa Y, Wieder R. Basic fibroblast growth factor confers a less malignant phenotype in MDA-MB-231 human breast cancer cells. Cancer Res 2000;60:733–40.

25. Koprowski H, Steplewski Z, Mitchell K, Herlyn M, Herlyn D, Fuhrer P. Colorectal carcinoma antigens detected by hybridoma antibodies. Som Cell Genet 1979;5:957–72.

26. Augusteyn RC, Rosen AM, Borja D, Ziebarth NM, Parel JM. Biometry of primate lenses during immersion in preservation media. Mol Vis 2006;12:740–7.

27. Wechsler-Reya R, Elliott K, Herlyn M, Prendergast GC. The putative tumor suppressor BIN1 is a short-lived nuclear phosphoprotein whose localization is altered in malignant cells. Cancer Res 1997;57:3258–63.

28. DuHadaway JB, Lynch FJ, Brisbay S, et al. Immunohistochemical analysis of Bin1/Amphiphysin II in human tissues: diverse sites of nuclear expression and losses in prostate cancer. J Cell Biochem 2003;88:635–42.

29. Stoner GD, Greisiger EA, Schut HA, et al. A comparison of the lung adenoma response in strain A/J mice after intraperitoneal and oral administration of carcinogens. Toxicol Appl Pharmacol 1984;72:313–23.

30. Mustacich D, Wagner A, Williams R, et al. Increased skin carcinogenesis in a keratinocyte directed thioredoxin-1 transgenic mouse. Carcinogenesis 2004;25:1983–9.

31. Park CB, Fukamachi K, Takasuka N, et al. Rapid induction of skin and mammary tumors in human c-Ha-ras proto-oncogene transgenic rats by treatment with 7,12-dimethylbenz[*a*]anthracene followed by 12-*O*-tetradecanoylphorbol 13-acetate. Cancer Sci 2004;95:205–10.

32. Sivadon P, Bauer F, Aigle M, Crouzet M. Actin cytoskeleton and budding pattern are altered in the yeast rvs161 mutant: the Rvs161 protein shares common domains with the brain protein amphiphysin. Mol Gen Genet 1995;246:485–95.

33. Chen F, Ma L, Parrini MC, et al. Cdc42 is required for PIP(2)-induced actin polymerization and early development but not for cell viability. Curr Biol 2000;10:758–65.

34. Manam S, Storer RD, Prahalada S, et al. Activation of the Ha-, Ki-, and N-ras genes in chemically induced liver tumors from CD-1 mice. Cancer Res 1992;52:3347–52.

35. Stewart TA, Pattengale PK, Leder P. Spontaneous mammary adenocarcinomas in transgenic mice that carry and express MTV/myc fusion genes. Cell 1984;38:627–37.

36. Crouzet M, Urdaci M, Dulau L, Aigle M. Yeast mutant affected for viability upon nutrient starvation: characterization and cloning of the RVS161 gene. Yeast 1991;7:727–43.

37. Shiels A, Hejtmancik JF. Genetic origins of cataract. Arch Ophthalmol 2007;125:165–73.

38. Favor J. Mutagenesis and human genetic disease: dominant mutation frequencies and a characterization of mutational events in mice and humans. Environ Mol Mutagen 1995;25 Suppl 26:81–7.

39. Graw J. Congenital hereditary cataracts. Int J Dev Biol 2004;48:1031–44.

40. Dalke C, Graw J. Mouse mutants as models for congenital retinal disorders. Exp Eye Res 2005;81:503–12.

41. Matsushima Y, Kamoto T, Iida F, Abujiang P, Honda Y, Hiai H. Mapping of rupture of lens cataract (rlc) on mouse chromosome 14. Genomics 1996;36:553–4.

42. Iida F, Matsushima Y, Hiai H, Uga S, Honda Y. Rupture of lens cataract: a novel hereditary recessive cataract model in the mouse. Exp Eye Res 1997;64:107–13.

43. Song CW, Okumoto M, Mori N, Kim JS, Han SS, Esaki K. Mapping of new recessive cataract gene (lr2) in the mouse. Mamm Genome 1997;8:927–31.

44. Song CW, Okumoto M, Mori N, et al. A new hereditary cataract mouse with lens rupture. Lab Anim 1997;31:248–53.

45. Bova GS, Carter BS, Bussemakers MJ, et al. Homozygous deletion and frequent allelic loss of chromosome 8p22 loci in human prostate cancer. Cancer Res 1993;53:3869–73.

46. Haggman MJ, Wojno KJ, Pearsall CP, Macoska JA. Allelic loss of 8p sequences in prostatic intraepithelial neoplasia and carcinoma. Urology 1997;50:643–7.

47. Kagan J, Stein J, Babaian RJ, et al. Homozygous deletions at 8p22 and 8p21 in prostate cancer implicate these regions as the sites for candidate tumor suppressor genes. Oncogene 1995;11:2121–6.

48. Oba K, Matsuyama H, Yoshihiro S, et al. Two putative tumor suppressor genes on chromosome arm 8p may play different roles in prostate cancer. Cancer Genet Cytogenet 2001;124:20–6.

49. El-Naggar AK, Coombes MM, Batsakis JG, Hong WK, Goepfert H, Kagan J. Localization of chromosome 8p regions involved in early tumorigenesis of oral and laryngeal squamous carcinoma. Oncogene 1998;16:2983–7.

50. Wistuba II, Behrens C, Virmani AK, et al. Allelic losses at chromosome 8p21-23 are early and frequent events in the pathogenesis of lung cancer. Cancer Res 1999;59:1973–9.

51. Kuszak JR, Peterson KL, Brown HG. Electron microscopic observations of the crystalline lens. Microsc Res Tech 1996;33:441–79.

52. Zhou CJ, Lo WK. Association of clathrin, AP-2 adaptor and actin cytoskeleton with developing interlocking membrane domains of lens fibre cells. Exp Eye Res 2003;77:423–32.

53. Lo WK, Shaw AP, Wen XJ. Actin filament bundles in cortical fiber cells of the rat lens. Exp Eye Res 1997;65:691–701.

54. Weber GF, Menko AS. Actin filament organization regulates the induction of lens cell differentiation and survival. Dev Biol 2006;295:714–29.

55. Rincon S, Coll PM, Perez P. Spatial regulation of Cdc42 during cytokinesis. Cell Cycle 2007;6:1687–91.

Tumor

Tumor-Draining Lymph Node
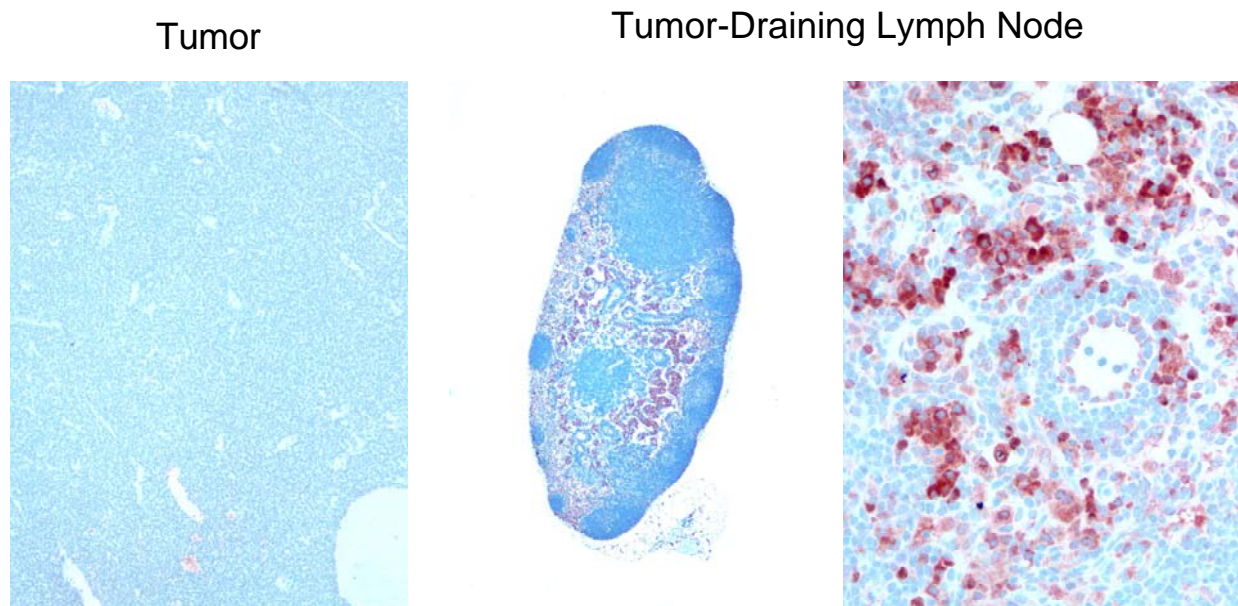
Figure 1. IDO expression is evident in the tumor draining lymph nodes but not in the autochthonous primary tumors formed in MMTV-*Neu* transgenic mice. Immunohistochemical staining with rabbit polyclonal antibody to mouse IDO. Left: Primary MMTV-*Neu* mammary gland tumor stained for IDO (red, x100). Right: Draining inguinal lymph node stained for IDO (red, x100 & x400).

A   WAP-Cre Transgenic Mouse Breeding Flowchart

WAP-Cre(+/−) X Bin1(KO/wt)
(M)   (F)

25% Bin1(wt/wt), WAP-Cre(−/−)   euthanize at weaning
25% Bin1(wt/wt), WAP-Cre(+/−)   euthanize at weaning
25% Bin1(KO/wt), WAP-Cre(−/−)   euthanize at weaning
*25% Bin1(KO/wt), WAP-Cre(+/−) X Bin1(KO/wt), WAP-Cre(+/−)
(M)   (F)

6.25% Bin1(wt/wt), WAP-Cre(−/−)   euthanize at weaning
12.5% Bin1(wt/wt), WAP-Cre(+/−)   euthanize at weaning
6.25% Bin1(wt/wt), WAP-Cre(+/+)   euthanize at weaning
6.25% Bin1(KO/KO), WAP-Cre(−/−)   perinatal lethal
12.5% Bin1(KO/KO), WAP-Cre(+/−)   perinatal lethal
6.25% Bin1(KO/KO), WAP-Cre(+/+)   perinatal lethal
12.5% Bin1(KO/wt), WAP-Cre(−/−)   euthanize at weaning
25% Bin1(KO/wt), WAP-Cre(+/−)   euthanize at weaning
*12.5% Bin1(KO/wt), WAP-Cre(+/+)
(F)

B   MMTV-cNeu Transgenic Mouse Breeding Flowchart

MMTV-cNeu(+/+) X Bin1(flox/flox)
(M)   (F)

100% MMTV-cNeu(+/−), Bin1(flox/wt) X Bin1(flox/flox)
(M)   (F)

25% MMTV-cNeu(−/−), Bin1(flox/wt)   euthanize at weaning
25% MMTV-cNeu(−/−), Bin1(flox/flox)   euthanize at weaning
25% MMTV-cNeu(+/−), Bin1(flox/wt)   euthanize at weaning
25% MMTV-cNeu(+/−), Bin1(flox/flox) X Bin1(KO/wt),WAP-Cre(+/+)
(M)   (F)

                                                   euthanize males
25% [12.5% F] MMTV-cNeu(−/−),Bin1(flox/wt),WAP-Cre(+/−)   euthanize
25% [12.5% F] MMTV-cNeu(−/−),Bin1(flox/KO),WAP-Cre(+/−)   euthanize
25% [12.5% F] MMTV-cNeu(+/−),Bin1(flox/wt),WAP-Cre(+/−)   control group
25% [12.5% F] MMTV-cNeu(+/−),Bin1(flox/KO),WAP-Cre(+/−)   experimental group
(F)

Figure 2. Breeding strategy for producing FVB-strain mammary gland targeted Bin1-null mice. The alleles for the Cre recombinase transgene controlled by the whey acidic protein promoter [WAP-Cre], the constitutive Bin1 knockout [Bin1(KO)], and the conditional Bin1 knockout [Bin1(flox)] were all individually introduced onto the FVB strain background by performing 5 or more generations of backcrossing prior to initiating these crosses. The two flowcharts diagram the breeding steps that were followed to generate experimental and control groups mice with the desired genotypes. This required (A) two generations of breeding to obtain Bin1(KO/wt),WAP-Cre(+/+) mice that were used in breeding scheme B where indicated by the arrow and (B) three generations of breeding to obtain experimental MMTV-cNeu(+/-), Bin1(flox/KO),WAP-Cre(+/-) and control MMTV-cNeu(+/-),Bin1(flox/wt),WAP-Cre(+/-)mice.
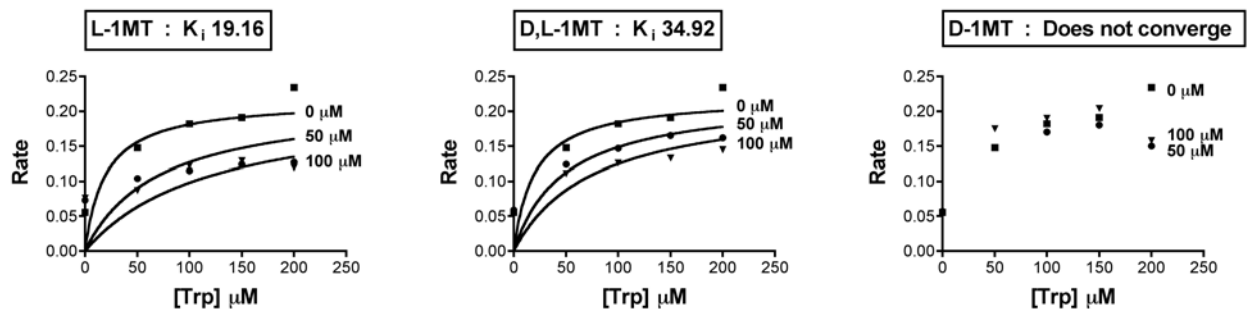
Figure 3. L-MT inhibits purified IDO enzyme activity more effectively than D-1MT. Enzyme kinetic data demonstrating the impact of the L and D 1MT isomers and the D,L racemate on purified, recombinant IDO enzyme activity in the presence of varying concentrations of L-tryptophan substrate. Global nonlinear regression analysis and computation of best fit Ki values, (shown for each compound), was performed using the Prism4 software package (GraphPad).

Hou, et al. 2007 Cancer Res. 67:792
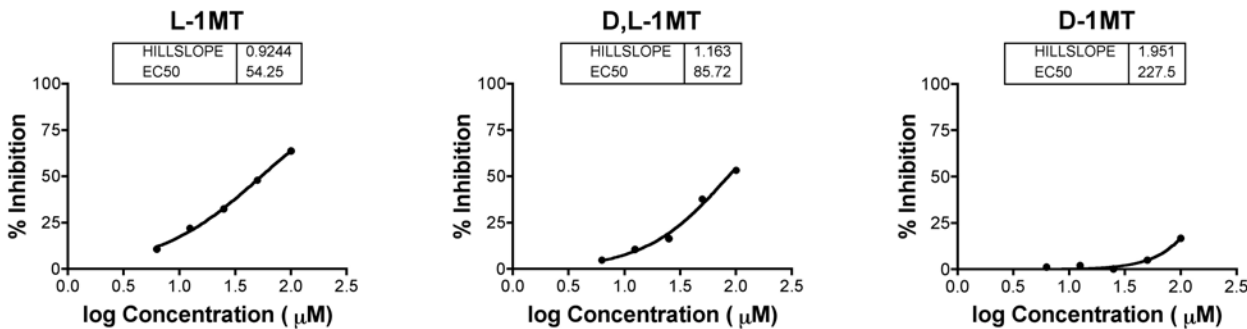
Figure 4. L-MT inhibits IDO enzyme activity in HeLa cells more effectively than D-1MT. The impact of dose escalation of the L and D 1MT isomers and the D,L racemate on IDO activity was evaluated in HeLa cells stimulated for 24h with IFN-γ. Nonlinear regression analysis and calculation of EC50 and Hillslope values, (shown for each compound), was performed using the Prism4 data analysis program (GraphPad).

Hou, et al. 2007 Cancer Res. 67:792
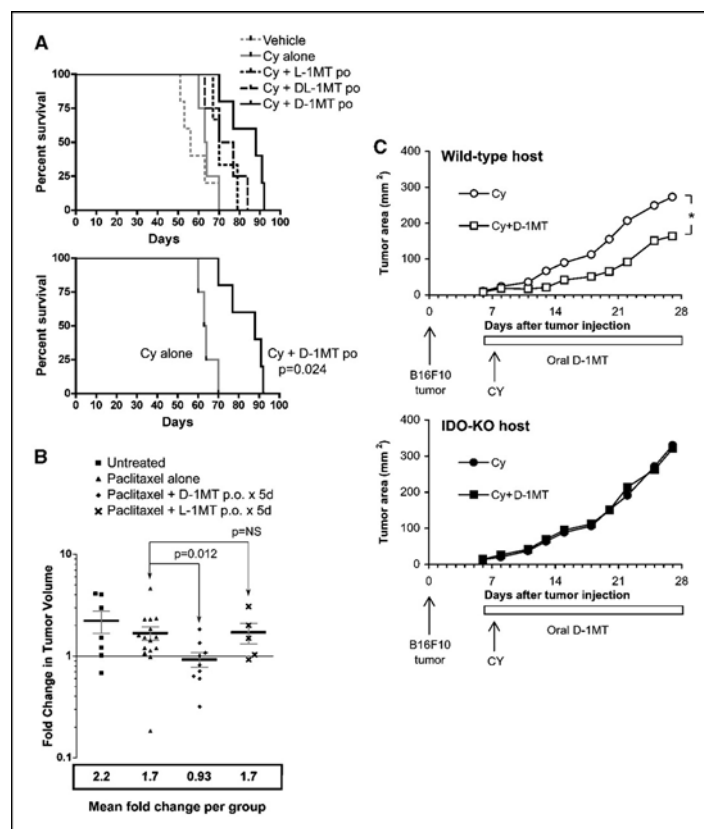
Figure 3. D-1MT provides greater survival benefit in combination therapy, in an IDO-dependent fashion.
A. 4T1-luc orthotopic isografts were established in the mammary fatpad. Cy was administered at 25 mg/kg orally qd 1×/week, and 1MT (D, L or DL) administered at 400 mg/kg by oral gavage twice daily 5×/week by gavage, beginning at the time of tumor implantation. The upper graph shows time to endpoint for all groups; the lower graph shows only the Cy vs Cy+D-1MT groups, for clarity. The comparisons of interest were between [D-1MT+CY vs CY] and [L-1MT+CY vs CY]. Since survival data were not censored, groups were analyzed using a two-group Wilcoxon exact test; statistical significance was determined at p<0.025. The combination of D-1MT+CY showed a significant survival benefit over CY alone (p=0.024), while L-1MT+CY was not different from CY alone (p=0.14).
B. MMTV-*Neu* mice with tumors were treated for 2 weeks, receiving either vehicle alone, paclitaxel alone or paclitaxel (13.3 mg/kg q. MWF) plus oral D-1MT or L-1MT for 5 days, as indicated. For statistical analysis, the comparisons of interest were [D-1MT+paclitaxel vs paclitaxel alone] and [L-1MT+paclitaxel vs paclitaxel alone]. Significance was determined at p<0.025 using a two-group Wilcoxon exact test. The fold change of the D-1MT+paclitaxel group was significantly smaller than that of paclitaxel alone (p=0.012), whereas paclitaxel+L-1MT was not different from paclitaxel alone (p=0.85).
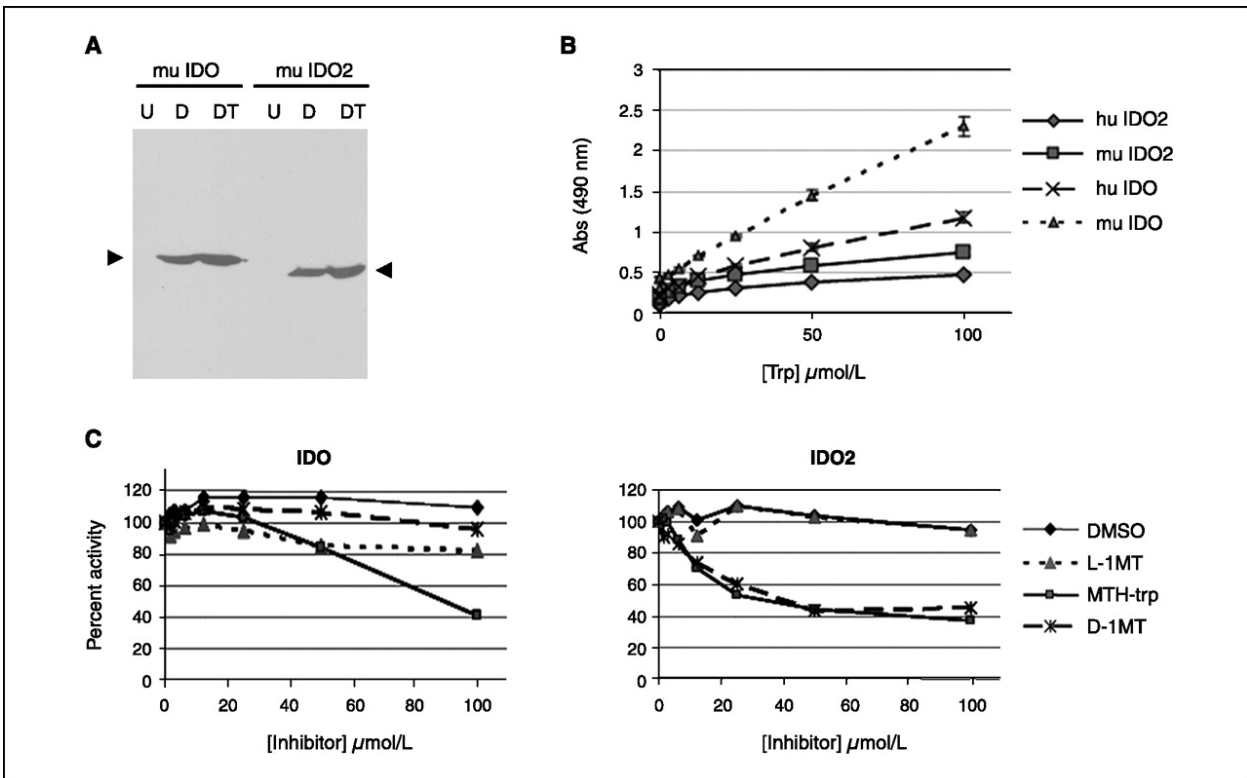*C.* The effects of the D isomer of 1MT require an intact host IDO gene. B16F10 tumors were grown in either wild-type B6 hosts or IDO-KO hosts on the B6 background, as shown. All groups received Cy, with or without oral D-1MT (2 mg/ml in drinking water). Analysis by ANOVA showed that Cy+D-1MT was significantly different (* p<0.05) than Cy alone for the wild-type hosts, but there was no effect of D-1MT when tumors were grown in IDO-KO hosts.

Hou, et al. 2007 Cancer Res. 67:792
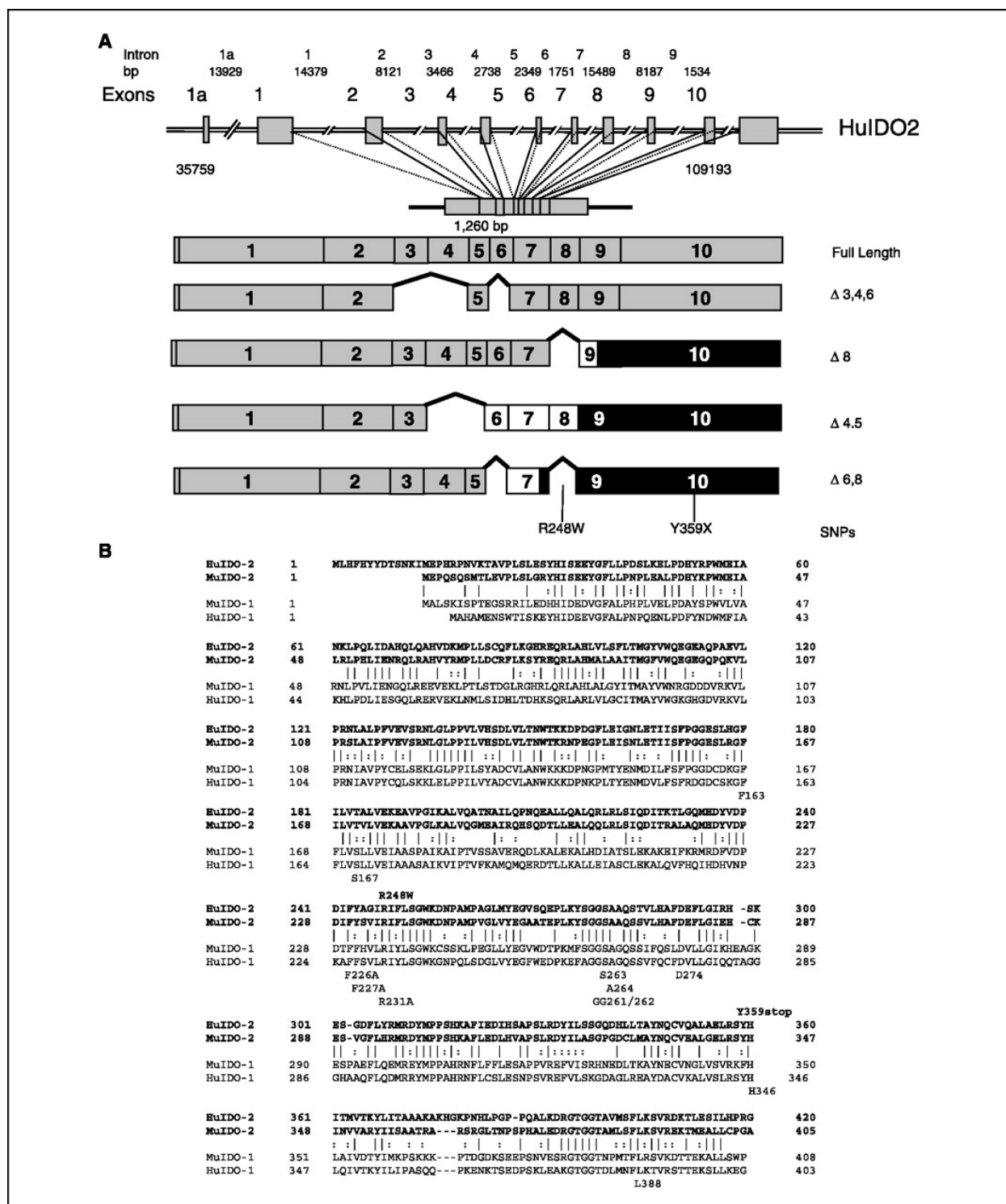
Figure 6. IDO2 structure and similarities to IDO. *A,* structure of human *IDO2* gene and transcripts. Complete coding region is 1,260 bp encoding a 420-amino-acid polypeptide. Alternate splice isoforms lacking the exons indicated are noted. *White boxes,* a frameshift in the coding region to an alternate reading frame leading to termination. *Black boxes,* 3' untranslated regions. Nucleotide numbers, intron sizes, and positioning are based on IDO sequence files NW_923907.1 and GI:89028628 in the Genbank database. *B,* amino acid alignment of IDO and IDO2. Amino acids determined by mutagenesis and the crystal structure of IDO that are critical for catalytic activity are positioned below the human IDO sequence. Two commonly occurring SNPs identified in the coding region of human IDO2 are shown above the sequence that alter a critical amino acid (R248W) or introduce a premature termination codon (Y359stop).
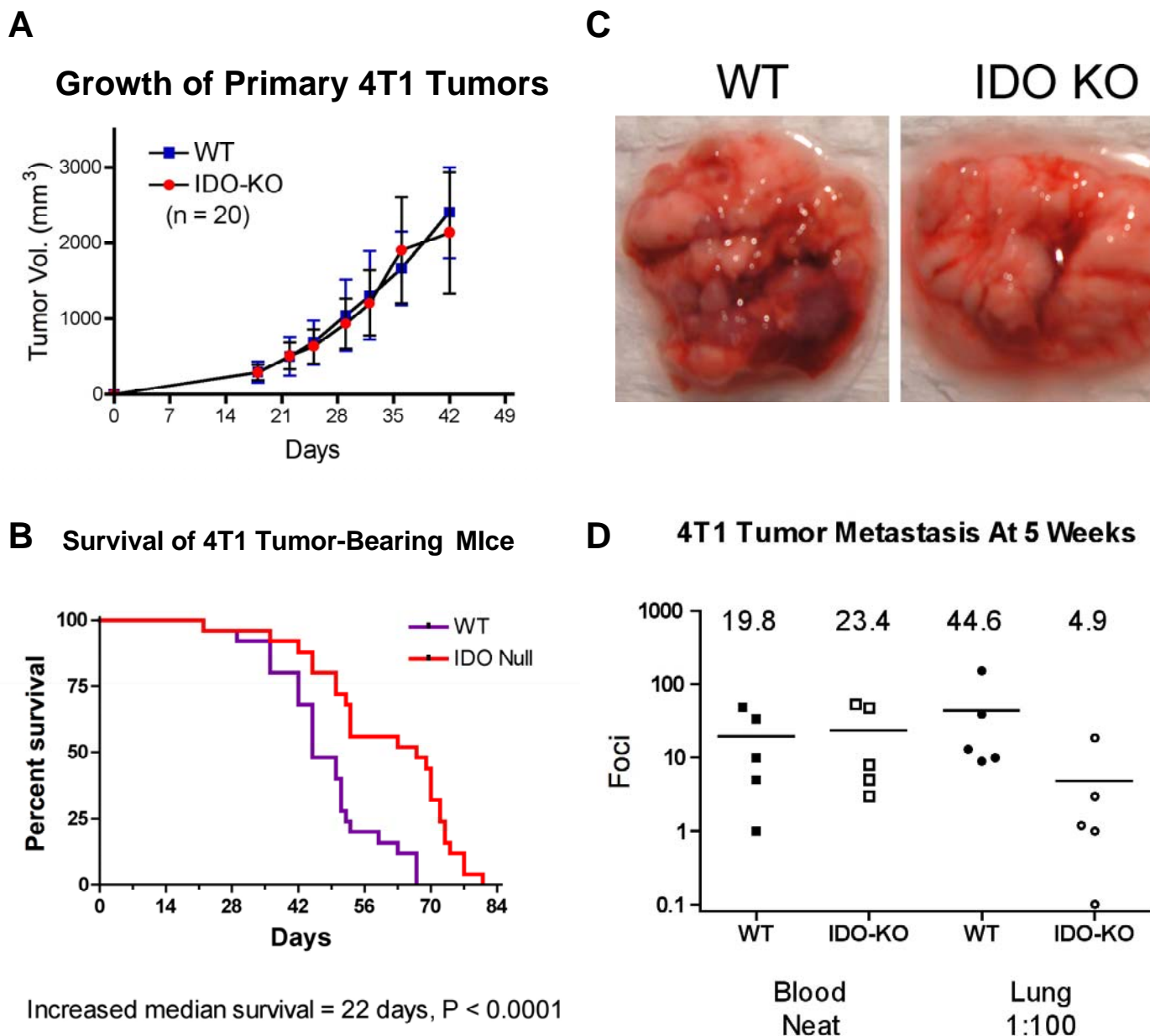
Metz, et al. 2007 Cancer Res. 67:7082

Figure 7. Tryptophan catabolic activity of IDO2 and inhibition by D-1MT. *A,* inducible expression of IDO and IDO2 in representative T-REX cells. Western blot analysis of the V5 epitope–tagged proteins indicated was done with a horseradish peroxidase–conjugated anti-V5 antibody (Invitrogen) in cells that were untreated (*U*), treated with 20 ng/mL doxycycline (*D*), or treated with doxycycline and 100 µmol/L tryptophan (*DT*). *B,* tryptophan catabolism. T-REX cells were seeded at 60% to 70% confluence in 96-well dishes in medium supplemented with 0 to 100 µmol/L tryptophan. Kyn production was determined 48 h later and normalized to protein levels as determined by sulforhodamine B assay. Each enzyme was catalytically active, based on increased Kyn levels with increasing substrate concentrations, although IDO2 seemed to be 2- to 4-fold less active than IDO when normalized to protein levels as determined by sulforhodamine B assay. *Points,* mean of values determined in triplicate and normalized to cellular protein levels. *Abs,* absorbance. *C,* effect of IDO inhibitors on IDO2 catalytic activity. T-REX cells were seeded and processed as above except for the addition to the medium of 0 to 100 µmol/L of the IDO inhibitors MTH-trp, L-1MT, D-1MT, or vehicle control (DMSO). *Points,* mean of values determined in triplicate and normalized to cellular protein levels as before.

Metz, et al. 2007 Cancer Res. 67:7082

72
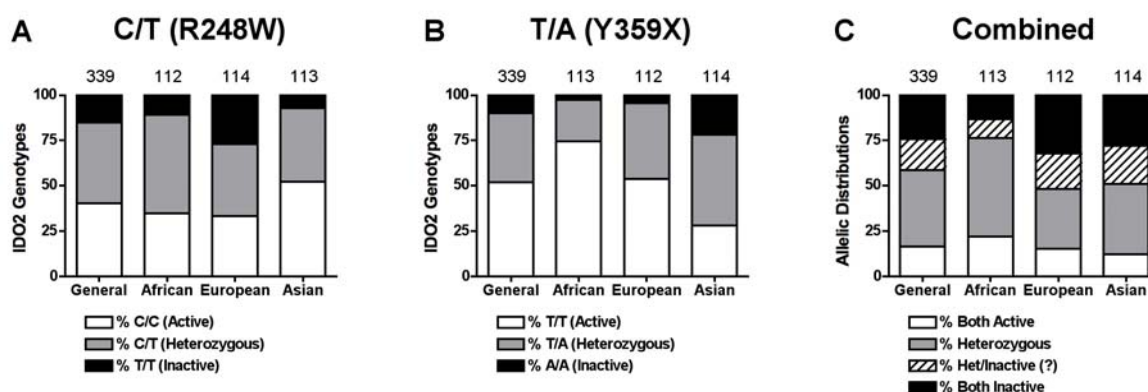
Figure 8. Non-functional *IDO2* SNPs are highly represented in the human population. A SNP database from 341 individuals was evaluated for the frequency of alternate alleles of the two functional SNPs identified in the human *IDO2* gene, rs10109853 (C/T; codon change R248W) and rs4503083 (T/A; codon change Y359Stop). Of the individuals represented in the databse, 114 were categorized as European, 114 as Asian, 23 as African American and 90 as Sub-Saharan African. The percent distribution of the different allelic pairs are graphed for **A)** the C/T alleles, **B)** the T/A alleles and **C)** the active vs. inactive alleles combining data from both allelic variants. The distribution pattern for the entire dataset is represented by the first bar on the left followed by separate analyses for the African, European, and Asian groups. The N for each analysis is listed at the top of the bar. In a few instances, the SNP analysis was uninformative resulting in the N values being somewhat lower than the total number of individuals evaluated. In panel C it was sometimes impossible to unequivocally determine whether two inactivating SNPs were located in the same or different alleles, and these instances are represented separately in the distribution pattern by a hatched segment on the graph. However, sequence data presented in this report indicating that the two polymorphism tend to be independently segregating alleles suggests that the distribution of these equivocal alleles is likely to be skewed toward both being inactive. The SNP datasets are available through the NCBI ENTREZ SNP web site at http://www.ncbi.nlm.nih.gov/entrez/query.fcgi?db=Snp.

Metz, et al. 2007 Cancer Res. 67:7082

A

Growth of Primary 4T1 Tumors

C

B   Survival of 4T1 Tumor-Bearing MIce

Increased median survival = 22 days, P < 0.0001

D   4T1 Tumor Metastasis At 5 Weeks

Figure 9. Loss of IDO in the stroma prolongs the survival of mice bearing 4T1 breast tumor isografts. by impairing metastasis. 4T1-luc orthotopic isografts were established by injection of 1×10^4 cells into the mammary fatpad of wild type and IDO knockout BALB/c strain mice. **A**) Growth of primary tumors as determined by caliper measurements. Graphed as the mean ± SEM. **B**) Survival of mice bearing 4T1 tumors. Since survival data were not censored, groups were analyzed by a two-group logrank test (equivalent to the Mantel-Haenszel test) using GraphPad Prism4 statistical analysis software; statistical significance was determined at $p < 0.05$. **C**) Lungs from mice taken at 7 weeks following challenge with 4T1 cells. **D**) Number of 6-thioguanine-resistant colonies formed from blood and lung biopsies taken from mice at 5 weeks following challenge with 4T1 cells.